Characterizing an in-situ fraction of Photosynthetic Active Radiation product for implementation in the validation of MODIS-derived fraction of Photosynthetic Active Radiation products using continuous-wavelet transforms.

by

Iain Sharp

A thesis submitted to fulfill the requirements of the degree of

Master of Science

Department of Earth and Atmospheric Sciences

University of Alberta

Abstract

The goal of this thesis is to address the need to improve forestry monitoring and satellite validation techniques to better contextualize the effects that human-induced climate change is having on tropical dry forests (TDFs). Climate change is expected to change regional and global precipitation patterns, intensifying and punctuating precipitation events, lengthening drought periods and shortening growing season length for photosynthesizing vegetation. Anthropogenically focused land use policies impose a top-down control of ecosystems by altering the disturbance regimes of ecosystems and determining the ability of ecosystems to regenerate based on its anthropogenic value. Understanding the interplay between the top-down anthropogenic control and bottom-up climate forces on TDF ecosystem functionality, resilience, and productivity is ailing, and remedying that ailment is the drive for this thesis. Therefore, the thesis aims to test previously established findings about the influences that increase the variance of an in-situ fraction of Photosynthetic Active Radiation (fPAR) product and establish the influences that are unique to TDFs for the creation of this product. Another purpose of this study is to bring to light the utilization of near-surface optical wireless sensor networks for the purpose of validating satellite-derived products and to monitor the health, productivity, and ecological functionality of TDFs. By passively observing the photosynthetic dynamics of TDFs, while collecting subsequent environmental data this study reveals the benefits of using wireless sensor network technology to monitor and assess leaf phenology, phenological drivers and how these can be used to validate the observations from satellite-derived fPAR products with a case study from the tropical dry forest located in Costa Rica's, Santa Rosa National Park Environmental Monitoring Super-Site (SRNP-EMSS).

Chapter one is used as an introduction into the motivation behind the methodologies presented in this thesis. Chapter two confirms that environmental and methodological influences that exist in the northern hemispherical deciduous broadleaf forests also influence the creation of an in-situ fraction of Photosynthetic Active Radiation (fPAR) product in tropical dry forests. The scope of influence that solar zenith angle, sky condition, wind speed, network configuration and mechanical PAR sensor calibration have on in-situ 2-flux fPAR is defined and isolated for each phenological phase that tropical dry forests undergo. Results from this chapter indicate that utilizing data captured when wind speeds are less than 5 m/s, when solar zenith angles are between 27° and 60°, and which are captured under diffuse sky conditions with seven or more sensors present results in the smallest degree of variance for the in-situ 2-flux fPAR product. Utilizing the findings from chapter two, chapter three slightly alters and then employs the in-situ fPAR product produced to test and validate if the MODIS-derived fPAR products are capable of accurately capturing the timing, length, and magnitude of phenological events and trends observed in the TDF of Costa Rica's SRNP-EMSS. Conclusions from chapter three indicate that while MODIS-derived fPAR products are capable of capturing broad phenological trends, they are incapable of capturing the magnitude of change that occurs in photosynthesizing vegetation throughout a phenological year, and that they are incapable of accurately capturing the timing of phenological patterns, such as the yearly, bi-annual peaking, or onset of green-up or senescence. Chapter four provides the conclusive statement to the thesis, reviewing the significance of these results and how the contributions of this thesis may further research in the fields of remote sensing and forest phenology. The results presented here may be specific to tropical dry forests and the MODIS satellite system, but the methodologies are not, and their implementation in other forest ecosystems should be considered when considering the standardization of satellite-

validation procedures and environmental monitoring as they can improve our understanding of the limitations or problems of satellite techniques and how vegetation seasonality is rapidly changing globally.

Preface

The research conducted for this thesis forms part of an international research collaboration called Tropi-Dry, led by Professor G.A. Sanchez-Azofeifa of the University of Alberta. The specific wireless sensor network referred to in chapters 2 and 3 are the realization of Dr. G.A. Sanchez-Azofeifa and were co-designed and manufactured by Onset® Communications and Lord-Microstrain Systems®, with the assistance of Mr. Doug Calvert of Hoskins Scientific®, and Cassidy Rankine a former PhD student of Professor G.A. Sanchez-Azofeifa.

Results from Chapter 2 of this thesis were presented as *Sharp, Iain, Sanchez-Azofeifa, Arturo, and Musilek, Petr, 2018. Land-product validation of the MODIS derived FAPAR product over the tropical dry-forest of Santa Rosa National Park, Guanacaste, Costa Rica. Poster Presentation in Biogeosciences at the European Geophysical Union General Assembly 2018, Vienna, Austria*. I was responsible for the experimental design, data collection and analysis as well as the poster creation. The co-authors were responsible for poster editing and contributing to results interpretation. The data analysis and results interpretation of Chapters 2 and 3 are my original work.

Acknowledgements

I would like to first and foremost, formally thank my supervisor and mentor Dr. Arturo Sanchez-Azofeifa for providing me with the opportunity to become a masters student in his laboratory, along with the years of support, enlightenment and opportunities that he has provided for me. I would not have become the dedicated professional that I have without the patience and support of Dr. Sanchez-Azofeifa. It has been an honour and privilege to work under your well-directed guidance throughout this process.

Additionally, I would like to thank all my co-workers, lab partners, and lab managers at the Center for Earth Observation Sciences – which includes Jose Antonio Guzman in particular – for providing me with guidance, support and cultivating a wonderful working environment that continues to make the CEOS research environment a productive, progressive light in the field of remote sensing science. It also would have been impossible to complete this work without the help of the instrumentation teams in the Department of Electrical Engineering and Computer Sciences, as well as the support teams at Hoskin Scientific Edmonton (Mr Doug Calvert et al.).

The realization of this thesis would not have been made possible without the Tropi-Dry Collaborative Research Network (CRN3-025) which provided me with the opportunity to execute many a successful field campaign at the SRNP-EMSS and beyond. The field support team cannot be forgotten either, as they provided me with the much-needed support and expertise necessary to maintain instruments and collect data in such a harsh and unforgiving environment (Saulo Castro, Peter Carlson, Rebeca Campos-Valverde, Ronny Hernandez, Jose Antonio Guzman, Carlos Campos-Valverede, Ana Cristina-Castro, and more). A special thank you to Dr. Hans Verbeeck of Ghent University, along with the MiTACS Globalink Travel Award, who provided me with wonderous Belgian hospitality and the opportunity to come and learn from himself and his esteemed team (Dr. Kim Calders and Sruthi Moorthy) for many months. Of course, I cannot forget the help that Dr. Joanne Nightingale and Niall Origo from the National Physical Laboratory provided me, with the calibration of the PAR sensors and providing insights into methods of satellite validation that could be utilized and would like to thank the entire National Physical Laboratory team for their assistance in this endeavour.

A tremendous thank you to my parents, Dr. Martin Sharp and Patricia Sharp for believing in me and that this path would lead me somewhere eventually. To my friends who, despite not understanding what I do, still encouraged my research and pushed me to the completion of this thesis.

Table of Contents

List of Tables:

List of Figures:

Chapter 1

Thesis Introduction

Background and Study Motivation

Earth is in a state of unprecedented change. As Earth's geologic history continues it officially enters the Anthropocene, an era in which two centuries of industrialization and economic globalization have transformed the face of the Earth (Wright, et al., 2018), including its forests. Continued population growth has forced humans to alter the landscapes in which they reside, resulting in massive-scale deforestation to accommodate the increased demands for energy, food, building materials, medicine, and space, all resources proffered by forests (Ghazoul, et al., 2015; Hosonuma et al., 2012; Ramsfield, et al., 2016; Temperli, et al., 2012). In a world defined by the utilization of its finite resources, it is impossible to continually extract resources from those forests that remain without repercussions to the balance of Earth's biogeochemical cycles, forest health, biodiversity, carbon sequestration capacity, and other ecosystem goods and services (Chave et al., 2014; Foley et al., 2007; Temperli et al., 2012; Zelazowski, et al., 2011). Of the remaining 3.9 billion ha of forest in 2015, 1.7 billion hectares or approximately 44% contained tropical forests while subtropical forests comprised an additional 316 million ha or 8% bringing tropical and sub-tropical forests to a total of 52% of the world's forests (FAO, 2015a, 2015b). Comprising the remaining tropical forests, approximately 37% are primary, with 57% resulting from secondary-growth indicating that these forests are typically younger, are capable of greater amounts of carbon sequestration and net primary productivity than primary forests (Drake, Davis, Raetz, & Delucia, 2011; Gower, McMurtrie, & Murty, 1996). Of the tropical and subtropical forests currently existing, approximately 22% and 85% of these forests are under a forest management plan leaving approximately 1.4 billion hectares of tropical and subtropical forest without a forest management plan (FAO, 2015a, 2015b). This massive extent of forest that has been left unmanaged is very vulnerable to exploitation and deforestation, which could prove devastating for those 1.6 billion people who rely on forests for their livelihoods and the subsequent 7.7 billion people who inadvertently rely on these forests to provide climate stability (Canadell & Raupach, 2008).

One of these original deforestation fronts occurred in Central America during colonization, specifically along the dry Pacific coast where land use policy and migration drove

the development of agricultural and ranch lands (Calvo-Alvarado, et al., 2009; Sánchez-Azofeifa et al., 2005). Due to this early agricultural development, deforestation rates of the Tropical Dry Forests (TDFs) found along the Pacific coast of Central America have decreased or stagnated (FAO, 2015a, 2015b), and in some cases like in Costa Rica, afforestation is occurring (Calvo-Alvarado, et al., 2009). In these regions where deforestation is still occurring and afforestation is starting to progress, the development of secondary growth forests is critical to replacing the significant loss of carbon sinks, habitat, and ecosystem goods and services necessary for the continued productivity of local communities.

Currently, climate change is destabilizing previously predictable precipitation patterns, temperatures and increasing the intensity and frequency of extreme weather events across the globe (Ramsfield et al., 2016; Seneviratne, et al., 2014; Trenberth, et al., 2015). The interplay between forests, forest land-cover extent and the atmosphere can moderate or exacerbate the intensity and extent of extreme weather patterns, as afforestation or deforestation can alter local precipitation patterns by strengthening or weakening land-atmosphere heat and moisture flux exchanges via changes in the amount of evapotranspiration and shading that occurs (Cao & Sanchez-Azofeifa, 2017; Power et al., 2016). This is especially true for the regions where TDFs exist, which already undergo 3-6 month-long seasonal droughts that limit the productivity of these regions (Kalacska, et al., 2005; Poulter, et al., 2009; Souza et al., 2016). Unfortunately, little is understood about the dynamics of deforestation, afforestation, regeneration and succession of TDFs as they are a highly underrepresented ecosystem in the scientific literature in comparison to tropical moist forests, leaving them as a convoluting parameter in our understanding of the resilience and productivity for the regions in which TDFs exist (Pineda-García, et al., 2012; Power et al., 2016). Understanding that all future tropical dry forest growth and expansion in the Neotropics will be a result of secondary succession, forest managers and policy-makers require new tools to evaluate the health, productivity and performance of these tropical dry forests to develop forest management plans that can efficiently regenerate sustainable forests, providing new carbon sinks and habitats to sustain the world's biodiversity.

With the increasing ubiquity of environmental sensors and their decreased costs, a whole host of new environmental data collection techniques are now available to forest researchers, managers, and policy makers permitting the investigation of ecosystem responses to human and

environmental disturbances. As extreme weather events become more frequent and the challenges of climate change become more prevalent, it is necessary to have real-time information to make informed decisions to manage regional ecosystem health and functionality. Thus far, satellite imagery and remote sensing techniques have been the most widely used tools for mapping forest extent, structure, and the long-term dynamics occurring within these forests (FAO, 2015a; Jensen, 1986; Zhang et al., 2003). While these satellite remote sensing tools have become more powerful as the technology progresses, they are still plagued by some perpetual problems such as atmospheric interference and cloud cover; which limit the availability and quality of data, or which require extensive ground validation campaigns to ensure the validity of algorithms and biophysical products extracted from complex post-processing of satellite imagery (Steinberg & Goetz, 2008; Yan et al., 2016). This inevitably leads to satellite remote sensing being unreliable for providing near real-time information. The advantages of using satellite remote sensing data come from the spatial resolution they offer, which permits for the large-scale monitoring of forests. However, the temporal unreliability of satellite imagery calls into question the ability of these satellite platforms to capture important phenological events (Ryu, et al., 2014), extreme weather events (Wang & D'Sa, 2010), diseases or insect infestation (Rullan-Silva, et al., 2013), or even subtle changes in forest productivity. Sporadic or short-term events can have significant effects on ecosystem productivity and are typically linked with effects caused by climate change, therefore these events are expected to increase in frequency and severity as climate change continues to accelerate. The frequency of these events is currently hard to know as the temporal limitations of satellite imagery restrict the ability to observe, in enough detail, the quantitative effects on forest ecosystem services (Martínez & Gilabert, 2009). Additionally, changes in forest productivity can occur over seasonal, multi-year, or even decadal time-periods, making it necessary to record forest productivity in conjunction with meteorological variables at a high temporal frequency to detect significant trends in seasonal phenology in response to climatic and weather events (Martínez & Gilabert, 2009; Verbesselt, et al., 2010). This is especially true of TDFs, which, are especially sensitive to precipitation events, due to their inherent drought-responses, making them significant indicator ecosystems for the monitoring of climatic-biosphere interactions in the regions which they exist.

One such technology that can work in tandem with satellite imagery to provide the temporal resolution necessary are *in-situ* wireless sensor networks (WSN). Thus far, these

networks of wirelessly communicating data loggers have been underutilized in the study of ecology and Earth Sciences, despite the potential that they hold to overcome some of the major challenges in forest ecophysiology monitoring or ecosystem assessments. The advantages that WSNs provide to overcome these challenges are the ability to provide continuous, automated, reliable observations of processes that occur rapidly or slowly while transmitting critical data in real-time (Putzenlechner, et al., 2019; Sánchez-Azofeifa, et al., 2011; Younis & Akkaya, 2008). While limited by the spatial area which they can cover, WSNs are capable of being replicated over a landscape providing pockets of real-time, highly-resolved data locations acting as anchors for interpolation over larger spatial areas. Due to the adaptability of these networks to attach multiple types of environmental sensors to them, it enables them to monitor different biophysical variables making them very adaptable for forest monitoring and satellite validation purposes. This makes WSNs especially appealing, due to the long-term cost-effectiveness and quick deployment of numerous data loggers that are typically cheaper than other long-term data logging systems that are not capable of being used in larger arrays. For instance, optical light sensors are utilized to detect the radiation plants utilize for photosynthesis, allowing for the estimation of photosynthesis dynamics and the phenology of deciduous forests based on measurements of canopy reflectance and the transmission of sunlight during different seasons. These instruments provide a more detailed and higher-resolution set of data than what is provided by space-borne surface reflectance measurements making them ideal for investigating ecosystem dynamics (Sanchez-Azofeifa et al., 2017). By ensuring that large-scale sensor arrays are employed in the collection of biophysical data, the reliability, and accuracy of these derived products increases, thereby increasing the reliability of satellite-derived biophysical variables to which they are compared. The implementation of wireless sensor systems has not occurred on a large scale, despite the advantages they offer. Therefore, exploring the utility of WSNs for the validation of satellite-derived products and for monitoring forest productivity and phenology is necessary to promote the usefulness of this technology for use in the Earth sciences and ecology.

Specific Hypotheses and Objectives

Having provided some context of the scientific research that has been undertaken in the past, the state of knowledge surrounding remote sensing science, its use in monitoring forest phenology, and the implementation of WSNs for validating satellite data and forest phenology

the purpose of this thesis can be introduced. While WSNs have primarily been experimented with in the deciduous and evergreen forests of the Northern hemisphere, it is necessary to continue to explore whether the same influences and effects that occur in those forests also occur in the forests of the tropics. Therefore, to address some remaining uncertainties and limitations that may remain related to the utilization of these technologies for forest research and management, this thesis evaluates two specific hypotheses:

1. The environmental factors that influence the creation of an *in-situ* fraction of Photosynthetic Active Radiation (fPAR) product, are the same in northern deciduous forests as in tropical deciduous forests. These include testing for how solar zenith angle, wind speed, sky conditions and season affect the creation of an *in-situ* fPAR product.
2. The Moderate Resolution Imaging Spectroradiometer (MODIS) satellite-derived fPAR products are incapable of replicating the phenological time-series created by the *in-situ* wireless sensor network fPAR product. This means that the MODIS fPAR product is incapable of accurately detecting the timing of phenological events, such as green-up, senescence, the timing of maximum photosynthetic productivity, the moment of minimum photosynthetic productivity and the monthly, quarterly, bi-annually, yearly or multi-year phenological cycles that occur.

Goals and Objectives:

a) To evaluate the ability for environmental sensors to be used in a plug-in-play mode without additional calibration and determine if post-deployment calibration is required for an *in-situ* fPAR product to be developed.
b) To evaluate the influence of environmental factors on the creation of an *in-situ* fPAR product, and to properly characterize and limit the influence of these factors to create a product that has less than 10% variability.
c) To assess the ability of the MODIS fPAR products to replicate the *in-situ* fPAR product time-series and predict phenological events that are consistent with those derived using the *in-situ* fPAR product.

Chapter Synopses

Chapter Two: *Characterization of PAR sensors and the in-situ fraction of Photosynthetic Active Radiation (fPAR) product in a tropical dry forest,* evaluates the need for sensor calibration, the effect of external environmental influences, and the sampling sizes necessary to create an *in-situ* 2-flux fPAR product that meets the GCOS 10% variability standard for the Environmental Monitoring Super-site in the TDF of Santa Rosa National Parks', Environmental Monitoring Super-site (SRNP-EMSS) in northwestern Costa Rica. The purpose of this study is to determine if the same factors that influence the creation of an *in-situ* 2-flux fPAR product in a deciduous broadleaf forest from the northern hemisphere, are found to influence the creation of an *in-situ* 2-flux fPAR product for a deciduous broadleaf forest from the tropics. Here, a five-year dataset is used to produce an empirical dataset (>16,000 data points) that includes environmental variables such as, wind speed, solar zenith angle, humidity, temperature, soil moisture, incoming photosynthetic active radiation, and transmitted photosynthetic active radiation, all of which are implemented in testing their relative or absolute effects on the *in-situ* 2-flux fPAR product. These variables are measured at a single location, at 10-minute intervals for the entire five year duration. This chapter tests for how environmental factors change the distribution of an *in-situ* 2-flux fPAR product, test for the minimum wireless sensor network size necessary for the creation of an *in-situ* 2-flux fPAR product that has less than 10% variability, and determines the significance of these factors in the prediction of 2-flux fPAR. Finally, the chapter demonstrates the implementation of the first known near real-time environmental monitoring sensor network for monitoring the fraction of photosynthetic active radiation in a tropical dry forest.

Chapter Three: *Employing wavelet-transforms and cross-wavelet analysis to validate the MODIS fPAR time-series over a tropical dry forest,* assesses the use of cross-wavelet transforms to compare the green fraction of Photosynthetic Active Radiation time-series developed from an *in-situ* wireless sensor network to those produced by the Moderate Resolution Imaging Spectroradiometer sensors on board the Terra and Aqua satellites. Two methods are used to identify and quantify phenological events that occur within the time-series of each fPAR product. The first is a derivative-based function that extracts the onset of green-up and senescence dates by retrieving the date based on the rate-of-change of the

curvature of the derived-slope, the second uses a univariate wavelet analysis to characterize the time-frequency patterns of an individual fPAR time-series, before conducting cross-wavelet analyses to understand how the univariate wavelets co-vary with each other as a function of time. This chapter evaluates the temporal accuracy of MODIS-derived fPAR products for the detection of green-up, senescence, $fPAR_{max}$ and $fPAR_{min}$ along with their capabilities for detecting weekly, monthly, quarterly, bi-annual, annual, and multi-year phenological patterns that may or may not be detectable within the *in-situ* fPAR product. It is the first study of its kind to use wavelet analysis for testing the capacity of a fraction of Photosynthetic Active Radiation product to detect phenological cycles within a deciduous broadleaf forest, let alone a tropical dry forest. Therefore, this chapter explores the capabilities of using cross-wavelet analysis techniques for the validation of satellite-derived biophysical products with ground-based biophysical products.

Limitations to research projects

The data collected in this thesis being primarily time-series observations which are either short-term, high frequency measurements or aggregated long-term measurements, there are limitations to the analyses that can be performed on the data. The environment in which these electronic data loggers were installed is characterized by high variability in air temperature and humidity, with the result that the loggers are exposed to both hot/dry and hot/wet conditions. As a result, data collection interruptions and data losses occur frequently due to data logger failure, wildlife interference, and power loss which plague the dataset. This makes achieving the conditions for standardizing the creation of a time-series, difficult. Additionally, the data loggers used in the creation of the wireless sensor network are custom made for this application and are regarded as being leading-edge technology with little user input to its design, and scarce environmental testing for performance, subjecting the hardware to greater rates of failure than would be expected for a commercially available product. Pairwise comparisons of Apogee-calibrated and National Physical Laboratory calibrated quantum sensors had to be limited to time-frames in which all data loggers were operational, limiting the amount of data that could be utilized for portions of this study. This is true of the meteorological data employed in this study as well, where temporal synchroneity is necessary to ensure that biases from transient phenomena are minimized. The

remote location of these sites meant that it was expensive and challenging to access these sites, making it impossible to address all technology failures in a timely manner, leading to some equipment failures that persisted for longer than desired. Data availability for the complete time-series used can be reviewed via the University of Alberta's Enviro-net® Cyber-Database.

The choice of study location is due to the availability of locations provided by the University of Alberta's Center for Earth Observation Science ecological remote sensing ground-truthing network, which provides the necessary research infrastructure for long-term deployment of wireless sensor networks and field campaigns. While all study sites within the University of Alberta's Center for Earth Observation Science research network include wireless sensor networks, the tropical dry forest was chosen due to the uniqueness of the biome, which has not been well studied in satellite-validation research.

This is the first study of its kind to monitor tropical dry forest phenology over a multi-year period using the fraction of photosynthetic active radiation biophysical variable. Consequently, this makes this study a baseline reference for future studies that aim to validate satellite-derived fPAR products, or that require a multi-year dataset to separate the long-term trends of vegetation phenology from the natural variability observed inter-seasonally. Each chapter presents a greater in-depth review of the study's limitations.

Final Opening Remarks

The chapters within this thesis highlight the factors that need to be taken into consideration when creating ground-based fraction of Photosynthetic Active Radiation products for tropical deciduous broadleaf forests that can be used for the validation of satellite-derived fPAR products and reveal whether those satellite-derived fPAR products accurately record phenological events. Applying emerging information and communication technologies for the fields of Ecology, Earth Sciences and Forest Productivity has the potential to advance our knowledge of forest ecological processes and provide the ability to predict future threats to ecosystem services that humanity relies upon to survive. This thesis provides an insight into the tools now available that can potentially improve upon the insights of old domains of forestry science, piercing the veil of unknown ecological processes and opening new frontiers in forest productivity monitoring and the remote sensing of forests.

The research conducted in this study is carried out as part of the University of Alberta's Center for Earth Observation Science Environmental Wireless Sensor Network development project, Enviro-Net®, and as part of the TROPI-DRY international collaborative research network whose goals and objectives are to improve our understanding of and ability to conserve, preserve, and expand Neotropical Dry Forests.

Literature Cited:

Calvo-Alvarado, J. C., McLennan, B., Sanchez-Azofeifa, G. A., & Garvin, T. (2009). Deforestation and forest restoration in Guanacaste, Costa Rica: Putting conservation policies in context. *For*, *258*, 931–940. https://doi.org/10.1016/j.foreco.2008.10.035

Calvo-Alvarado, J., McLennan, B., Sánchez-Azofeifa, A., & Garvin, T. (2009). Deforestation and forest restoration in Guanacaste, Costa Rica: Putting conservation policies in context. *Forest Ecology and Management*, *258*(6), 931–940. https://doi.org/10.1016/j.foreco.2008.10.035

Canadell, J. G., & Raupach, M. R. (2008, June 13). Managing forests for climate change mitigation. *Science*, Vol. 320, pp. 1456–1457. https://doi.org/10.1126/science.1155458

Cao, S., & Sanchez-Azofeifa, A. (2017). Modeling seasonal surface temperature variations in secondary tropical dry forests. *International Journal of Applied Earth Observation and Geoinformation*, *62*(October), 122–134. https://doi.org/10.1016/j.jag.2017.06.008

Chave, J., Réjou-Méchain, M., Búrquez, A., Chidumayo, E., Colgan, M. S., Delitti, W. B. C., … Vieilledent, G. (2014). Improved allometric models to estimate the aboveground biomass of tropical trees. *Global Change Biology*, *20*(10), 3177–3190. https://doi.org/10.1111/gcb.12629

Drake, J. E., Davis, S. C., Raetz, L. M., & Delucia, E. H. (2011). Mechanisms of age-related changes in forest production: The influence of physiological and successional changes. *Global Change Biology*, *17*(4), 1522–1535. https://doi.org/10.1111/j.1365-2486.2010.02342.x

FAO. (2015a). Global Forest Resources Assessment 2015. In *FAO Forestry*. https://doi.org/10.1002/2014GB005021

FAO. (2015b). *How are the world's forests changing?* Retrieved from www.fao.org/publications

Foley, J. A., Asner, G. P., Costa, M. H., Coe, M. T., DeFries, R. S., Gibbs, H. K., … Snyder, P. K. (2007). Amazonian revealed: Forest degradation and loss of ecosystem goods and services in the Amazon Basin. *Frontiers in Ecology and the Environment*, *5*(1), 25–32. Retrieved from http://www.jstor.org/stable/20440556

Ghazoul, J., Burivalova, Z., Garcia-Ulloa, J., & King, L. A. (2015, October 1). Conceptualizing Forest Degradation. *Trends in Ecology and Evolution*, Vol. 30, pp. 622–632. https://doi.org/10.1016/j.tree.2015.08.001

Gower, S. T., McMurtrie, R. E., & Murty, D. (1996). Aboveground net primary production

decline with stand age: Potential causes. *Trends in Ecology and Evolution*, Vol. 11, pp. 378–382. https://doi.org/10.1016/0169-5347(96)10042-2

Hosonuma, N., Herold, M., De Sy, V., De Fries, R. S., Brockhaus, M., Verchot, L., … Romijn, E. (2012, December 1). An assessment of deforestation and forest degradation drivers in developing countries. *Environmental Research Letters*, Vol. 7, p. 044009. https://doi.org/10.1088/1748-9326/7/4/044009

Jensen, J. R. (1986). *Original Title: Introductory Digital Image Processing (Prentice Hall Series in Geographic Information Science) Introductory Digital Image Processing*.

Kalacska, M. E. R., Sanchez-Azofeifa, G. a, & … J. C. C.-. (2005). Effects of Season and Successional Stage on Leaf Area Index and Spectral Vegetation Indices in Three …. *Biotropica*, *37*(4), 486–496. Retrieved from http://www.ingentaconnect.com/content/bsc/btp/2005/00000037/00000004/art00002

Martínez, B., & Gilabert, M. A. (2009). Vegetation dynamics from NDVI time series analysis using the wavelet transform. *Remote Sensing of Environment*, *113*(9), 1823–1842. https://doi.org/10.1016/j.rse.2009.04.016

Pineda-García, F., Paz, H., & Meinzer, F. C. (2012). *Drought resistance in early and late secondary successional species from a tropical dry forest: the interplay between xylem resistance to embolism, sapwood water storage and leaf sheddingp ce_2582 405..418*. https://doi.org/10.1111/j.1365-3040.2012.02582.x

Poulter, B., Heyder, U., & Cramer, W. (2009). Modeling the sensitivity of the seasonal cycle of GPP to dynamic LAI and soil depths in tropical rainforests. *Ecosystems*, *12*(4), 517–533. https://doi.org/10.1007/s10021-009-9238-4

Power, M. J., Whitney, B. S., Mayle, F. E., Neves, D. M., de Boer, E. J., & Maclean, K. S. (2016). Fire, climate and vegetation linkages in the bolivian chiquitano seasonally dry tropical forest. *Philosophical Transactions of the Royal Society B: Biological Sciences*, *371*(1696). https://doi.org/10.1098/rstb.2015.0165

Putzenlechner, B., Marzahn, P., Kiese, R., Ludwig, R., & Sanchez-Azofeifa, A. (2019). Assessing the variability and uncertainty of two-flux FAPAR measurements in a conifer-dominated forest. *Agricultural and Forest Meteorology*, *264*(October 2018), 149–163. https://doi.org/10.1016/j.agrformet.2018.10.007

Ramsfield, T. D., Bentz, B. J., Faccoli, M., Jactel, H., & Brockerhoff, E. G. (2016). Forest health in a changing world: Effects of globalization and climate change on forest insect and pathogen impacts. *Forestry*, *89*(3), 245–252. https://doi.org/10.1093/forestry/cpw018

Rullan-Silva, C. D., Olthoff, A. E., Delgado de la Mata, J. A., & Pajares-Alonso, J. A. (2013). Remote monitoring of forest insect defoliation. A review. *Forest Systems*, *22*(3), 377–391. https://doi.org/10.5424/fs/2013223-04417

Ryu, Y., Lee, G., Jeon, S., Song, Y., & Kimm, H. (2014). Monitoring multi-layer canopy spring phenology of temperate deciduous and evergreen forests using low-cost spectral sensors. *Remote Sensing of Environment*. https://doi.org/10.1016/j.rse.2014.04.015

Sanchez-Azofeifa, A., Antonio Guzmán, J., Campos, C. A., Castro, S., Garcia-Millan, V.,

Nightingale, J., & Rankine, C. (2017). Twenty-first century remote sensing technologies are revolutionizing the study of tropical forests. *Biotropica*, Vol. 49, pp. 604–619. https://doi.org/10.1111/btp.12454

Sánchez-Azofeifa, G. A., Quesada, M., Rodríguez, J. P., Nassar, J. M., Stoner, K. E., Castillo, A., … Cuevas-Reyes, P. (2005). Research priorities for neotropical dry forests. *Biotropica*, *37*(4), 477–485. https://doi.org/10.1111/j.1744-7429.2005.00066.x

Sánchez-Azofeifa, G. A., Rankine, C., Do Espirito Santo, M. M., Fatland, R., & Garcia, M. (2011). Wireless sensing networks for environmental monitoring: Two case studies from tropical forests. *Proceedings - 2011 7th IEEE International Conference on EScience, EScience 2011*, (December 2011), 70–76. https://doi.org/10.1109/eScience.2011.18

Seneviratne, S. I., Donat, M. G., Mueller, B., & Alexander, L. V. (2014). No pause in the increase of hot temperature extremes. *Nature Climate Change*, *4*(3), 161–163. https://doi.org/10.1038/nclimate2145

Souza, R., Feng, X., Antonino, A., Montenegro, S., Souza, E., & Porporato, A. (2016). Vegetation response to rainfall seasonality and interannual variability in tropical dry forests. *Hydrological Processes*, *30*(20), 3583–3595. https://doi.org/10.1002/hyp.10953

Steinberg, D. C., & Goetz, S. (2008). Assessment and extension of the MODIS FPAR products in temperate forests of the eastern United States. *International Journal of Remote Sensing*, *30*(1), 169–187. https://doi.org/10.1080/01431160802244276

Temperli, C., Bugmann, H., & Elkin, C. (2012). Adaptive management for competing forest goods and services under climate change. *Ecological Applications*, *22*(8), 2065–2077. https://doi.org/10.1890/12-0210.1

Trenberth, K. E., Fasullo, J. T., & Shepherd, T. G. (2015, July 24). Attribution of climate extreme events. *Nature Climate Change*, Vol. 5, pp. 725–730. https://doi.org/10.1038/nclimate2657

Verbesselt, J., Hyndman, R., Newnham, G., & Culvenor, D. (2010). Detecting trend and seasonal changes in satellite image time series. *Remote Sensing of Environment*, *114*(1), 106–115. https://doi.org/10.1016/j.rse.2009.08.014

Wang, F., & D'Sa, E. J. (2010). Potential of MODIS EVI in identifying hurricane disturbance to coastal vegetation in the Northern Gulf of Mexico. *Remote Sensing*, *2*(1), 1–18. https://doi.org/10.3390/rs2010001

Wright, C., Nyberg, D., Rickards, L., & Freund, J. (2018, July 1). Organizing in the Anthropocene. *Organization*, Vol. 25, pp. 455–471. https://doi.org/10.1177/1350508418779649

Yan, K., Park, T., Yan, G., Liu, Z., Yang, B., Chen, C., … Myneni, R. B. (2016). Evaluation of MODIS LAI/FPAR product collection 6. Part 1: Consistency and Improvements. *Remote Sensing*, *8*(6), 1–16. https://doi.org/10.3390/rs8060460

Younis, M., & Akkaya, K. (2008). Strategies and techniques for node placement in wireless sensor networks: A survey. *Ad Hoc Networks*, *6*(4), 621–655. https://doi.org/10.1016/J.ADHOC.2007.05.003

Zelazowski, P., Malhi, Y., Huntingford, C., Sitch, S., & Fisher, J. B. (2011). Changes in the potential distribution of humid tropical forests on a warmer planet. *Philosophical Transactions of the Royal Society A: Mathematical, Physical and Engineering Sciences*, *369*(1934), 137–160. https://doi.org/10.1098/rsta.2010.0238

Zhang, X., Friedl, M. A., Schaaf, C. B., Strahler, A. H., Hodges, J. C. F., Gao, F., … Huete, A. (2003). Monitoring vegetation phenology using MODIS. *Remote Sensing of Environment*. https://doi.org/10.1016/S0034-4257(02)00135-9

Chapter 2: Characterization of PAR sensors and the *in-situ* fraction of Photosynthetic Active Radiation (fPAR) product in a tropical dry forest.

Abstract:

The fraction of Photosyntethic Active Radiation (fPAR) attempts to quantify the amount of Photosynthetic Active Radiation that is absorbed by vegetation for use in photosynthesis. Despite the importance of fPAR, there has been little research into how fPAR may change with biome and latitude, or the extent of ground networks required to validate satellite observations. This study provides the first attempt to quantify the uncertainties related to *in-situ* 2-flux fPAR estimations within a tropical dry forest. Using the Wireless Sensor Network (WSN) found at the Santa Rosa Natioanl Park Environmental Monitoring super-site this study analyzes the response of 2-flux fPAR to seasonal, environmental, and meteorological influences over five years (2013-2017). Using statisitical tests on the distribution of fPAR measurements throughout the days and seasons based on the sky condition, solar zenith angle and wind speed, we determine which conditions reduce variability, and their relative impact on fPAR estimation. Additionally, using a Generalized Linear Mixed Effects Model, we determine the relative impact of the factors above, as well as soil moisture on the prediction of fPAR.

Our findings suggest that similar to other broadleaf deciduous forests diffuse light conditions and low wind patterns reduce variability in fPAR. Additionally, calibration methodology does not significantly change the fPAR measurements, and a network of at least eight sensors is required to characterize the variability in the tropical dry forest. Finally, we found that soil moisture is a significant predictor of the distribution and magnitude of fPAR, and particularly impacts the onset of senescence for tropical dry forests.

Additional keywords: fPAR, tropical-dry forests, liana, soil moisture, wind speed, solar zenith angle, sky conditions, wireless sensor networks, spatial distribution.

1.0 - Introduction:

One of the prominent fields in the remote sensing community is monitoring forest productivity and its changes over time in response to disturbances and climate change (McDowell et al., 2015). Since 1996, one method has been to measure the fraction of Phosynthetically Active radiation (fPAR) which has been defined in many ways; however, fPAR has consistently been

considered a useful biophysical product in quantifying the amount of Photosynthetic Active Radiation (PAR; 400-700nm) absorbed for photosynthesis by vegetation (Chen, 1996; Claverie et al., 2013; Gobron et al., 2006a; Gower, et al., 1999; Knyazikhin, et al., 1998; Li & Fang, 2015; Myneni et al., 1999; Myneni, 1997; Thomas et al., 2006; Widlowski, 2010). As research into fPAR continues, it has been recognized as an essential variable for monitoring forest and ecosystem health and productivity, being declared as such by both the Global Climate Observation System (GCOS) and Global Terrestrial Observation System (GTOS).

Due to its status, many partners and leaders in the remote sensing community have integrated fPAR products into the suite of biophysical products produced by its satellites. This proliferation of satellite-derived fPAR products, such as those from the Moderate Resolution Imaging Spectroradiometer (MODIS) run by NASA (Myneni et al., 1999), creates a need for these products to undergo a validation process (Nightingale, et al., 2011). The validation of satellite-derived products can be determined at a local level either through direct measurements (Carrara et al., 2018; D'Odorico et al., 2014; Majasalmi, 2015; Majasalmi, Stenberg, & Rautiainen, 2017; Nestola et al., 2017a; Putzenlechner, Marzahn, Kiese, Ludwig, & Sanchez-Azofeifa, 2019; Senna, 2005; Widlowski, 2010) or through derivations from a radiative transfer model (Disney, et al., 2000; Stenberg, et al., 2016; Thomas et al., 2006; Van der Zande, et al., 2010).

The challenges facing the remote sensing community are related to scale, as forests can cover many hundreds or thousands of kilometers, but also includes limitations in the technology available. Direct methods usually result in large, costly, and technical experimental field setups (Gobron et al., 2006; Nestola et al., 2017; Putzenlechner, et al., 2019; Senna, 2005; Steinberg, et al., 2006) while, indirect methods in general use the gap fractions retrieved from hemispherical photographs (Wenjuan Li et al., 2015) which in turn relate the leaf are index (LAI) to fPAR (Fensholt, et al., 2004; Pinty et al., 2011). Consequently, modeling approaches have become more common due to financial and time constraints (Ahl et al., 2006; Li & Fang, 2015; Myneni, 1997; Pickett-Heaps et al., 2014; Zhang, et al., 2017). These studies have acknowledged the complexities of light environments, especially in forests which exhibit a high degree of spatial heterogeneity (Gu et al., 2002; Leuchner, Hertel, & Menzel, 2011; Shabanov et al., 2003; Thomas et al., 2006); however these experimental methods are dependent on radiation

measurements from a few sensors and neglect the uncertainty of the light fields they are measuring (D'Odorico et al., 2014).

Scientific bodies, such as the CEOS-LPV sub-group, have therefore called for the expansion and diversification of in-situ calibration and validation sites, to provide a robust and globally representative quality assured product (Nightingale et al., 2011). Subsequently, these scientific bodies have also called for the establishment of standardized protocols for the measurement and reporting of uncertainties for *in-situ* fPAR products. In turn, this will raise the profile of fPAR, as higher quality products can be produced from these validation results, as outlined by the CEOS-LPV validation hierarchy (Table 2-2, (Nightingale et al., 2011)). To date, there have been no sites used to quantify the uncertainty of fPAR in the Tropical Dry Forest, a biome which accounts for 40% of tropical ecosystems (D. H. Janzen, 1988; Portillo-Quintero & Sánchez-Azofeifa, 2010; G. Arturo Sánchez-Azofeifa et al., 2005). Given the extensive nature of this biome, its extremely heterogenous nature, quantifying and validating fPAR in this biome is crucial.

In response to an increasing need for standardization in validation methodologies, the definitions and methodologies of measuring fPAR will replicate the methods and definitions presented by Widlowski, (2010), furthered by Nestola et al. (2017) and Putzenlechner et al., (2019). Of the different definitions of fPAR that Widlowski (2010) tested, his study determined that the 2-flux fPAR formula was the most invariant of the *in-situ* fPAR fluxes. Both Nestola et al. (2017) and Putzenlechner, et al., (2019) utilized a 2-flux fPAR product but expanded the scale of the experiment, both temporally and spatially. These studies illustrated how a Wireless Sensor Network (WSN) composed of data loggers (or nodes) and equipped with environmental sensors capable of sampling and storing understorey micrometeorological data can be utilized in the analysis of fPAR (Nestola et al., 2017; Putzenlechner et al., 2019). The use of an expansive network of data loggers permits the observation of the uncertainty and variability in the understorey of heterogenous forests at the minute-scale to the multi-year scale (Pastorello, et al., 2011; Rawat, et al., 2014; Sanchez-Azofeifa et al., 2017; Sanchez-Azofeifa, et al., 2011).

As a result, this study employs a WSN in its study of 2-flux fPAR in the Tropical Dry Forest of Santa Rosa National Park. We will investigate the spatial, temporal, and environmental factors

that cause variability in the *in-situ* 2-flux fPAR product within a TDF, focusing on the following questions:

1. Is it necessary to recalibrate Apogee SQ-110 PAR sensors before deploying them in the field?
2. How much does solar zenith angle influence the measurement of *in-situ* 2-flux fPAR in a TDF site?
3. What is the influence of sky conditions (cloudy, mix of sun and clouds, or clear) on the measurement of *in-situ* 2-flux fPAR in a TDF site?
4. Is there an ideal number of nodes within a WSN needed to create a robust *in-situ* 2-flux fPAR product that can meet the standards outlined by the GCOS (2011)?
5. Are there other meteorological or environmental variables that influence the estimation of *in-situ* 2-flux fPAR?

2.0 Materials and Methods:

2.1 *Study Site*

This study was conducted at the Santa Rosa National Park Environmental Monitoring Super-site (SRNP-EMSS) located in Guanacaste, Costa Rica (Figure 2-1). Santa Rosa is considered a transitional tropical dry-forest to tropical moist forest that experiences ranges of precipitation from 900-2500mm per year, of which most arrives in a 6 month period (June – December) giving a distinct wet-dry seasonal cycle to the area permitting average temperatures ≥ 25°C (G. Sánchez-Azofeifa et al., 2005). The uplands of the park host a mosaic of secondary tropical dry forest (TDF) which are in various stages of forest succession, which include just as varied histories of anthropogenic land use (Janzen, 2000; Janzen & Hallwachs, 2016; M. Kalacska et al., 2004). These areas of forest succession can be characterized by the species composition found within the forest, the species richness, tree height, and by their leaf area index (Kalácska, et al., 2004; Kalácska, et al., 2004; Sánchez-Azofeifa et al., 2017). An updated map and classification of these forest age stands in the SRNP-EMSS can be found in Li, et al., (2017) and as such the wireless sensor network (WSN) sites will be classified in accordance with this forest age classification map.

In June 2018, a forestry inventory was conducted for the 1ha plot surrounding the WSN (Figure 2-1) to determine the species, diameter at breast height (DBH), and tree height within the WSN. The area of the WSN itself is a 75x65m (4875m^2) area containing a total of 48 subplots that measured 10x10m (100m^2). From those 48 subplots a total of 307 stems were counted from 39 different species, with an average DBH of 0.131m, and an estimated average tree height of 9m. The forest inventory for the entire hectare resulted in a basal area of 445m^2 ha^{-1} and 1200 stems ha^{-1}, with basal area per subplot, within the WSN, ranging from 124.6m^2 ha^{-1} to 714.2m^2 ha^{-1}. Of the 39 species found within the footprint of the WSN, *Guazuma ulmifolia*, *Luehea speciosa*, and *Lueahea candida* accounted for 18%, 11% and 8% of the total stems respectively. Included in the inventory was a count for the number of lianas, which totaled 9 individuals with 5 of the 9 individuals clustered together in an 30x30m (900m^2) subsection located between nodes 1, 2, 3, 10 and 12 (Figures 2-8/2-9). All species found within the WSN were classified as deciduous broadleaf trees, exhibiting seasonal leaf loss during the dry-season or senescence period.

2.2 Instrumentation

For this study, the network with the longest and most complete record was selected, with data from 2013-2017 being analyzed. Collectively, there are 13 self-powered nodes in the network (model ENV-Link-Mini-LXRS, Lord Microstrain, Cary, NC, USA). Each node is equipped with a temperature and relative humidity sensor, along with a soil moisture and quantum PAR sensor (model SQ-110, Apogee, Logan, UT, USA, field of view 180°) mounted 1.3m from the forest floor. The PAR sensors measure PAR (µE) that is transmitted (tPAR) from the atmosphere through the canopy and into the understory. As per the manufacturer, PAR sensors have uncertainty estimates as follows: cosine response +/- 5% at 75° solar zenith angle (SZA), temperature response 0.06 +/- 0.06% per °C, calibration uncertainty +/- 5% and non-stability <2%/year. Establishing the reliability of these sensors is crucial, as noted by researchers such as Akitsu, et al., (2017) who compared the measurements from the Apogee SQ-110 PAR sensors to a reference standard and found a difference of -7.7 x 10^{-4} an accuracy well within the 10% threshold set by GCOS, (2011).

Locations, and the distribution of nodes within the network was chosen based on the following criteria: a) nodes were installed >80m from the edge of forests as to avoid the edge and

disturbance effects from roads/trails, b) due to its proximity (< 200m) to a meteorological tower and c) it was possible for the network to encompass a domain of interest larger than 30m x 30m (Widlowski, 2010) which is necessary to minimize the horizontal fluxes captured by multiple sensors, which creates an unacceptably high bias for two-flux fPAR. A star-like (Figure 2-1) arrangement of nodes within the network was chosen to: a) maximize the area covered by the nodes, b) to prevent the formation of gaps between sensors resulting in the incomplete characterization of the overhead canopy, and c) to guarantee wireless sensor connectivity across the network (Putzenlechner et al., 2018; Rankine, 2016; Sánchez-Azofeifa, et al., 2011; Younis & Akkaya, 2008). These formations have also been found to be less influenced by solar zenith angle (*SZA*) when compared with other sampling schemes (Widlowski, 2010).

Furthermore, a companion meteorological tower is located within 200m of all the nodes in the network (Figure 1). This tower is equipped with SQ-110 quantum PAR sensors mounted at 30m from the ground, measuring the incoming PAR (iPAR) from the atmosphere, and the total reflected PAR (rPAR) coming from the soil, leaf litter, and canopy back into the atmosphere, a necessary measurement for 3-flux fPAR (Table 2-1). An Onset Hobo Data logger accompanies the PAR sensors at the top of the tower, which measures wind speed, gust speed, wind direction, air temperature, relative humidity, barometric pressure, incoming net radiation and reflected net radiation. Sampling is set at a 2-second interval which are aggregated to a 30-minutes mean value. These observations are then wirelessly transmitted via satellite to Enviro-net.org©.

2.3 Calibration of PAR sensors

An 8-month experiment was conducted to determine the need for standardized calibration, or for the recalibration of PAR sensors in experimental setups. The experiment paired six National Physical Laboratory (NPL, Teddington, UK) calibrated SQ-110 PAR sensors with six manufacturer calibrated SQ-110 PAR sensors. Of these six sensors, only 5 acquired sufficient data for comparison. Measurements between the two calivrated sensors, after their respective calibration coefficients were applied, were compared 1:1 to assess their similarity. If these measurements agree with the stated uncertainties, they can be considered compliant.

Apogee compares its sensors to the LiCOR 1800-02 Optical Radiation Calibrator (*Apogee Quantum Sensor Calibration Certificate*, 2019; *QUANTUM SENSOR Models SQ-100 and SQ-300 Series (including SS models)*, 2019), for calibration. Apogee compares a suite of SQ-110

sensors against several reference sensors to derive a calibration coefficient (and uncertainty) which is applied for all SQ-100 sensors (*QUANTUM SENSOR Models SQ-100 and SQ-300 Series (including SS models)*, 2019). This means that each sensor does not come with its own calibration coefficient, and it is unclear whether this calibration coefficient is monitored between different batches of sensors. Likewise, since the SQ-110 spectral response differs significantly from the reference sensor, there may be large spectral errors associated with looking at different targets to that used in the original calibration (sky conditions).

The calibration procedure at the NPL is split into two parts: a broadband absolute calibration and a spectral responsivity calculation. The absolute calibration involves recording the voltage output of the Apogee SQ-110s when illuminated by a calibrated irradiance source allowing for the derivation of the calibration coefficient. The lamp is set to the same voltage and current under which it was calibrated, and the sensor is placed at the same calibration distance (0.5 m). For PAR, which generally uses quantum units, a conversion is required which accounts for the spectral irradiance and the spectral response function of the PAR sensor. This is required because the energy of a single photon is dependent on its wavelength.

The uncertainty associated with the calibration coefficient is calculated by propagating the input uncertainties (e.g. dark current, alignment, etc.) through the calibration equation using the law of propagation of uncertainties (JCGM, 2008). Field operation (such as differences between the calibration source and illumination conditions) uncertainties are not accounted for in calibration.

2.4 Data processing

In processing fPAR data, it is necessary to filter out all the time-steps where tPAR > iPAR as this phenomenon is theorized to be caused by clouds passing overhead the iPAR but not the rPAR sensors. *SZA* and air temperature corrections were applied to the PAR values, as these corrections can adjust values by up to 0.06 ± 0.06% per °C departed from 20°C and by -5% for *SZA* > 75°.

For this study, 2-flux fPAR was calculated using:

$$2 - flux\ fPAR = 1 - \frac{tPAR}{iPAR} \qquad (1)$$

Where tPAR is the PAR transmitted through the canopy into the understory, and iPAR is the incident PAR from the tower. This version of fPAR was chosen because it is robust and offers a low degree of variability, especially for in-situ and WSN analyses (Putzenlechner et al., 2019; Widlowski, 2010). The 2-flux fPAR was calculated for every node, every 10 minutes during daylights hours. The nodes were synchronized using time-stamps and then averaged to create a single network-wide 2-flux fPAR product (2-flux $fPAR_{Domain}$).

To conduct analysis on the effects of illumination conditions, fPAR was divided by sky conditions, which were classified as clear (CS), mixed (MS), or diffuse (DS) based on the cleark-sky calculator developed by Walter et al., (2002). Sky conditions are therefore categorized as diffuse when iPAR < 900µE, mixed when 900µE < iPAR < 1100µE, and clear when iPAR > 1100µE. This characterization was necessary due to the absence of sunshine pyranometers. These sensors allow for the determination of diffuse-to-total incident radiation, a metric used by other studies (Wenjuan Li & Fang, 2015; Putzenlechner et al., 2019; Widlowski, 2010).

To avoid the confounding effects of season in the analyses, the data was also divided into three phenophases. The transitional phenophases (green-up and senescence) encompass large ranges of fPAR (0.01 – 0.85) while maturity remains more stable (0.7 – 0.99). Phenophases for this study were determined using a threshold method, which takes the first derivative of the time-series and sets a threshold based on the rate-of-change for the curvature of the time-series. When the rate-of-change increases beyond a certain rate, the threshold is breached and until the rate-of-change slows breaking the threshold again, data taken within those periods is determined to be part of the corresponding phenophase (Doktor, et al., 2009; Lange & Doktor, 2017; Zhang et al., 2003). This resulted in a time-series (2013-2017) that has six senescence (n = 4548), five green-up (n = 1331) and five maturity (n = 9711) phases in total (Figure 2-2).

All PAR and meteorological data was acquired from the website Enviro-net.org run by the Center of Earth Observation Sciences at the University of Alberta (https://enviro-net.org/). Further processing and analysis of data was done in the statistical software R (https://cran.r-project/org/). Within R the *SZA* were calculated for the coordinates overtop of the network location using the package “insol” (https://meteoexploration.com/R/insol/index.html).

2.5 Data analysis

When working with the fPAR fluxes, the fluxes represented non-parametric probability distributions which was determined using the kurtosis and skewness of each phenophase. As such, it was decided that analyzing the differences in distributions caused by external factors such as wind speed (*WS*), solar zenith angle (*SZA*), and sky conditions (*SC*) should be conducted by employing Kolmogorov-Smirnov (KS) and Mann-Whitney (MW) tests. KS tests were used for determining the normality of each distribution. Once determined non-normal, the KS test was used to compare the cumulative probability distributions against one another for significant ($p < 0.05$) differences. MW tests were utilized for determining if the central tendencies of two distributions were detectably different ($p < 0.05$) and were reported with a *Cliff's d* effect size (Cliff, 1993) to contextualize if detected differences were meaningful. Each set of distributions was subjected to different selection schemes, to isolate variables under examination and determine these individual variables effects (Table 2-3).

To ensure that the study captures the effects of the external forces, instead of internal or sampling sources, spatio-temporal variability of fPAR needs to be tested. Individual nodes fPAR were tested against the domain-level fPAR using the non-parametric KS and MW tests to test for differences in the central tendencies and distributions ($p < 0.05$). Inherently, these tests also permitted the testing for the optimal number of sensors required to capture the spatial variability of 2-flux $fPAR_{Domain}$ and eliminate the "sampling bias" of fPAR (Widlowski, 2010) per phenophase. To determine the optimal number of sensors, the coefficient of variation (CV) is calculated for different nunbers and spatial configurations of sensors (Putzenlechner, et al., 2019). Additionally, to test for the effects of external factors on the variation of fPAR within a network, CVs were calculated using different *SZA,* sky conditions, and wind-speeds for each phenophase, therefore determining the number of sensors necessary to build fPAR products with a maximum CV < 10% and the environmental filters necessary for meeting the GCOS standards (Table 2-3).

To characterize the spatial variability of fPAR across the network, simple kriging was employed between each node within the network. Simple Kriging assumes that the univariate data (2-flux fPAR) is stationary (Li & Heap, 2014). The fPAR of each node was averaged across 8-day periods, selected to coincide with the Moderate resolution Imaging Spectroradiometer (MODIS)

satellite product time-frames, for the periods of 2013– 2017 (n = 225). To determine if patterns of spatial autocorrelation were occurring the Moran I statistic (Moran, 1950) for all time periods was calculated. Results from the spatial autocorrelation were split into the phenophase which they belonged (Figure 2-2) with the semi-variogram (Figure 2-11).

Finally, to test if the external factors selected in this study had an impact on 2-flux $fPAR_{Domain}$ two General Linear Mixed Equation (GLME) models were tested, one using only the external factors selected, the other including soil moisture measurements. The impact of soil moisture was tested because TDF's are water-limited ecosystems with green-up occurring after the first precipitation events (Chadwick, et al., 2016; Kalácksa, et al., (2005); Zelazowski, et al., 2011). Therefore, these models tested the relative contribution of each external factor in the presence and absence of the site-limiting factor, for each phenophase. A stepwise logistic regression was applied for several reasons, a) it can be applied to restrictive ranges such as those found in 2-flux $fPAR_{Domain}$ ($0 \leq fPAR \leq 1$) (Wang, 2006), and b) it permits the study to find the best fitting model for each phenophase by employing the minimum Akaike information criterion (AIC).

3.0 – Results

3.1 Sensor calibration and network variability

When comparing between the uncalibrated and calibrated PAR sensors, employing all available data, 4 of 5 sensor pairs had high correlations ($R^2 > 0.89$, Figure 2-3). Node 5 demonstrated the largest degree of variance between the calibrated and uncalibrated sensors, which is especially prevalent during senescence when PAR > 1200 (μE) (RMSE ~30% larger than estimates during green-up or maturity, Appendix B, Figure 2-1). Some of this variance can be attributed to the fact that more than 60% of measurements were taken under clear-sky conditions compared with measurements the 21% during green-up or 36% during maturity. Measurements taken under clear-sky conditions have a variance (*RMSE* = 206.3, Appendix B, Figure 2-2) quadruple that of measurements taken under mixed-sky (*RMSE* = 74.8, Appendix B Figure 2-3) or diffuse-sky conditions (*RMSE* = 56.2, Appendix B Figure 2-4). Of the 5 sensor pairs tested, 3 of the 5 NPL calibrated sensors under-estimated measurements compared with the manufacturer-calibrated sensors. (Appendix B, Figure 2-3).

Filters were implemented in conjunction with an increase in the number of sensors employed to determine both the spatial variability of the site and the best environmental filters to use within each phenophase to achieve a minimum variance. During green-up (Appendix B, Figure 2-7a) filtering to only use data taken during diffuse sky conditions reduced variation by 7% between the use of two and thirteen sensors. The next best filter, $SZA < 27°$, only decreases it by 2%. Compare this to maturity, where filtering for diffuse skies reduces variability by 3%, but using a combination of $27° < SZA < 60°$ & $WS < 3$m/s (Appendix B, Figure 2-7b) reduces variability by 4%. However, regardless of the phenophase the one filter that works best is the $27° < SZA < 60°$, reducing the variability by 9%, 3.2% and 8% during green-up, maturity, and senescence, respectively (Appendix B, Figure 2-7). This filter is also the most dependable to use, regardless of the size of network employed as it will reduce the variability in networks with 7 or fewer sensors by 3.2% and by 7.3% for networks using all 13 sensors.

Each phenophase has its own magnitude of variation to deal with, resulting in a different number of nodes necessary to characterize the spatial variability occurring. For the transitional phenophases (green-up and senescence) it takes up to 7-8 sensors before the rate of change in the coefficient of variation is reduced to < 0.5% per additional sensor; while, during maturity, only 3 sensors were required to reduce the rate of change in the coefficient of variation < 0.5% per additional sensor. Despite the incremental rate of change, 8+ sensors were required to reduce the variation to < 10% during maturity, the acceptable range as dictated by the GCOS (2011). Therefore, at least 8 sensors are necessary to properly characterize the spatial variability of 2-flux $fPAR_{Domain}$ at this site.

Determining the spatial variability of 2-flux $fPAR_{Domain}$ within the network entails understanding if spatial autocorrelation is occurring within the network. For 228 8-day aggregated periods, a total of 16 periods were identified as having high degrees of spatial autocorrelation, 10 during senescence ($p < 0.05$, Figure 2-9) and 6 during maturity ($p < 0.05$, Figures 2-8). Relating these spatial autocorrelated periods with the forestry inventory data, it appears that 81% of autocorrelated instances can be associated with the presence of lianas, which may cause higher estimates of fPAR in the north-northwest section of the network (Figure 2-9). During the maturity phenophase, Nodes 8, 9 & 13 are associated with 3/6 instances of autocorrelated periods. These aggregates estimate a 10-16% decrease in 2-flux $fPAR_{Domain}$ compared with the

rest of the network. Regarding senescence, nodes 8, 9, & 13 are involved in every instance where aggregates of decreased 2-flux $fPAR_{Domain}$ exist (Figure 2-9), creating a clear dichotomy between the south-southwest nodes and north-northeast nodes. The mean 2-flux $fPAR_{Domain}$ estimates of the south-southwest group are 16-22% lower than the north-northwest group but had a decreased variability of 4-6% (Figure 2-9).

3.2 Variability caused by external influences

3.2.1 – Green-up

Examining the effect of *SZA* and sky condition on 2-flux $fPAR_{Domain}$ estimation, the green-up phenophase displayed that during periods in which $27° < SZA < 60°$ that there was no difference in the central tendencies between the pairs of sky conditions (Figure 2-4b) using a MW test ($p > 0.35$). This is reflected in the similar medians (*Mdn*) and inter-quartile ranges (*IQR*) in the fPAR distributions per sky condition (CS: *Mdn* = 0.716, *IQR* = 0.625-0.807; MS: *Mdn* = 0.725, *IQR* = 0.615-0.781; DS: *Mdn* = 0.742, *IQR* = 0.618-0.794, Figure 2-4b). Towards midday when the *SZA* < 27° (Figure 2-4a) detectable differences emerge between CS and DS distributions (KS: $p = 4.777^{-5}$, MW: $p = 0.0434$, *Cliff d* = -0.101), and between MS and DS conditions (KS: $p = 0.0127$); despite these differences, they are not reflected in the inter-quartile ranges in each fPAR distribution (CS: *Mdn* = 0.716, *IQR* = 0.625-0.807; MS: *Mdn* = 0.725, *IQR* = 0.615-0.781; DS: *Mdn = 0.742*, *IQR* = 0.618-0.794). The difference detected by the MW and KS tests which are not reflected in the IQR may result from a change in the modality of the distributions, as CS exhibit a unimodal distribution (*skewness* = -0.501, *kurtosis* = -0.122, *mode* = 0.746, Figure 2-4a), which shifts to a bimodal distribution under MS and DS condtions (MS: *skewness* = -1.126, *kurtosis* = 0.491, *modes* = 0.356 & 0.732/ DS: *skewness* = -1.039, *kurtosis* = 0.270, *modes* = 0.487 & 0.789).

Another external factor considered is wind, in the green-up phase (Figure 2-6a) it is when *WS* > 5m/s that variability is at its lowest (*mean* = 0.699, *sd* = 0.117, *RMSE* = 0.00470). When wind speed is in its lowest category (*WS's* < 3m/s), fPAR variability is at its highest due to the formation of a bimodal distribution (*Mdn* = 0.758, *skewness* = -0.589, *kurtosis* = -0.882, *mean* = *0.*687, *sd* = 0.198, *RMSE* = 0.00991). Testing for discernable differences between the three categories of wind speed, using the KS test ($p < 0.05$) confirmed that differences existed,

whereas when employing MW tests, the only detectable difference found is between *WS* < 3m/s and *WS* > 5m/s ($p = 0.0396$, *Cliff's d* = 0.0763).

3.2.2 Maturity

The distribution of fPAR in the maturity phenophase (Figure 2-4c, d), regardless of sky conditions, *SZA* or wind speed is always extremely skewed (Figure 2-4c, 4d/ Figure 2-6b). When considering the *SZA* between 27° and 60° there is a measurable difference between CS and DS sky conditions (KS: $p = 2.2^{-16}$; MW: $p = 1.45^{-26}$, *Cliff's d* = 0.180). This difference remains between MS and DS conditions (KS: $p = 3.027^{-9}$, MW: $p = 7.95^{-8}$, *Cliff's d* = 0.150). In both instances, there is a low, but significant probability that DS conditions will result in lower estimates of 2-flux $fPAR_{Domain}$. No detectable differences between CS and MS occur ($p > 0.05$).

When *SZA* < 27° the modality of fPAR changes as SC shifts between DS and CS conditions, resulting in a shift from a unimodal to a slightly bimodal distribution (Figure 2-4c). This second mode results in an increase in the medians of fPAR (DS: *Mdn* = 0.918/MS: *Mdn* = 0.927/CS: *Mdn* = 0.928), but results in a smaller measurable difference in the cumulative distribution and central tendencies for CS conditions and DS conditions (KS: $p = 3.019^{-6}$; MW: $p = 9.46^{-4}$, *Cliff's d* = 0.0678) than when *SZA* is between 27° and 60°. There is no significant difference between the distributions of MS and either CS or DS conditions ($p > 0.05$).

When considering the effect of wind speed during maturity, all distributions maintain a unimodal shape regardless of the wind speed category employed. Those measurements made under conditions when *WS* > 5m/s have the largest variability and lowest median (*Mdn* = 0.909, *IQR* = 0.803-0.951). In contrast when *WS* < 3m/s (*Mdn* = 0.949*, IQR* = 0.902-0.972) the fPAR distribution has its lowest variability and highest median. The differences between each set of distributions are detectable with a KS test ($p < 0.05$). Comparing the central tendencies also yielded demonstrable differences in all paired cases ($p < 0.0001$) with the *Cliff's d* indicating that *WS's* < 3m/s or *WS's* that are between 3-5m/s yield higher fPAR estimates than when *WS's* > 5m/s (*Cliff's d* = 0.341/0.268).

3.2.3 Senescence

Depending on the external factors there can be differences in the distributions of fPAR, while low or midday SZA (*SZA* < 27°) result in normal or near-normal distributions, fPAR distributions when the *SZA* is between 27° and 60° or when divided by the wind speed categories results in non-normal distributions (Figure 2-4e, f/ Figure 2.6c). Distributions for both MS and DS when *SZA* < 27° are normally distributed according to a Shapiro-Wilks test (p = 0.226 & p = 0.131, respectively) while CS is nominally non-normally distributed ($p = 1.028^{-5}$, *skewness* = 0.215, *kurtosis* = -0.279). Consequently, the first analysis will employ the Welch's t-test to detect differences in the distributions. In this case, the only detectable difference occurs between CS and DS conditions (t = -2.77, df = 129, p = 0.00641, *95% CI* = -0.0744: -0.0124), with no differences found between mixed skies and other sky conditions (p > 0.05).

As *SZA* increases the results invert as CS conditions (*Mdn* = 0.653, *skewness* = 0.0113, *kurtosis* = -0.634) are skewed less than either MS (*median* = 0.712, *skewness* = -0.950, *kurtosis* = -0.348) or DS conditions (*median* = 0.736, *skewness* = -0.397, *kurtosis* = -1.139). Additionally, under DS conditions the distribution becomes bimodal, exhibiting the largest variability (*Modes* = 0.486 & 0.906, *IQR* = 0.51-0.918). These changes in the mode led to noteworthy differences in the central tendencies between CS and both MS and DS (MW Test: CS:MS, p = 0.00406, *Cliff's d* = 0.101; CS:DS, $p = 9.14^{-5}$, *Cliff's d* = 0.221; MS:DS, p = 0.202, *Cliff's d* = 0.023). While differences in the distributions between all sky conditions could also be found (KS Test; CS:MS, $p = 8.19^{-5}$; CS:DS, $p = 1.19^{-11}$; MS:DS, p = 0.00808).

When considering wind speed, senescence exhibited the largest discrepancies between the central tendencies and distributions of the different wind speeds (Figure 2.6c). Detectable differences in the central tendencies and distributions were found between the highest and lowest wind-speed conditions (KS: $p = 1.05^{-6}$, MW: $p = 2.46^{-6}$, *Cliff's d* = 0.152) with WS < 3m/s also yielding a higher median fPAR. When WS are less than 3m/s or when WS is between 3 and 5m/s bimodal distributions form with the same modes (*Modes* = 0.923 & 0.704), with a heavier positive tail forming for 3 < *WS* < 5m/s (Figure 2-6c). The difference in the tails between *WS* < 3m/s and 3 < *WS* < 5m/s creates a weak difference in the central tendencies (MW test: p = 0.0330, *Cliff's d* = 0.0808), but not for the cumulative distributions as determined by the KS test (p = 0.0779). There are also detectable differences between when 3< *WS* <5 m/s and *WS* > 5m/s

between the distributions (KS test: $p = 6.48^{-4}$) and its central tendencies (MW test: $p = 8.25^{-3}$, *Cliff's d* = 0.658) with a large likelihood that when $3 < WS < 5$ m/s there are higher estimates of 2-flux $fPAR_{Domain}$.

3.3 – Time of Day

When examining the daily cycle of 2-flux $fPAR_{Domain}$ (Figure 2-5a) a diurnal cycle appears which can be deconstructed into three separate phenomena. The first phenomena occur during the early (06:00 – 07:00, Figure 2-5a) and late (16:40 – 18:00) hours of the day, resulting in the lowest mean estimates of 2-flux $fPAR_{Domain}$ (*mean* = 0.809, *sd* = 0.0737; *mean* = 0.817, *sd* = 0.0433, respectively). The second occurs when the *SZA* is between 27° & 60°, during the morning hours between 07:10 & 10:00 (*mean* = 0.910, *sd* = 0.0536, Figure 2-5b) or the afternoon hours between 14:00 & 16:30 (*mean* = 0.910, *sd* = 0.0460, Figure 2-5d) resulting in the maximum fPAR measured with the lowest variability. The third occurs around solar noon (10:10 – 13:50), when *SZA* < 27° which has a variance 24% greater and mean 4% lower (*mean = 0.87, sd = 0.0619*, Figure 2-5c) than those measurements taken when the *SZA* is between 27° and 60°.

3.4 General Linear Mixed Effect's Model

Two generalized linear mixed effect's models were tested, one (Model A, Figure 2-10) with the variables *WS, SZA,* and *SC* and the other (Model B, Figure 2-10) with the same variables in addition to *SM*. Model B consistently outperforms Model A based on the AIC criteria, with Model B having approximately half the AIC score of Model A in all phenophases. During green-up, neither model provided independent variables capable of significantly predicting ($p < 0.05$) 2-flux $fPAR_{Domain}$. During maturity, all the independent variables were significant in Model A ($p < 0.05$), but wind speed had the largest coefficient (-0.155), with *SZA* (0.0138) and *SC* (0.000321) having significant, but negligible impacts predicting 2-flux $fPAR_{Domain}$ (Figure 2-10). Employing Model B, *WS* was no longer significant, while *SZA* (*coef* = 0.00888) and *SC* (*coef* = 0.000348) remained despite their negligible coefficients and soil moisture became the strongest predictor of 2-flux $fPAR_{Domain}$ (*coef* = 0.0709). In senescence, Model B displays a similar pattern seen in maturity, where *SM* became the strongest predictor of fPAR (*coef* = 0.0706) with *SZA* (*coef* = 0.0250) also being determined as significant. Model A, has both *WS* (*coef* = -0.0374) and *SZA* (*coef* = 0.0282) as being significant predictors of 2-flux $fPAR_{Domain}$ (Figure 2-10).

4.0 – Discussion

4.1 Methodological considerations

During the setup of data loggers and PAR sensors many studies assume that PAR sensor calibration is valid, and that sensors are recording accurate estimates of PAR (Wenjuan Li & Fang, 2015; Majasalmi, 2015). In this study, it was found that in only 4/5 tests the $R^2 \geq 0.89$ and that RMSE $\leq$ 190 (Figure 2-3). The final sensor had a divergence occur when values of PAR > 1200 μE which primarily occurs during the senescence phase (Figure 2-3). As a result, the Apogee calibrated sensors overestimate tPAR. Overestimation, especially under clear sky conditions (PAR $\geq$ 1200μE) can occur as a result of sunflecking (Chazdon & Fetcher, 1984). Sunflecking is the phenomenon where due to the organization of leaves in the canopy partial shading of the understorey occurs and where shading does not occur sun flecks exist hitting vegetation, or in this case sensors, that reside in the understorey (Chazdon & Fetcher, 1984; Vierling & Wessman, 2000). This is a likely explanation for the increase in the tPAR variance that occurs under clear-sky conditions, with this phenomenon being especially prevalent during senescence when canopy structure is more random and heterogenous as leaves are shed and LAI drops (Kalácska, Calvo-Alvarado, & Sánchez-Azofeifa, 2005). The lower variability between sensor pair 5 (Figure 2-3) that occurs during maturity supports this idea, as LAI $\geq$ 3 during these periods (Kalácska et al., 2005) creating a homogenous canopy with less spatial variability, as witnessed in the coefficient of variation tests (Figure 2-7). Sensor drift may also be a cause for divergence, as Apogee calibrated sensor had been installed for 3 years prior to the installation of the NPL calibrated sensor, permitting up to 6% drift. Drift would account for only a fraction of the observed difference. Given the agreement between the sensors during maturity and lack of additional data (i.e. hemispherical pictures), we cannot determine if the deviance is caused by sun flecks or sensor error. Considering the strong agreement, especially during maturity and under diffuse sky conditions (Figure 2-15) it is argued that recalibration of PAR sensors is unnecessary step in WSN setup.

When setting up a WSN network in a TDF the high spatial variability that exists within all phenophases needs to be considered. When filtered for *SZA* between 27° - 60° and *WS* < 3m/s, only two sensors are necessary to characterize the light field in the understorey during maturity; however, in all other cases during maturity, 8+ sensors are necessary to constrain the variability

across the site to the GCOS 10% threshold (2011). In the transitional phenophases (green-up and senescence), the *CV* never approaches the 10% threshold set by GCOS (2011), regardless of the number of sensors in the network. These transitional phenophases are periods of dynamic physiological and physical change in the environment, where the LAI changes from 0 to > 3 (Kalácska et al., 2005), which is distinguished by the bimodal distributions, especially during diffuse sky conditions (Figure 2-4), indicative of fPAR observations being made under two distinctly different canopies (Li & Fang, 2015; Majasalmi, 2015). Subsequently, because these phenophases are capturing a transforming canopy and its associated conditions, with a much larger *IQR* range than during maturity which prevents the *CV* from < 10% and indicates that physical measurements of the canopy state is necessary to contextualize the transitional phenophase data.

These findings translate to other broadleaf deciduous forests, which also demonstrate high variability in fPAR based on the LAI of the site (Atkins, et al., 2018; Li & Fang, 2015; Myneni, 1997; Putzenlechner et al., 2019; Shabanov et al., 2003). These studies also describe how small-scale spatial heterogeneity can be due to complex interactions of absorbance, reflectance in complex forest canopies (Ahl et al., 2006; Wenjuan & Fang, 2015; Shabanov et al., 2003; Vierling & Wessman, 2000). Given the high variability found in this and other broadleaf forest studies, it is recommended that the methodologies proposed by Widlowski (2010) and Putzenlechner et al.'s (2019) should be followed, especially when validating satellite products. Additionally, our results suggest that the inclusion of *SZA* and *WS* filters may be useful to constrain the variability of 2-flux $fPAR_{Domain}$ to reflect only the heterogeneity imposed by differences in canopy structure.

While it has been highlighted that a physical measure of the canopy condition is necessary for better context, the thresholding method still captured the phenophases accurately. Extreme seasonality is one of the primary characteristics of TDFs, reflected by the change in 2-flux $fPAR_{Domain}$ (±0.85) during a phenological cycle (Figure 2-2). As such, this needed to be accounted for when conducting a study that investigates the dynamic changes of photon flux and light fields within a spatially and temporally heterogenous forest. The approach this study took was to divide the phenological year into three separate phenophases: green-up, maturity and senescence based on a thresholding technique that took into consideration the rate-of-change for

the fPAR time-series. The purpose for dividing the phenological year is to capture and categorize what is occurring to fPAR in the context of the unique environmental and physiological circumstances, as described by Janzen (1988). In this context employing a threshold method was effective in categorizing the different physiological changes occurring, as demonstrated by the difference in the median, *IQR* ranges, and the length of each season which respected the definitions for TDF phenology as described by Sánchez-Azofeifa et al., (2005).

Despite the phenophases of green-up and senescence both embodying a period of dramatic physical change, as indicated by overlapping *IQR* ranges the thresholding method still captured the unique differences in the physiological changes. For example, senescence still yields a median 20.8% lower than that of green-up and has a rate-of-change for fPAR of -0.637% per day for a 136-day season, which compared to green-up's 1.43% per day for an average 26-day season, indicates that the degree of physiological changes within the TDF are differing considerably. It seems the thresholding method is capturing the entirety of senescence, from the denaturing of chlorophyll pigments to the abscission of leaves and the absence of photosynthesizing foliage that occurs in the latter months (February – March) of this phenophase (Kalácska, et al., 2005; Wilson, et al., 2001); while also capturing the rapid change onset by the first rains during green-up from leaf absence to almost full-leaf maturity. This is supported by the GLME's for each phenophase, as regardless of the model, each has its own unique set of significant environmental predictors for 2-flux $fPAR_{Domain}$, indicating that different environmental factors are important for each phenophase.

The threshold method was also effective in capturing the maturity phenophase. The median for maturity is 38% higher than senescence's and the *IQR* does not overlap either of green-up or maturities, while remaining in the top 20% of the fPAR-scale, estimates of fPAR indicative of a fully-mature canopy (Ahl et al., 2006; Knyazikhin, et al., 1998; Myneni et al., 1999; Tian et al., 2002). This allowed for an analysis of the influence of environmental factors on a fully mature canopy, preventing the 2-flux $fPAR_{Domain}$ distribution from spreading and subsequently convoluting environmental influences with a change in canopy structure. Therefore, the thresholding method is adequate at isolating the time-series into periods of separate physiological and environmental change.

4.2 Influence of environmental conditions on the uncertainty of 2-flux fPAR

Of the two variables indicative of illumination conditions, *SZA* exhibits a higher significance in the prediction of 2-flux $fPAR_{Domain}$ during maturity and senescence in the GLME (Figure 2-10). The influence of *SZA* can have drastic effects on the measurement of fPAR, regardless of the canopy state. It is known that as *SZA* values increase (> 27°), fPAR converges at higher fPAR values, regardless of the canopy state or LAI observed (Wenjuan & Fang, 2015). Convergence of fPAR at lower *SZA* occurs due to the path of incident radiation lengthening, causing an increased probability that the radiation will be intercepted before reaching the sensor in the understorey therefore artificially increasing the fPAR estimated (Wenjuan & Fang, 2015; Shabanov et al., 2003; Thomas et al., 2006). This is especially crucial to account for during periods of lower LAI (LAI < 4; (Wenjuan & Fang, 2015)) as taking measurements at larger *SZA* will overestimate the maturity of the canopy, which may explain why the median of 2-flux $fPAR_{Domain}$ is consistently higher when 27° < *SZA* < 60° regardless of the phenophase or the sky condition. Other studies have found that under direct radiation, at times of nadir observations, fPAR can be underestimated by up to 10% when LAI < 2 as it often is during these transitional phenophases, especially during green-up and the latter months of senescence (Goward & Huemmrich, 1992; Kalácska et al., 2005; Kalacska et al., 2005). The differences in the central tendencies and distributions of 2-flux $fPAR_{Domain}$ between the two *SZA* categories are not significant during green-up or maturity, but are during senescence when LAI changes are slower (Kalacska et al., 2005) and therefore need to be accounted for during this phenophase.

The illumination conditions, determined by the sky conditions, regardless of phenophase showed that direct illumination under clear skies and diffuse illumination under cloudy skies create fPAR estimates with different central tendencies and distributions. This is most evident during the transitional phenophases, where clear sky conditions have a decreased standard deviation, root mean square error, and median compared to diffuse sky conditions, which becomes inverted during maturity. This may be due to diffuse radiation being more readily absorbed by photosynthesising materials as suggested by Atkins et al., (2018), Gu et al., (2002) and Wenjuan & Fang (2015). Not only is diffuse radiation more readily absorbed, but it is also capable of permitting the deeper penetration of photons which increases the light use efficiency of plant canopies while decreasing the frequency of photosynthetic saturation (Gu et al., 2002; Wenjuan

& Fang, 2015; Majasalmi, 2015). Consequently, it should be anticipated that measurements taken under diffuse skies are measuring only the effect of the canopy condition, and that the amount of PAR absorbed is proportional to the LAI, which yields both an increase in the 2-flux $fPAR_{Domain}$ and accurately represents the canopy condition being observed for that period. This is evident during the transitional phenophases, where often a bimodal distribution can be observed under diffuse skies. The bimodal distribution is reflective of the 2-flux $fPAR_{Domain}$ estimates anticipated under variable LAI values (Kalácska et al., 2005; Wenjuan & Fang, 2015). This bimodal distribution could explain why *SC*'s were not as significant to the GLME (Figure 2-10), as the bimodality increases the *RMSE* of the relationship between *SC* and 2-flux $fPAR_{Domain}$. This also supports the argument that any measurements of fPAR, especially during the transitional phenophase needs to be linked with measurements of the canopy condition, such as LAI.

Wind speed is a convoluting variable, as results differed depending on the phenophase (Figure 2-6) and likely the canopy condition (Putzenlechner et al., 2019). During canopy maturity, wind speeds greater than 5 m/s were found to increase the spatial variability of the understory light environment, causing an underestimation in the 2-flux fPAR estimated. Regardless, *WS* did not present any explanatory power in the GLME except in Model A during maturity. These findings are consistent with those found in a coniferous dominated forest (Putzenlechner et al., 2019). The wind-speeds that create these conditions are present at the end of maturity, and throughout senescence aiding in the leaf-shedding process, before receding as the rains return at the start of green-up. While the process of how wind speed influences fPAR estimation has not been investigated, this thesis poses that underestimation of 2-flux $fPAR_{Domain}$ during periods of high wind could be due to rapid changes in leaf angle orientation and an increase in the spatial heterogeneity of understorey illumination conditions. As wind speed increases, branch movement increases along with leaf movement and inherently leaf angle orientation. Leaves may change from being planophile to erectophile or plagiophile, permitting photons to reflect off the plagiophile or erectophile leaves allowing photons to penetrate deeper into the canopy, therefore increasing the tPAR readings in the understorey and decreasing the fraction of PAR absorbed by the canopy (Asner & Wessman, 1997; Verhoef, 1984). The shifting and reorientation of branches and leaves may also increase the frequency and the spatial distribution of sunflecks in the understorey, therefore increasing the variability of fPAR and decreasing its estimation. Contrasting results from the green-up phenophase may be a result of canopy condition, as

exhibited by the bimodal distribution (Figure 2-6) and the timing of high wind speeds, which typically occur with higher frequency early in green-up (Figure 2-17) when LAI is low and fPAR estimates are low. Asner & Wessman (1997), created model predictions for this canopy behaviour with the resulting impact on fPAR, which exhibited similar behaviour to that observed at the SRNP-EMSS canopy during maturity as wind speeds increase.

Investigating the results of the GLME, (Figure 2-10) the significance of *SM* for all three phenophases in Model B reinforces the well-established understanding that TDFs are water-limited ecosystem (Campos, 2018; Castillo-Núñez et al., 2011; Janzen, 1988; Power et al., 2016; Sánchez-Azofeifa et al., 2005) with precipitation and soil moisture controlling the onset of green-up, while influencing the photosynthetic capacities of tree canopies relative to the water available in the area (Hwang et al., 2017). This is reaffirmed with the data collected during maturity, as seen with the dry-period that occurs for two weeks in the middle of maturity. Even during this minor drought, the physiological stress response from the tropical dry forest is observed as 2-flux $fPAR_{Domain}$ decreases by 0.1-0.2 (Figure 2-2) until precipitation starts again and soil moisture increases. Additionally, it appears that *SM* occurs concurrently with the presence of lianas, which are known to delay the abscission of their leaves during senescence and can create matts in the canopy, decreasing the canopy openness and providing shade for the understorey below (Sánchez-Azofeifa, et al., 2009). The delay in leaf abscission by lianas during senescence (Cai, et al., 2009) would increase the LAI of the canopy and consequently increase fPAR for that area, which may explain the spatial autocorrelation observed during the senescence phenophase (Figure 2-9).

Overall, during phenological maturity, significant differences were only found between the central tendencies of 2-flux $fPAR_{Domain}$ estimated under clear-sky and diffuse sky conditions when *SZA* was between 27° and 60°. Therefore, controlling for *SZA* eliminates the need for considering illumination condition during canopy maturity. Consequently, *SZA* is a variable that should be controlled for when estimating 2-flux $fPAR_{Domain}$, especially for those measurements taken during senescence where its effect is most pronounced. Wind speed is another variable that needs to be considered when estimating 2-flux $fPAR_{Domain}$ during phenological maturity, as high *WS* are highly likely to underestimate fPAR as indicated by the *Cliff's d* (Figure 2-6). Controlling for these variables requires permanent monitoring sites, which is made possible by the WSN

technology employed in this study. Furthermore, if WSN technology continues to be employed, it should be coupled with time-lapse or a periodic photography campaign which helps links physical phenomenon with observed phenomenon in the WSN fPAR time-series.

5.0 Conclusions

This study was designed to evaluate the methodological procedures surrounding the collection of ground fPAR fluxes in a tropical dry-forest, for the purpose of validating satellite fPAR products. Unique to this study was its study location, being in a Tropical Dry Forest, and as such external variables, sensor calibration, and network size were tested. Overall, sensor calibration needs to be considered when employing Wireless Sensor Networks over the long-term, otherwise incidents like those observed in node 5 may occur where fPAR sensor measurement differs considerably. The measurements of fPAR collected between diffuse and clear sky conditions were considered significant, but as the *Cliff's d* effect size indicated the probability of different estimations occurring as a result was only of a concern when *SZA* was between 27° and 60°. Therefore, by taking measurements when the $SZA < 27°$ this eliminates the need for considering illumination condition during canopy maturity. If this recommendation is to be considered, then the Wireless Sensor Network needs to consist of 10+ sensors and take into consideration *WS*, otherwise it will not be able to meet the GCOS standards. While controlling for higher *SZA* had the most significant effect on reducing the variability of 2-flux $fPAR_{Domain,}$ regardless of season, this could be due to the spatial homogenization that occurs as fewer photons reach the sensors, inflating fPAR estimates artificially. Therefore, to realize a 2-flux $fPAR_{Domain}$ product that meets the GCOS standard, while remaining representative of true canopy conditions in a tropical dry forest, a network of 10+ sensors is necessary with the condition that measurements are taken when $WS < 3$ m/s and when $SZA < 27°$. Utilizing the comparisons and results found in this study the findings presented here could be used in the development of experimental designs in tropical areas which exhibit substationally less representation in the validation of satellite-derived fPAR products.

A permanent Wireless Sensor Network in combination with local meteorological towers, can be used to further quantify the sources of uncertainty and variability of fPAR in forest environments. Sites such as these are instrumental for the progression of satellite-derived fPAR products over forested areas, especially in the tropics where very few validation sites exist. If

satellite-derived fPAR products continue to expand, there will be a need for field validation sites to asses the influence of various environmental variables and to determine how assumptions differ by biome. No other method permits the high temporal and spatial resolution necessary for the validation of upcoming decametric satellite products, and as such, this method needs to be considered in the validation of these upcoming satellite products. Further investigations, however, into the effects of soil reflectance and top-of-canopy reflectance on fPAR during times of canopy turbidity should be assessed moving forward, especially during short-term sampling.

Acknowledgements

This study was conducted with the aid of a grant from the Inter-American Institute for Global Change Research (IAI), which is supported by the US National Science Foundation. We are also grateful for the financial, technical and infrastructural support provided by International Business Machines (IBM). We would also like to thank Roger Blanco and Maria Marta Chavarría from the Santa Rosa National Park. Finally, we would like to thank the field assistants from the University of Alberta and the Instituto Tecnologico de Costa Rica for their help in the collection of data and the maintenance of equipment at the Santa Rosa National Park Environmental Monitoring Super-site.

Table Legends

Table 2-1 **The definitions of the fraction of Photosynthetic Active Radiation.** *iPAR*: the total incoming Photosynthetic Active Radiation above the canopy. *tPAR*: the amount of Photosynthetic Active Radiation transmitted through the canopy to the forest floor. *rPAR*: the amount of Photosynthetic Active Radiation reflected off soil, leaf litter, and the top of the canopy back into the atmosphere.

Table 2-2 **Committee for Earth Observation Sciences- Land Product Validation Sub-group validation hierarchy scheme for satellite-derived products.** Products are to be classified according to the following criteria, with stage 3 products being products of the highest quality with their uncertainties well documented (Nightingale et al., 2011).

Table 2-3 **Selection Criteria and Classification Schemes.** Selection criteria and classification schemes for filtering 2-flux $fPAR_{Domain}$ to isolate variables being tested for their influence on 2-flux $fPAR_{Domain}$. Each set of classification schemes and selection criteria are implemented for each phenophase.

Figure Legends

Figure 2-1 The location of the Santa Rosa National Park - Environmental Monitoring Super-site (SRNP-EMSS). Network 1 refers to the WSN that is employed in the creation of the in-situ Green FPAR product.

Figure 2-2 **Breakdown of the 2-flux fPAR time-series into phenophases.** The entirety of the time-series is on display here and is broken down into its respective phenophases. These phenophases were determined using the R package "Phenex" and is based off local thresholds determined per year.

Figure 2-3 **A 1:1 comparison between NPL calibrated and Apogee calibrated PAR sensors.** NPL & Apogee PAR sensors were paired and mounted on 5 individual data. Node # is assigned to the location in which they are found within the WSN. Red line indicates the linear regression between the sensors, whereas the black line indicates a 1:1 line. Axis labelled "uncalibrated" refer to the Apogee calibrated sensors, whereas axis labelled "calibrated" refer to the NPL calibrated sensors

Figure 2-4 **The influence of solar zenith angles and sky conditions on the distribution of 2-flux domain fPAR.** These three sets of panels (a, b, c, d, e and f) are split into the respective phenophases: a & b) Green-up, c & d) Maturity, and e & f) Senescence. Further division between upper and lower panels displays the influence that a change in *SZA*, in conjunction with differing sky conditions, has on the distribution of 2-flux $fPAR_{Domain}$. Upper panels (a, c, & e) display the distribution of 2-flux $fPAR_{Domain}$ when: $0° < SZA < 27°$. Lower panels (b, d & f) display the distribution of 2-flux $fPAR_{Domain}$ when: $27° < SZA < 60°$.

Figure 2-5 **Distribution of 2-flux domain fPAR over the course of a day.** Panel a) displays the distribution of 2-flux $fPAR_{Domain}$ over the sunlit hours of a day. During a day, a diurnal pattern emerges where the median values and *IQR* ranges of 2-flux domain fPAR both increase and decrease, respectively. This is reflected in the panels b) Morning, c) Noon, & d) Afternoon. Panels b) & d) are subsets of when: $27° < SZA < 60°$. Whereas panel c) represents when: $SZA < 27°$. Median values increase during morning and afternoon subsets by 6% and 3% respectively, in comparison with the noontime median. Inter-quartile ranges from both the morning and afternoon subsets of data also shrink by an average of 12% and 22% respectively, in comparison with the *IQR* from the noon subsets.

Figure 2-6 **The influence of wind speed on the distribution of 2-flux domain fPAR by phenophase.** Each panel represents a different phenophase: a) green-up, b) maturity, c) senescence. Estimates of 2-flux domain fPAR in the context of investigating the influence of wind speed on its distribution were made during clear sky and mixed sky conditions. While there is no change in the mean or a significant change in the distribution of 2-flux domain fPAR during green-up, there are significant changes to the distribution and mean of 2-flux domain fPAR during both maturity (b) and senescence (c) between $WS<3$m/s and $WS>5$m/s.

Figure 2-7 **The coefficient of variation of 2-flux domain fPAR, by phenophase.** Each panel represents a different phenophase: a) Green-up, b) Maturity, c) Senescence. Calculating the maximum coefficient of variation takes all possible combinations of sensors, calculates the mean 2-flux $fPAR_{Domain}$ value for those combinations and the ratio of standard deviations to that mean. Here, an increasing number of sensors are

involved in the combinations, until all 13 data loggers in the network are considered. Therefore, as the sample size increases (from 2 – 13) it should be expected that the standard deviation of the 2-flux domain fPAR decreases towards the mean of the 2-flux domain fPAR.

Figure 2-8 **Instances of high spatial autocorrelation within the WSN during the maturity phenophase.** Each panel represents a week, in reverse chronological order, in which there was a high degree of spatial autocorrelation or clumping within the WSN. These periods were determined by Moran I's statistic and visualized to see where clumping occurred. a) Week of 06/01/2016, b) Week of 12/11/2014, c) Week of 11/25/2014, d) Week of 10/8/2014, e) Week of 9/30/2014, f) Week of 11/1/2013. It should be noted here that all instances of high spatial autocorrelation occur in the second half of maturity, once 2-flux domain fPAR peaks, excluding a). The network here displays a degree of symmetry, where certain nodes are always grouped together. Such as node #'s 1, 2, 3, 11, and 12 or nodes 8, 9 and 13. These groups typically display mean weekly fPAR values that are within 10% of one another.

Figure 2-9 **Instances of high spatial autocorrelation within the WSN during the senescence phenophase.** Each panel represents a week, in reverse chronological order, in which there was a high degree of spatial autocorrelation or clumping within the WSN. These periods were determined by Moran I's statistic and visualized to see where clumping occurred. a) Week of 02/18/2016, b) Week of 02/10/2016, c) Week of 02/02/2016, d) Week of 01/25/2016, e) Week of 01/17/2016, f) Week of 01/09/2016, g) Week of 02/26/2015, h) Week of 02/18/2015, i) Week of 02/10/2015, j) Week of 02/02/2015. Periods of high spatial autocorrelation here seem to be in consecutive periods during senescence and display periods of similar spatial distribution and autocorrelation. Panels a – f is from consecutive periods during 2016 and display that nodes 7, 8, 9, and 13 consistently have lower 2-flux fPAR estimates than the rest of the network. Panels g – j represents consecutive periods during 2015 where nodes 5, 6, 7, 8, 9, and 13 have consistently lower estimates of 2-flux fPAR than the rest of the network.

Figure 2-10 **The influence of independent variables on 2-flux $fPAR_{Domain}$ for two GLME models**. Each of these two GLME models were subjected to a logistic stepwise regression, which permitted the best fit model to be chosen based off its *AIC* score. In every instance, Model B, which included the variable soil moisture (*SM*) had an *AIC* score ½ the magnitude of Model A's. * indicate those variables with significant ($p < 0.05$) influence. Black arrows indicate positive coefficients, red arrows indicate negative coefficients, with the thickness of the arrow indicating relative effect of the variable, compared to other variables of significance. Arrows associated with variables that do not display the * symbol are variables selected by the logistic stepwise regression, which did not significantly impact the results of the GLME.

Figure 2-11 **Semi variogram of WSN**. This is the semi variogram utilized in the analysis of the Moran I spatial autocorrelation statistic. Only those periods which exhibited detectableautocorrelation are displayed in this figure.

Figure 2-12 A comparison between calibrated and uncalibrated PAR sensors during the senescence phase under all sky conditions.

(Table 2-1)

Type of fraction of Photosynthetic Active Radiation	Definition	Reference
Total fPAR	The ratio between the total absorbed PAR to incoming PAR at the top of canopy.	(Li & Fang, 2015)
White-sky fPAR or Diffuse fPAR	The ratio between the total absorbed PAR **under diffuse** (cloudy) light conditions to incoming PAR at the top of canopy.	(Gobron et al., 2006b; Wenjuan Li & Fang, 2015; Thomas et al., 2006)
Black-sky fPAR or Direct fPAR	The ratio between the total absorbed PAR **under direct** (sunny) light conditions to incoming PAR at the top of canopy.	(Gobron et al., 2006b; Wenjuan Li & Fang, 2015; Thomas et al., 2006)
Instantaneous fPAR	The PAR absorbed by the canopy **only** and excludes PAR absorbed by soil, understorey vegetation, or woody elements.	(Chen, 1996)
Green fPAR	The ratio between the total absorbed PAR by **all green elements** to incoming PAR at the top of canopy.	(Chen, 1996)
Fraction of Intercepted PAR	$FIPAR = \frac{iPAR - tPAR}{iPAR}$ where foliage and woody material is completely absorbing, and soil/ground is non-reflective.	(Gobron et al., 2006b; Widlowski, 2010)
2-flux fPAR	$2\ flux\ fPAR = 1 - \frac{tPAR}{iPAR}$	(Widlowski, 2010)
3-flux fPAR	$3\ \text{flux fPAR} = \frac{iPAR - tPAR - rPAR}{iPAR}$	(Widlowski, 2010)
4-flux fPAR	$4\ flux\ fPAR = \frac{iPAR - tPAR - rPAR - hPAR}{iPAR}$	(Widlowski, 2010)

(Table 2-2)

Stage	
Stage 1	Product accuracy is assessed from a small (<30) set of locations from and time periods by comparison with *in situ* or other suiTable 2-reference data.
Stage 2	Product accuracy is estimated over a significant set of locations and time periods by comparison with reference *in situ* or other suiTable 2-reference data. Spatial and temporal consistency of the product has been evaluated over a globally representative locations and time periods. Results are published in peer-reviewed journals.
Stage 3	Uncertainties in the product and its associated structure are well-quantified from comparison with reference *in situ* or other suiTable 2-data. Uncertainties are characterized in a statistically robust way over multiple locations and time periods representing global conditions. Spatial and temporal consistency of the product and consistency with similar products have been evaluated over globally representative locations and periods. Results are published in peer-reviewed journals.

(Table 2-3)

Variable(s)	Classification Scheme	Selection Scheme
Illumination (SZA & SC)	SZA < 27° 27° < SZA < 60° Clear Sky: iPAR > 1100µE Mixed Sky: 900µE < iPAR < 1100µE Diffuse Sky: iPAR < 900µE	WS < 3m/s
Wind Speed (WS)	WS < 3m/s 3m/s < WS < 5m/s WS > 5m/s	Diffuse Sky (iPAR < 900µE)

(Figure 2-1)

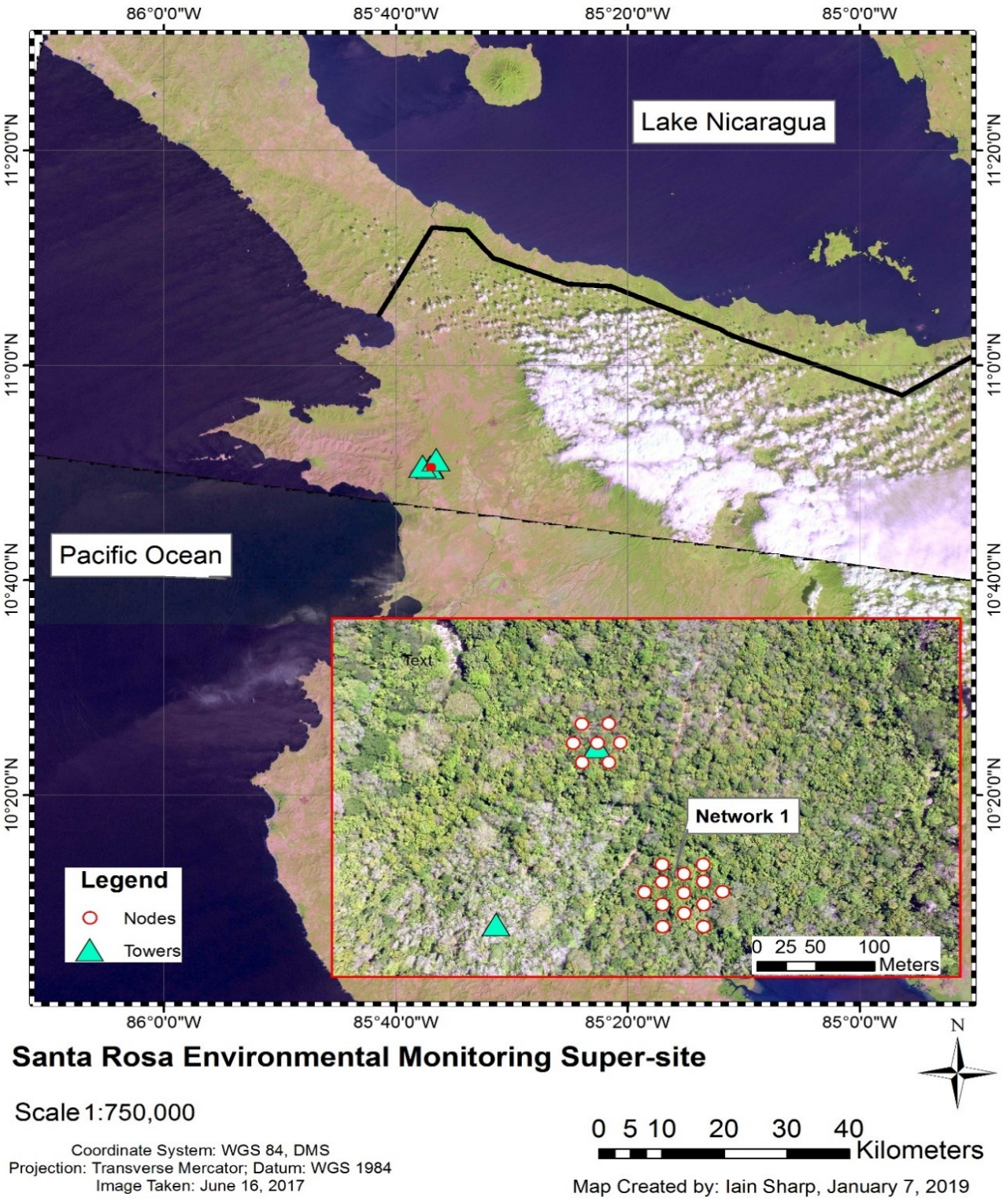
86°0'0"W
85°40'0"W
85°20'0"W
85°0'0"W
11°20'0"N
11°0'0"N
10°40'0"N
10°20'0"N
Lake Nicaragua
Pacific Ocean
Text
Network 1
Legend
Nodes
Towers
0 25 50 100
Meters
N
Santa Rosa Environmental Monitoring Super-site
Scale 1:750,000
Coordinate System: WGS 84, DMS
Projection: Transverse Mercator; Datum: WGS 1984
Image Taken: June 16, 2017
0 5 10 20 30 40
Kilometers
Map Created by: Iain Sharp, January 7, 2019

(Figu

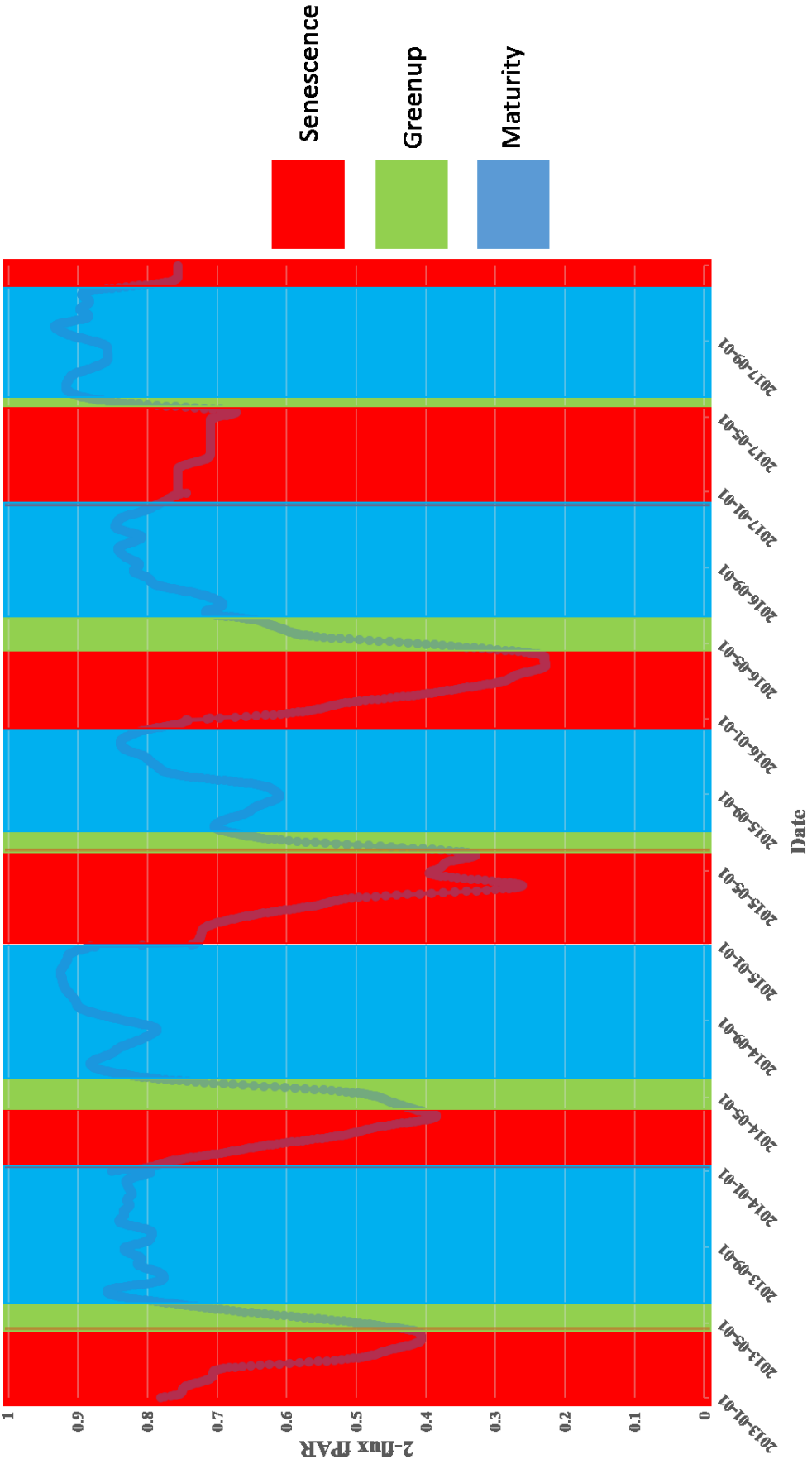
Senescence
Greenup
Maturity
2-flux fPAR
1
0.9
0.8
0.7
0.6
0.5
0.4
0.3
0.2
0.1
0
2013-01-01
2013-05-01
2013-09-01
2014-01-01
2014-05-01
2014-09-01
2015-01-01
2015-05-01
2015-09-01
2016-01-01
2016-05-01
2016-09-01
2017-01-01
2017-05-01
2017-09-01
Date

(Figure 2-3)

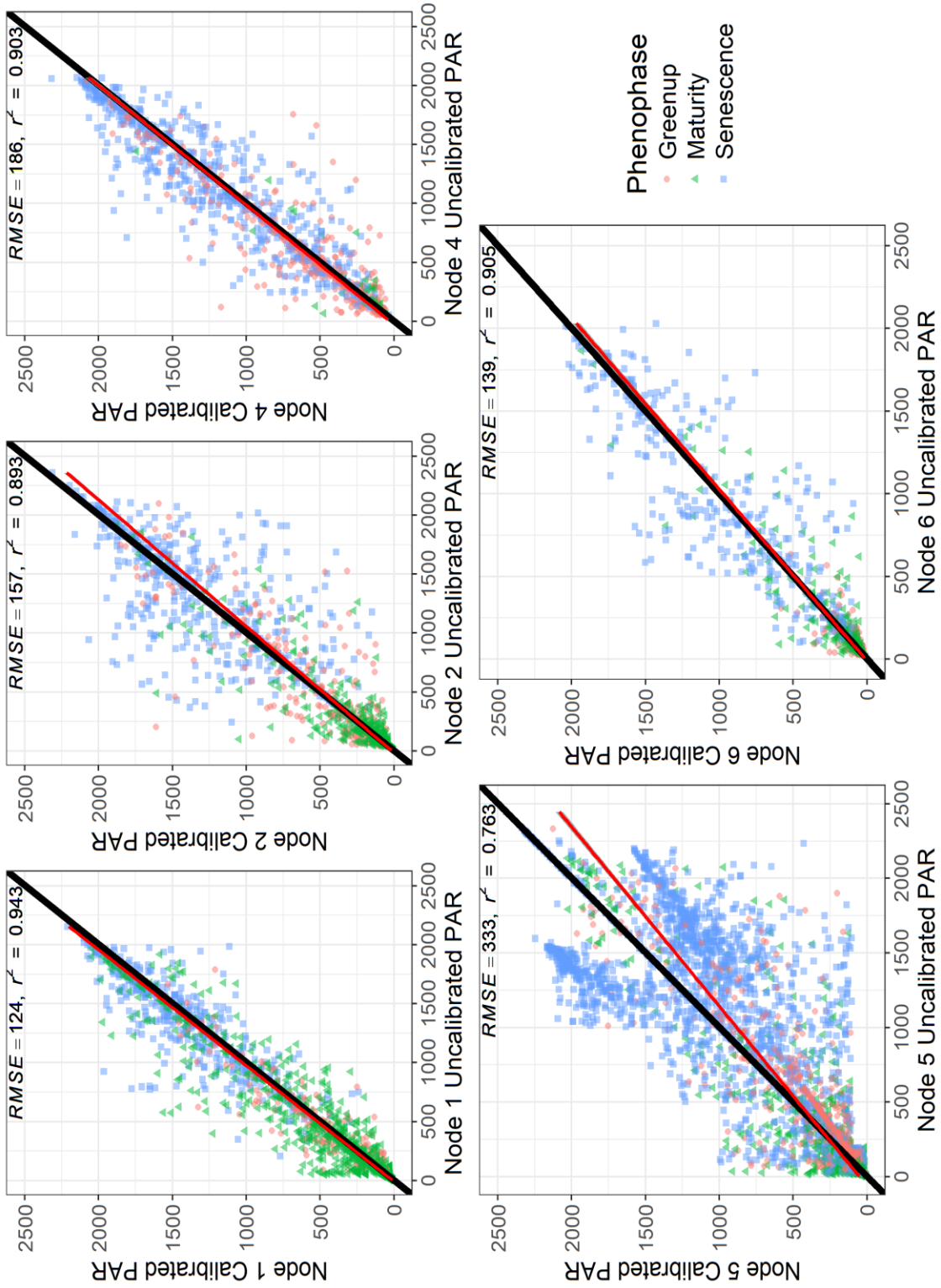
RMSE = 124, r² = 0.943
Node 1 Calibrated PAR
Node 1 Uncalibrated PAR
RMSE = 157, r² = 0.893
Node 2 Calibrated PAR
Node 2 Uncalibrated PAR
RMSE = 186, r² = 0.903
Node 4 Calibrated PAR
Node 4 Uncalibrated PAR
RMSE = 333, r² = 0.763
Node 5 Calibrated PAR
Node 5 Uncalibrated PAR
RMSE = 139, r² = 0.905
Node 6 Calibrated PAR
Node 6 Uncalibrated PAR
Phenophase
Greenup
Maturity
Senescence
0
500
1000
1500
2000
2500

(Figure 2-4)

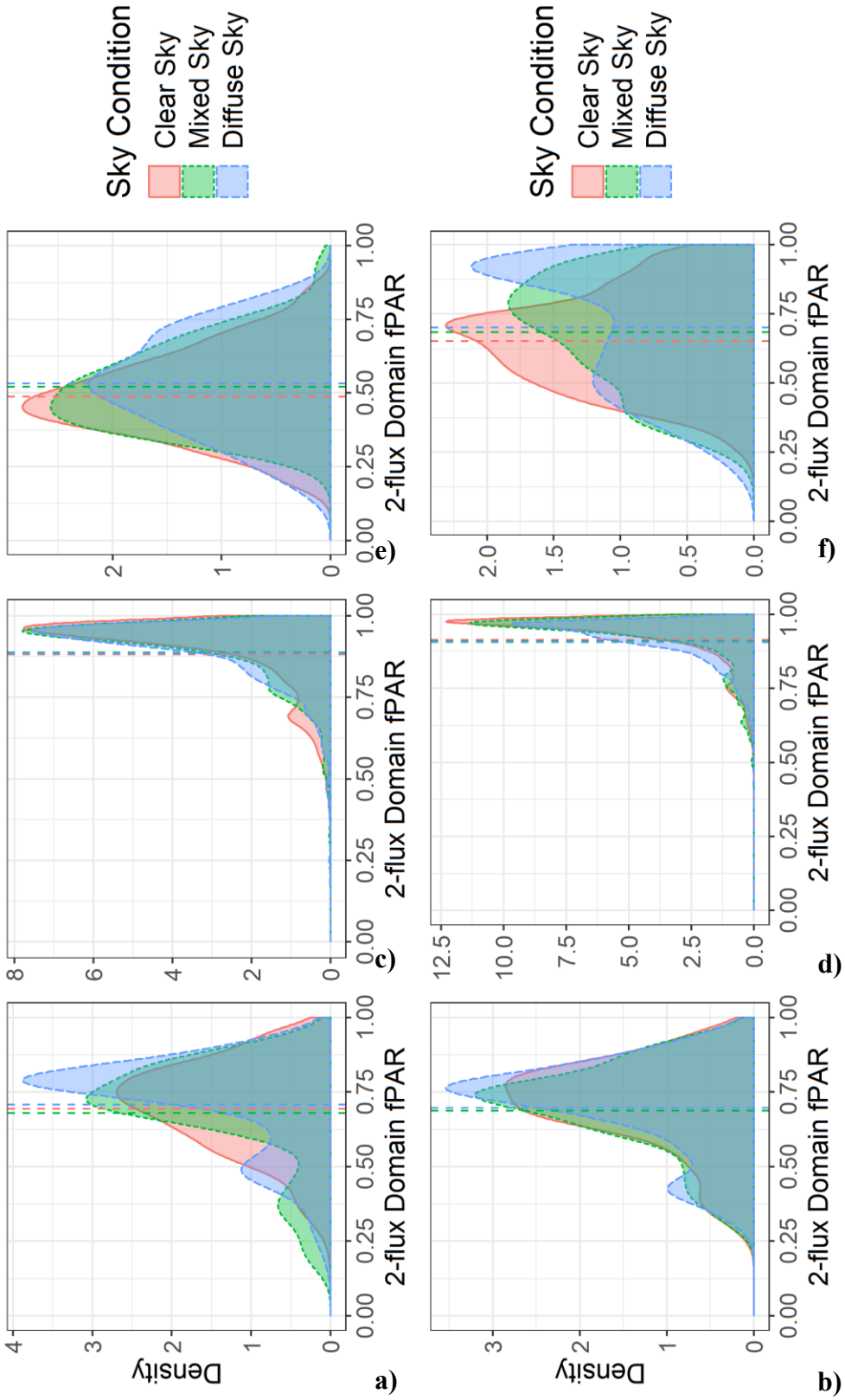
Sky Condition
Clear Sky
Mixed Sky
Diffuse Sky
Density
2-flux Domain fPAR
a)
b)
c)
d)
e)
f)

(Figure 2-5)

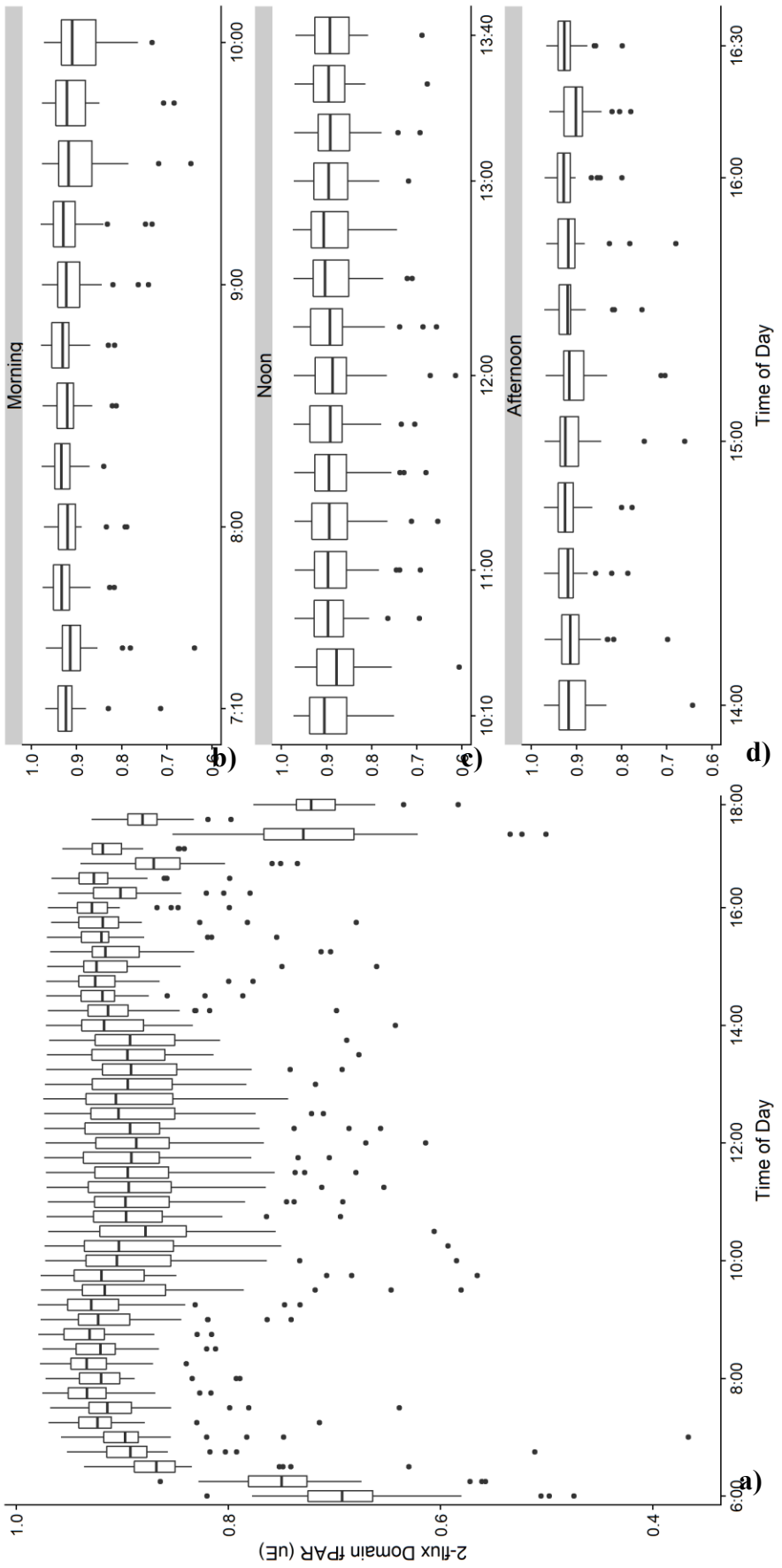
a)
b)
c)
d)
Morning
Noon
Afternoon
Time of Day
2-flux Domain fPAR (uE)

(Figure 2-6)

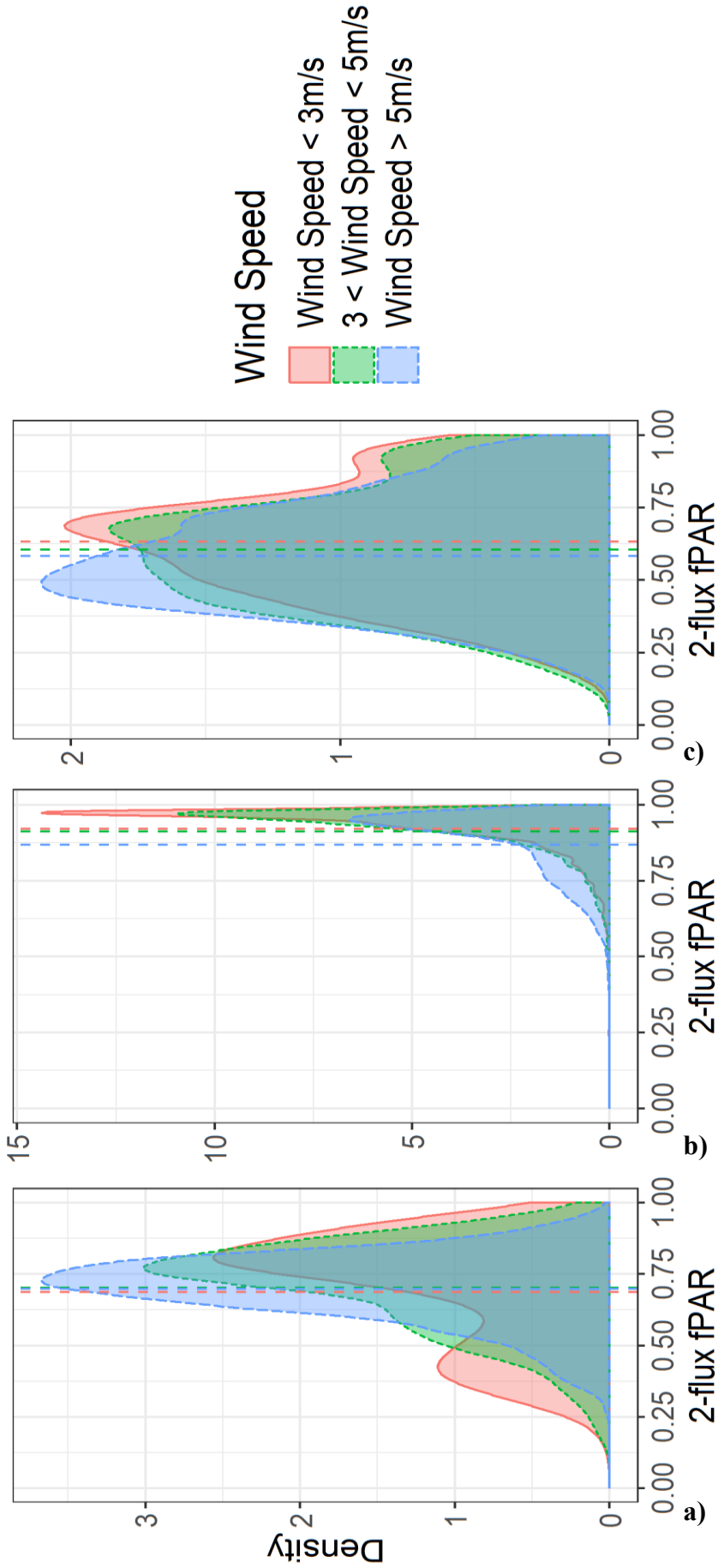
Wind Speed
Wind Speed < 3m/s
3 < Wind Speed < 5m/s
Wind Speed > 5m/s
Density
2-flux fPAR
a)
b)
c)

(Figure 2-7)

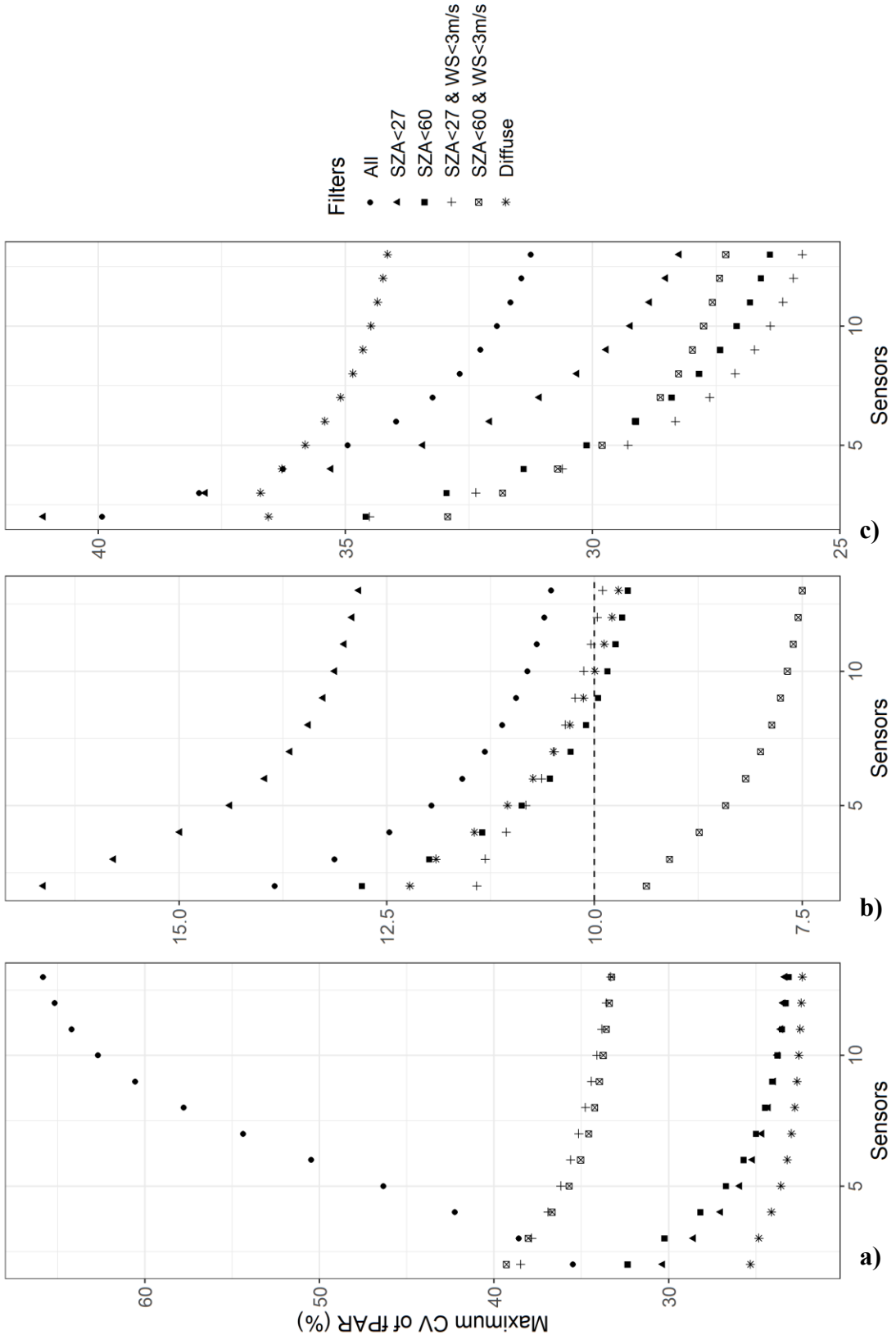
Filters
All
SZA<27
SZA<60
SZA<27 & WS<3m/s
SZA<60 & WS<3m/s
Diffuse
Maximum CV of fPAR (%)
Sensors
a)
b)
c)

(Figure 2-8, bottom) (Figure 2-9, top)

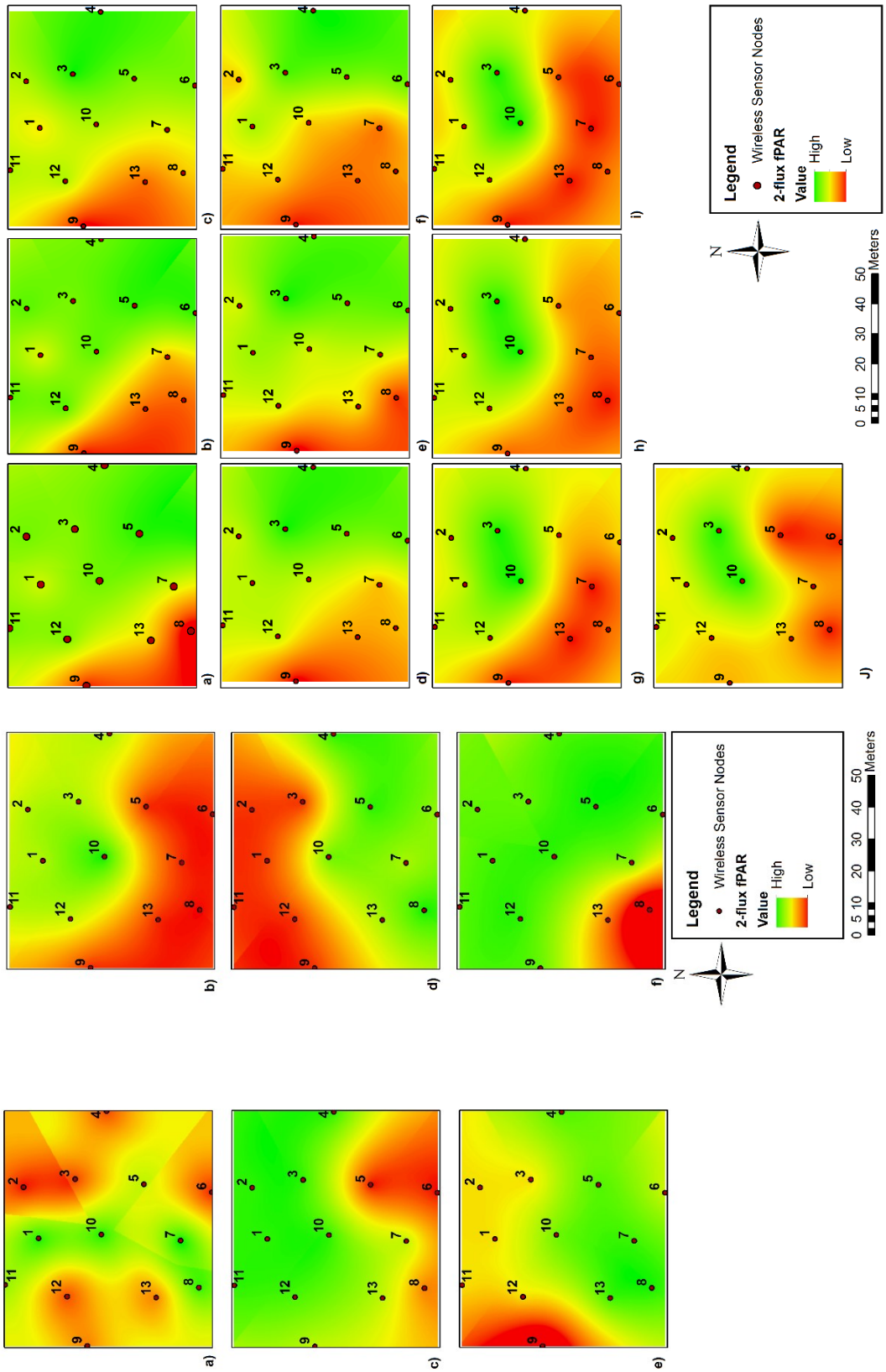

(Figure 2-10)

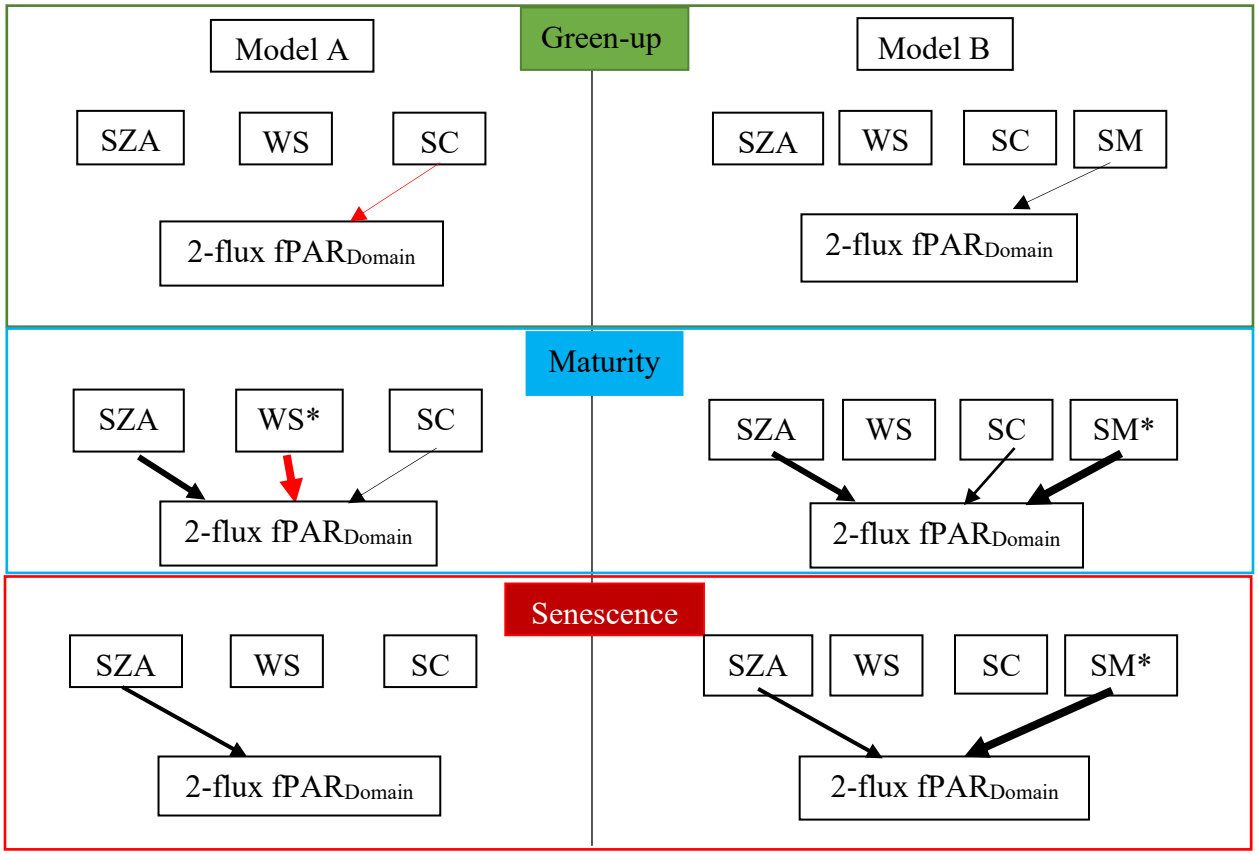
Green-up
Model A
SZA
WS
SC
2-flux fPARDomain
Model B
SZA
WS
SC
SM
2-flux fPARDomain
Maturity
SZA
WS*
SC
2-flux fPARDomain
SZA
WS
SC
SM*
2-flux fPARDomain
Senescence
SZA
WS
SC
2-flux fPARDomain
SZA
WS
SC
SM*
2-flux fPARDomain

Figure (2-11)

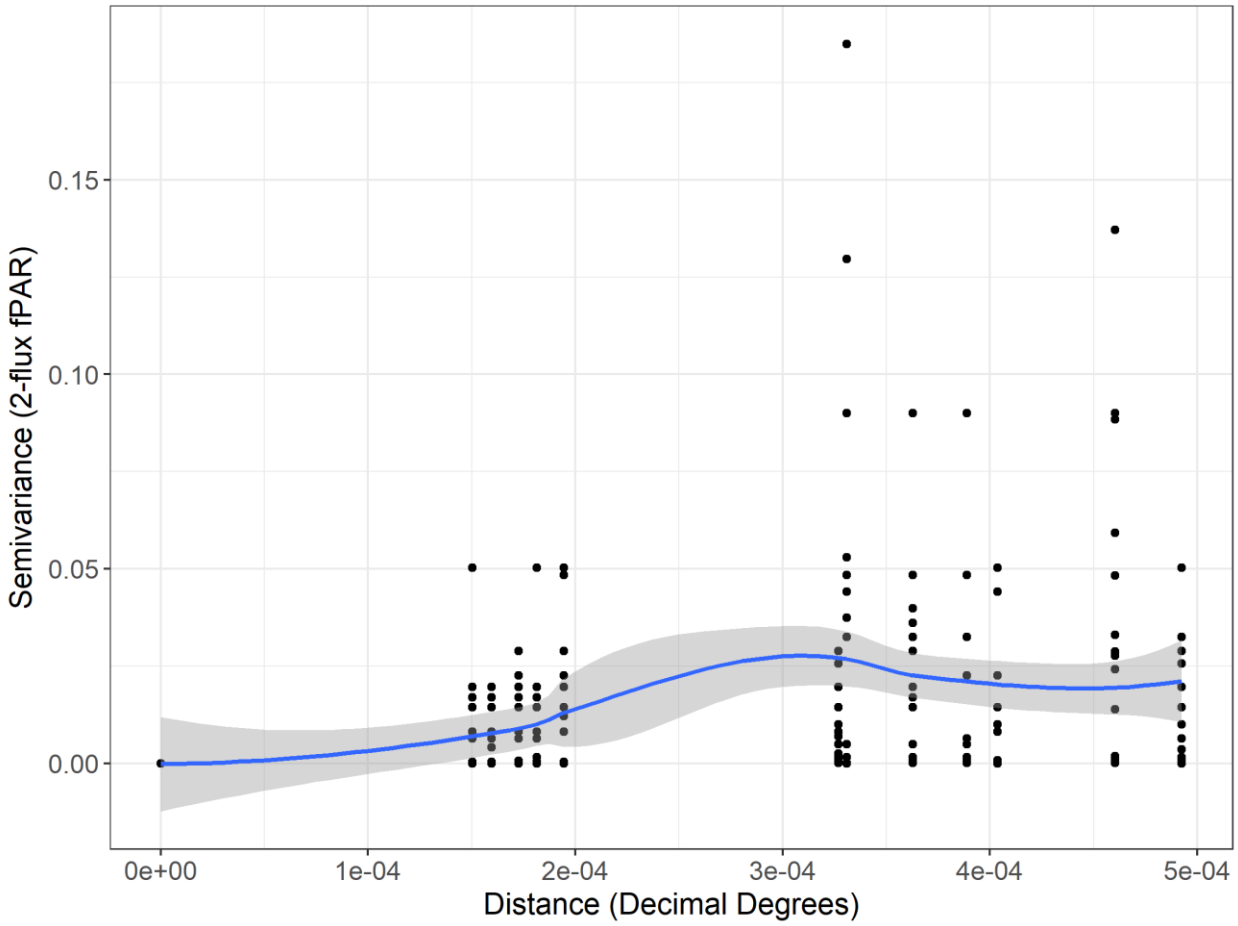
Semivariance (2-flux fPAR)
0.15
0.10
0.05
0.00
0e+00
1e-04
2e-04
3e-04
4e-04
5e-04
Distance (Decimal Degrees)

(Figure 2-12)

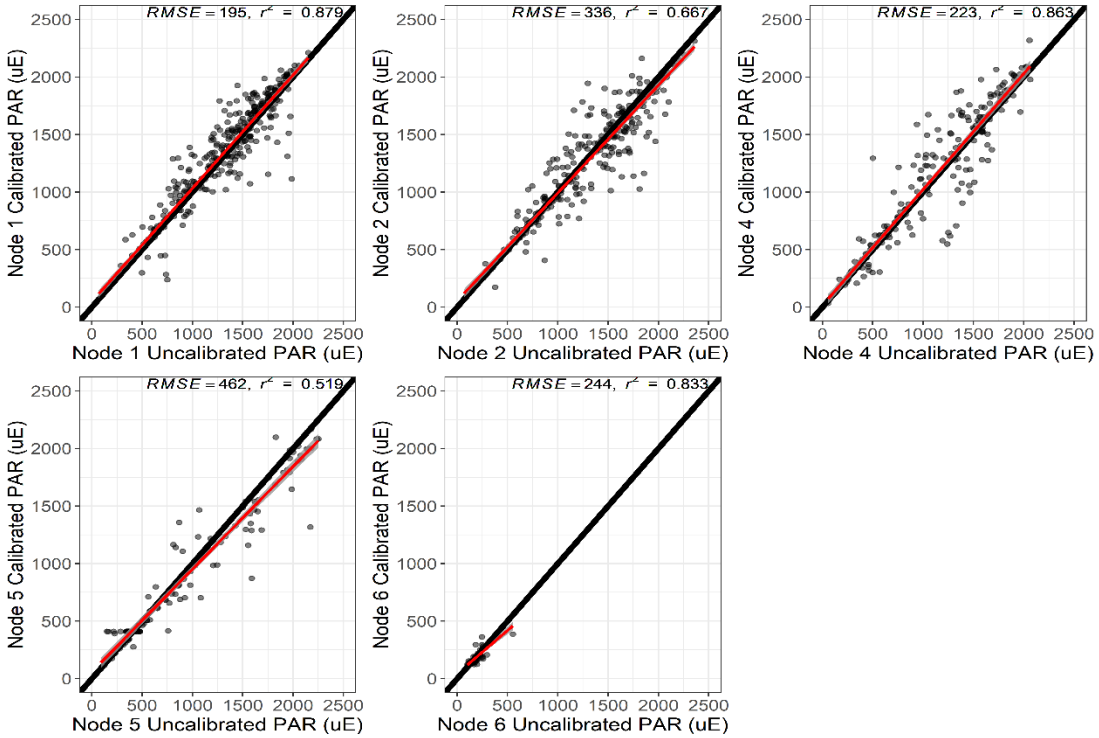

(Figure 2-13)

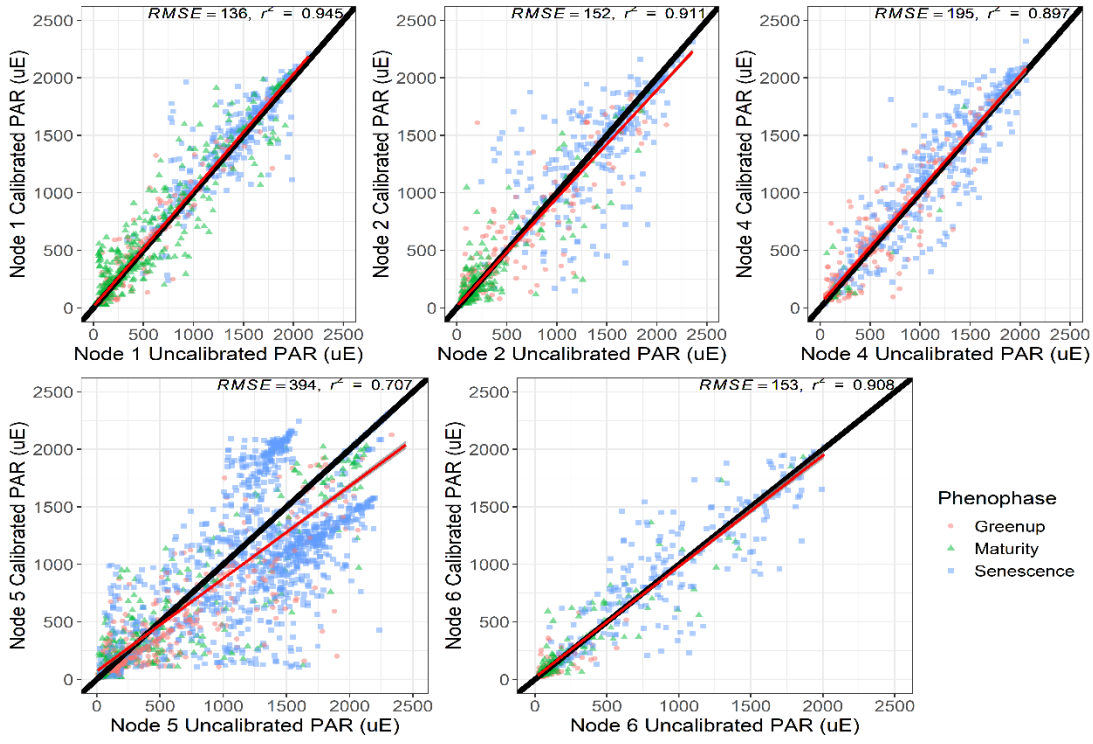

(Figure 2-14)

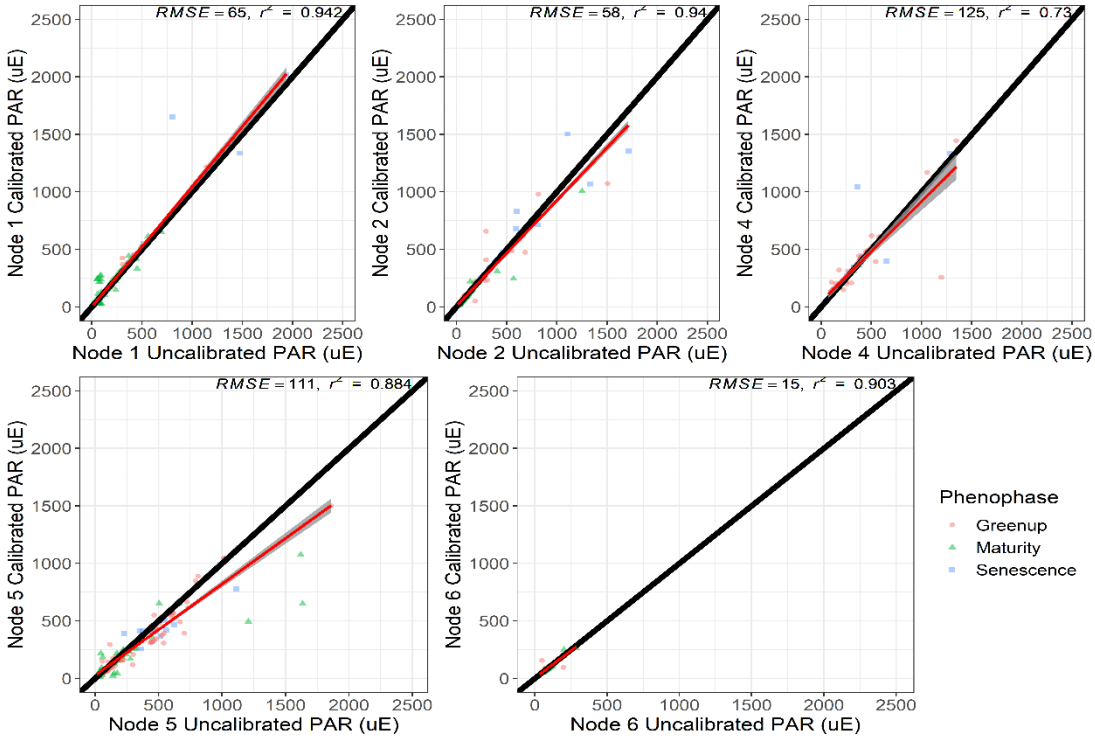

(Figure 2-15)

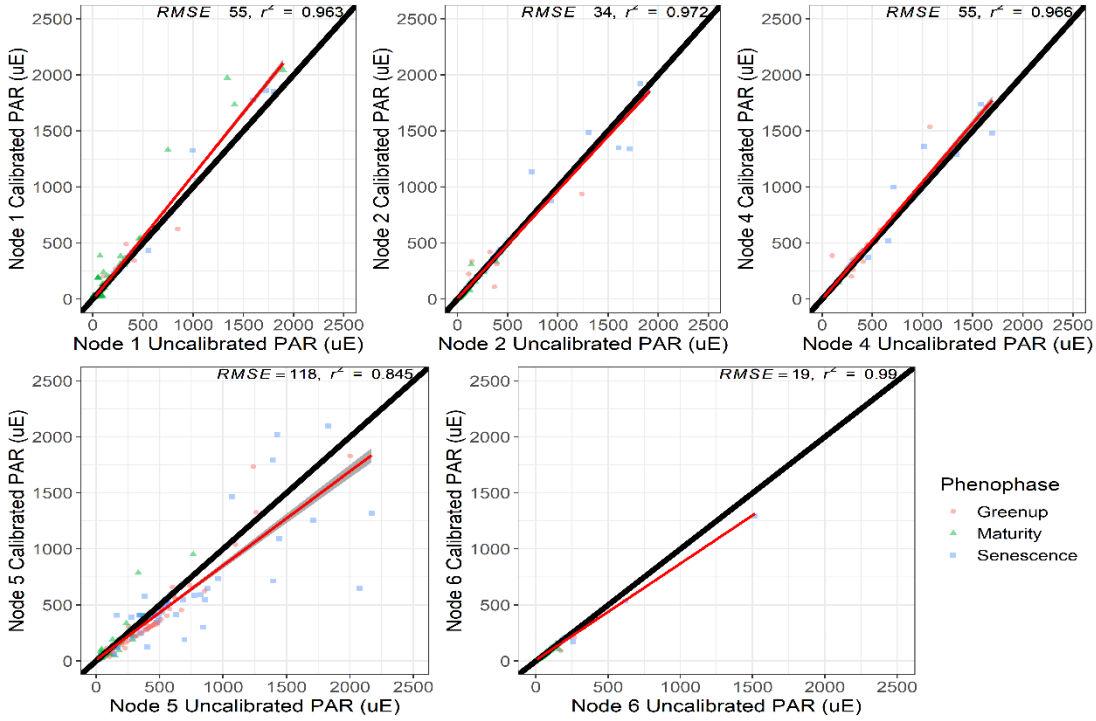

(Figure 2-16)

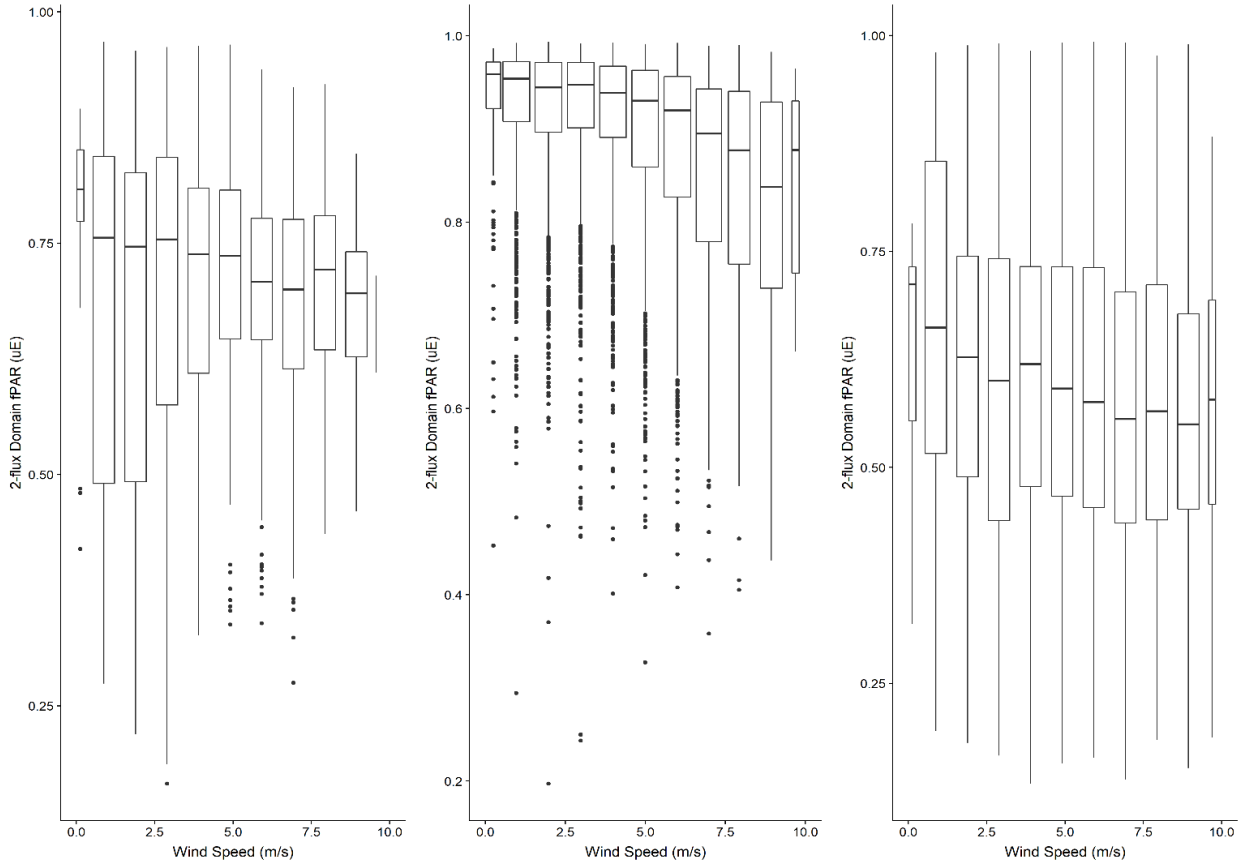
1.00
0.75
0.50
0.25
2-flux Domain fPAR (uE)
0.0
2.5
5.0
7.5
10.0
Wind Speed (m/s)
1.0
0.8
0.6
0.4
0.2
2-flux Domain fPAR (uE)
0.0
2.5
5.0
7.5
10.0
Wind Speed (m/s)
1.00
0.75
0.50
0.25
2-flux Domain fPAR (uE)
0.0
2.5
5.0
7.5
10.0
Wind Speed (m/s)

(Figure 2-17)

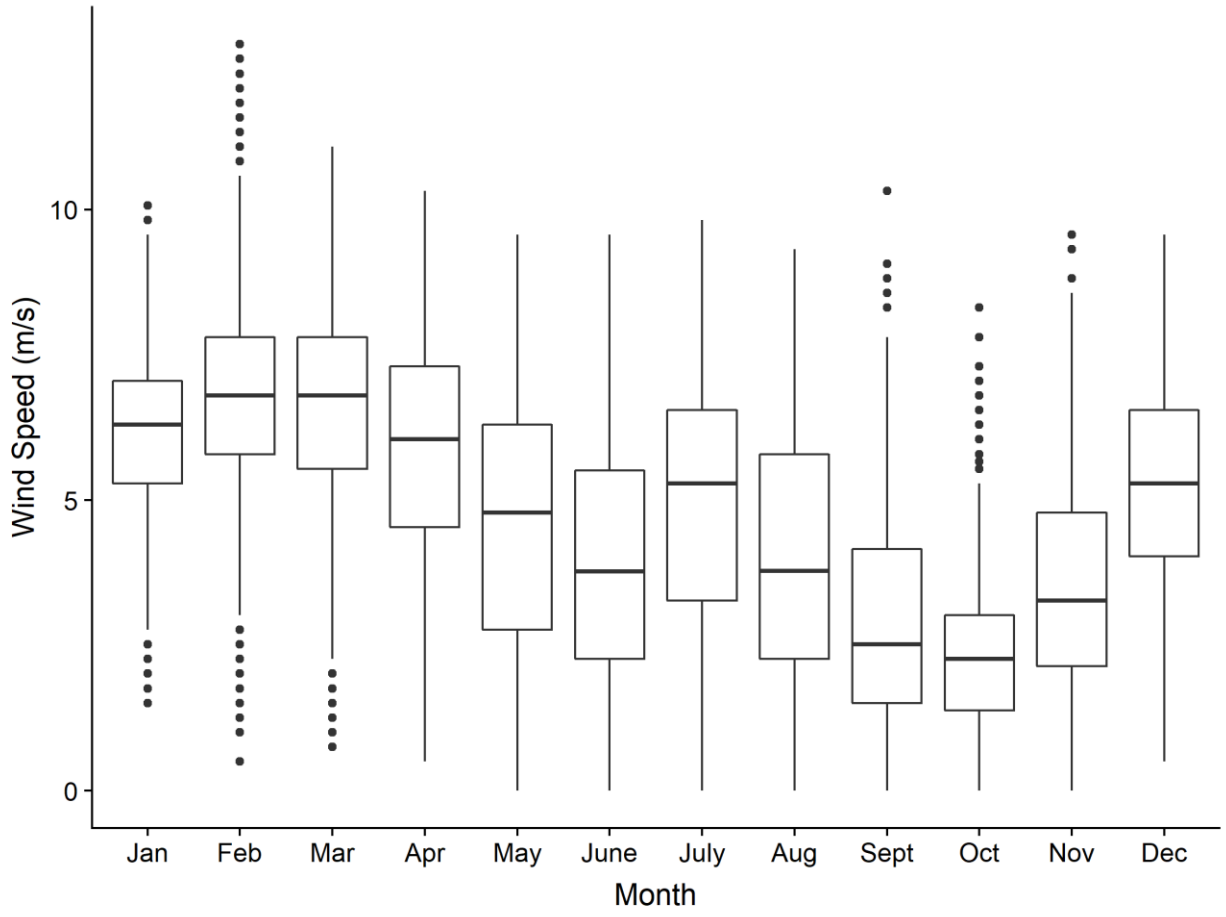

Literature Cited:

Ahl, D. E., Gower, S. T., Burrows, S. N., Shabanov, N. V., Myneni, R. B., & Knyazikhin, Y. (2006). Monitoring spring canopy phenology of a deciduous broadleaf forest using MODIS. *Remote Sensing of Environment*, *104*(1), 88–95. https://doi.org/10.1016/J.RSE.2006.05.003

Akitsu, T., Nasahara, K. N., Hirose, Y., Ijima, O., & Kume, A. (2017). Quantum sensors for accurate and stable long-term photosynthetically active radiation observations. *Agricultural and Forest Meteorology*, *237–238*, 171–183. https://doi.org/10.1016/J.AGRFORMET.2017.01.011

Apogee Quantum Sensor Calibration Certificate. (2019).

Asner, G. P., & Wessman, C. A. (1997). Scaling PAR absorption from the leaf to landscape level in spatially heterogeneous ecosystems. *Ecological Modelling*, *103*(1), 81–97. https://doi.org/10.1016/S0304-3800(97)00080-X

Atkins, J. W., Fahey, R. T., Hardiman, B. H., & Gough, C. M. (2018). Forest Canopy Structural Complexity and Light Absorption Relationships at the Subcontinental Scale. *Journal of*

Geophysical Research: Biogeosciences, *123*(4), 1387–1405. https://doi.org/10.1002/2017JG004256

Cai, Z. Q., Schnitzer, S. A., & Bongers, F. (2009). Seasonal differences in leaf-level physiology give lianas a competitive advantage over trees in a tropical seasonal forest. *Oecologia*, *161*(1), 25–33. https://doi.org/10.1007/s00442-009-1355-4

Campos, F. A. (2018). *A Synthesis of Long-Term Environmental Change in Santa Rosa, Costa Rica*. https://doi.org/10.1007/978-3-319-98285-4_16

Carrara, A., Kolari, P., Op De Beeck, M., Arriga, N., Berveiller, D., Dengel, S., … Biraud, S. C. (2018). Radiation measurements at ICOS ecosystem stations. *Int. Agrophys*, *32*, 589–605. https://doi.org/10.1515/intag-2017-0049

Castillo-Núñez, M., Sánchez-Azofeifa, G. A., Croitoru, A., Rivard, B., Calvo-Alvarado, J., & Dubayah, R. O. (2011). Delineation of secondary succession mechanisms for tropical dry forests using LiDAR. *Remote Sensing of Environment*, *115*(9), 2217–2231. https://doi.org/10.1016/j.rse.2011.04.020

Chadwick, R., Good, P., Martin, G., & Rowell, D. P. (2016). Large rainfall changes consistently projected over substantial areas of tropical land. *Nature Climate Change*, *6*(2), 177–181. https://doi.org/10.1038/nclimate2805

Chazdon, R. L., & Fetcher, N. (1984). Photosynthetic Light Environments in a Lowland Tropical Rain Forest in Costa Rica. In *The Journal of Ecology* (Vol. 72). https://doi.org/10.2307/2260066

Chen, J. M. (1996). Canopy architecture and remote sensing of the fraction of photosynthetically active radiation absorbed by boreal conifer forests. *IEEE Transactions on Geoscience and Remote Sensing*, *34*(6), 1353–1368. https://doi.org/10.1109/36.544559

Claverie, M., Vermote, E. F., Weiss, M., Baret, F., Hagolle, O., & Demarez, V. (2013). Validation of coarse spatial resolution LAI and FAPAR time series over cropland in southwest France. *Remote Sensing of Environment*, *139*, 216–230. https://doi.org/10.1016/j.rse.2013.07.027

Cliff, N. (1993). Dominance statistics: Ordinal analyses to answer ordinal questions. *Psychological Bulletin*, *114*(3), 494.

D'Odorico, P., Gonsamo, A., Pinty, B., Gobron, N., Coops, N., Mendez, E., & Schaepman, M. E. (2014). Intercomparison of fraction of absorbed photosynthetically active radiation products derived from satellite data over Europe. *Remote Sensing of Environment*, *142*, 141–154. https://doi.org/10.1016/j.rse.2013.12.005

Disney, M., Lewis, P., & North, P. (2000). Monte Carlo ray tracing in optical canopy reflectance modelling. *Remote Sensing Reviews*, *18*(February), 163–196. https://doi.org/10.1080/02757250009532389

Doktor, D., Bondeau, A., Koslowski, D., & Badeck, F. W. (2009). Influence of heterogeneous landscapes on computed green-up dates based on daily AVHRR NDVI observations. *Remote Sensing of Environment*, *113*(12), 2618–2632. https://doi.org/10.1016/j.rse.2009.07.020

Fensholt, R., Sandholt, I., & Rasmussen, M. S. (2004). Evaluation of MODIS LAI, fAPAR and the relation between fAPAR and NDVI in a semi-arid environment using in situ measurements. *Remote Sensing of Environment*, *91*(3–4), 490–507. https://doi.org/10.1016/J.RSE.2004.04.009

GCOS. (2011). *WORLD METEOROLOGICAL ORGANIZATION INTERGOVERNMENTAL OCEANOGRAPHIC COMMISSION SYSTEMATIC OBSERVATION REQUIREMENTS FOR SATELLITE-BASED DATA PRODUCTS FOR CLIMATE 2011 Update Supplemental details to the satellite-based component of the "Implementation Pl*. Retrieved from https://library.wmo.int/doc_num.php?explnum_id=3710

Gobron, N., Pinty, B., Aussedat, O., Chen, J. M., Cohen, W. B., Fensholt, R., … Widlowski, J. L. (2006a). Evaluation of fraction of absorbed photosynthetically active radiation products for different canopy radiation transfer regimes: Methodology and results using Joint Research Center products derived from SeaWiFS against ground-based estimations. *Journal of Geophysical Research Atmospheres*, *111*(13), D13110. https://doi.org/10.1029/2005JD006511

Gobron, N., Pinty, B., Aussedat, O., Chen, J. M., Cohen, W. B., Fensholt, R., … Widlowski, J. L. (2006b). Evaluation of fraction of absorbed photosynthetically active radiation products for different canopy radiation transfer regimes: Methodology and results using Joint Research Center products derived from SeaWiFS against ground-based estimations. *Journal of Geophysical Research Atmospheres*, *111*(13), 1–15. https://doi.org/10.1029/2005JD006511

Goward, S. N., & Huemmrich, K. F. (1992). Vegetation canopy PAR absorptance and the normalized difference vegetation index: An assessment using the SAIL model. *Remote Sensing of Environment*, *39*(2), 119–140. https://doi.org/10.1016/0034-4257(92)90131-3

Gower, S. T., Kucharik, C. J., & Norman, J. M. (1999). Direct and indirect estimation of leaf area index, f(APAR), and net primary production of terrestrial ecosystems. *Remote Sensing of Environment*, *70*(1), 29–51. https://doi.org/10.1016/S0034-4257(99)00056-5

Gu, L., Baldocchi, D., Verma, S. B., Black, T. A., Vesala, T., Falge, E. M., & Dowty, P. R. (2002). Advantages of diffuse radiation for terrestrial ecosystem productivity. *Journal of Geophysical Research: Atmospheres*, *107*(D6), ACL 2-1-ACL 2-23. https://doi.org/10.1029/2001JD001242

Hwang, T., Gholizadeh, H., Sims, D. A., Novick, K. A., Brzostek, E. R., Phillips, R. P., … Rahman, A. F. (2017). Capturing species-level drought responses in a temperate deciduous forest using ratios of photochemical reflectance indices between sunlit and shaded canopies. *Remote Sensing of Environment*, *199*, 350–359. https://doi.org/10.1016/J.RSE.2017.07.033

Janzen, D. H. (1988). Tropical dry forests. *Biodiversity*, 130–137.

Janzen, Daniel H. (2000). Costa Rica's Area de Conservación Guanacaste: A long march to survival through non-damaging biodevelopment. *Biodiversity*, *1*(2), 7–20. https://doi.org/10.1080/14888386.2000.9712501

Janzen, Daniel H, & Hallwachs, W. (2016). Biodiversity Conservation History and Future in Costa Rica: The Case of Área de Conservación Guanacaste (ACG). *Costa Rican*

Ecosystems, 290.

JCGM. (2008). *Evaluation of measurement data-Guide to the expression of uncertainty in measurement Évaluation des données de mesure-Guide pour l'expression de l'incertitude de mesure*. Retrieved from www.bipm.org

Kalácska, M., Calvo-Alvarado, J. C., & Sánchez-Azofeifa, G. a. (2005). Calibration and assessment of seasonal changes in leaf area index of a tropical dry forest in different stages of succession. *Tree Physiology*, *25*(6), 733–744. https://doi.org/10.1093/treephys/25.6.733

Kalacska, M. E. R., Sanchez-Azofeifa, G. a, & … J. C. C.-. (2005). Effects of Season and Successional Stage on Leaf Area Index and Spectral Vegetation Indices in Three …. *Biotropica*, *37*(4), 486–496. Retrieved from http://www.ingentaconnect.com/content/bsc/btp/2005/00000037/00000004/art00002

Kalacska, M., Sanchez-Azofeifa, G. A., Calvo-Alvarado, J. C., Quesada, M., Rivard, B., & Janzen, D. H. (2004). Species composition, similarity and diversity in three successional stages of a seasonally dry tropical forest. *Forest Ecology and Management*, *200*(1–3), 227–247. https://doi.org/10.1016/j.foreco.2004.07.001

Kalácska, M., Sánchez-Azofeifa, G. A., Rivard, B., Calvo-Alvarado, J. C., Journet, A. R. P., Arroyo-Mora, J. P., & Ortiz-Ortiz, D. (2004). Leaf area index measurements in a tropical moist forest: A case study from Costa Rica. *Remote Sensing of Environment*, *91*(2), 134–152. https://doi.org/10.1016/j.rse.2004.02.011

Knyazikhin, Y., Martonchik, J. V., Myneni, R. B., Diner, D. J., & Running, S. W. (1998). Synergistic algorithm for estimating vegetation canopy leaf area index and fraction of absorbed photosynthetically active radiation from MODIS and MISR data. *Journal of Geophysical Research*, *103*(D24), 32257. https://doi.org/10.1029/98JD02462

Leuchner, M., Hertel, C., & Menzel, A. (2011). Spatial variability of photosynthetically active radiation in European beech and Norway spruce. *Agricultural and Forest Meteorology*, *151*(9), 1226–1232. https://doi.org/10.1016/J.AGRFORMET.2011.04.014

Li, J., & Heap, A. D. (2014). Spatial interpolation methods applied in the environmental sciences: A review. *Environmental Modelling & Software*, *53*, 173–189. https://doi.org/10.1016/J.ENVSOFT.2013.12.008

Li, Wei, Cao, S., Campos-Vargas, C., & Sanchez-Azofeifa, A. (2017). Identifying tropical dry forests extent and succession via the use of machine learning techniques. *International Journal of Applied Earth Observation and Geoinformation*, *63*(April), 196–205. https://doi.org/10.1016/j.jag.2017.08.003

Li, Wenjuan, & Fang, H. (2015). Estimation of direct, diffuse, and total FPARs from Landsat surface reflectance data and ground-based estimates over six FLUXNET sites. *Journal of Geophysical Research: Biogeosciences*, *120*(1), 96–112. https://doi.org/10.1002/2014JG002754

Li, Wenjuan, Weiss, M., Waldner, F., Defourny, P., Demarez, V., Morin, D., … Baret, F. (2015). A generic algorithm to estimate LAI, FAPAR and FCOVER variables from SPOT4_HRVIR and landsat sensors: Evaluation of the consistency and comparison with

ground measurements. *Remote Sensing*, *7*(11), 15494–15516. https://doi.org/10.3390/rs71115494

Majasalmi, T. (2015). *Estimation of leaf area index and the fraction of absorbed photosynthetically active radiation in a boreal*. https://doi.org/10.14214/df.187

Majasalmi, T., Stenberg, P., & Rautiainen, M. (2017). Comparison of ground and satellite-based methods for estimating stand-level fPAR in a boreal forest. *Agricultural and Forest Meteorology*, *232*, 422–432. https://doi.org/10.1016/j.agrformet.2016.09.007

McDowell, N. G., Coops, N. C., Beck, P. S. A., Chambers, J. Q., Gangodagamage, C., Hicke, J. A., … Allen, C. D. (2015). Global satellite monitoring of climate-induced vegetation disturbances. *Trends in Plant Science*. https://doi.org/10.1016/j.tplants.2014.10.008

Moran, P. A. P. (1950). Notes on Continuous Stochastic Phenomena. *Biometrika*, *37*(1/2), 17. https://doi.org/10.2307/2332142

Myneni, R. B., Hoffman, S., Knyazikhin, Y., Privette, J. L., Glassy, J., Tian, Y., … Running, S. W. (2002). Global products of vegetation leaf area and fraction absorbed PAR from year one of MODIS data. *Remote Sensing of Environment*, *83*(1–2), 214–231. https://doi.org/10.1016/S0034-4257(02)00074-3

Myneni, R.B., Knyazikhin, Y., Privette, J. L., Running, S. W., Nemani, R., Zhang, Y., … Votava, P. (1999). MODIS Leaf Area Index (LAI) And Fraction Of Photosynthetically Active Radiation Absorbed By Vegetation (FPAR) Product. *Modis Atbd*, *Version 4.*(4.0), 130. https://doi.org/http://eospso.gsfc.nasa.gov/atbd/modistables.html

Myneni, Ranga B. (1997). Estimation of global leaf area index and absorbed par using radiative transfer models. *IEEE Transactions on Geoscience and Remote Sensing*, *35*(6), 1380–1393. https://doi.org/10.1109/36.649788

Nestola, E., Sánchez-Zapero, J., Latorre, C., Mazzenga, F., Matteucci, G., Calfapietra, C., & Camacho, F. (2017a). Validation of PROBA-V GEOV1 and MODIS C5 & C6 fAPAR products in a deciduous beech forest site in Italy. *Remote Sensing*, *9*(2). https://doi.org/10.3390/rs90201026

Nestola, E., Sánchez-Zapero, J., Latorre, C., Mazzenga, F., Matteucci, G., Calfapietra, C., & Camacho, F. (2017b). Validation of PROBA-V GEOV1 and MODIS C5 & C6 fAPAR products in a deciduous beech forest site in Italy. *Remote Sensing*, *9*(2), 126. https://doi.org/10.3390/rs90201026

Nightingale, J., Schaepman-Strub, G., & Nickeson, J. (2011). Assessing satellite-derived land product quality for Earth system science applications: overview of the CEOS LPV sub-group. *Proceedings of the 34th International Symposium on Remote Sensing of Environment*, (1).

Pastorello, G. Z., Sanchez-Azofeifa, G. A., & Nascimento, M. A. (2011). Enviro-Net : A Network of Ground-based Sensors for Tropical Dry Forests in the Americas. *Sensors*, *11.6*, 6454–6479.

Pickett-Heaps, C. A., Canadell, J. G., Briggs, P. R., Gobron, N., Haverd, V., Paget, M. J., … Raupach, M. R. (2014). Evaluation of six satellite-derived Fraction of Absorbed

Photosynthetic Active Radiation (FAPAR) products across the Australian continent. *Remote Sensing of Environment*, *140*, 241–256. https://doi.org/10.1016/j.rse.2013.08.037

Pinty, B., Jung, M., Kaminski, T., Lavergne, T., Mund, M., Plummer, S., … Widlowski, J. L. (2011). Evaluation of the JRC-TIP 0.01° products over a mid-latitude deciduous forest site. *Remote Sensing of Environment*, *115*(12), 3567–3581. https://doi.org/10.1016/j.rse.2011.08.018

Portillo-Quintero, C. A., & Sánchez-Azofeifa, G. A. (2010). Extent and conservation of tropical dry forests in the Americas. *Biological Conservation*, *143*(1), 144–155. https://doi.org/10.1016/j.biocon.2009.09.020

Power, M. J., Whitney, B. S., Mayle, F. E., Neves, D. M., de Boer, E. J., & Maclean, K. S. (2016). Fire, climate and vegetation linkages in the bolivian chiquitano seasonally dry tropical forest. *Philosophical Transactions of the Royal Society B: Biological Sciences*, *371*(1696). https://doi.org/10.1098/rstb.2015.0165

Putzenlechner, B., Marzahn, P., Kiese, R., Ludwig, R., & Sanchez-Azofeifa, A. (2019). Assessing the variability and uncertainty of two-flux FAPAR measurements in a conifer-dominated forest. *Agricultural and Forest Meteorology*, *264*(October 2018), 149–163. https://doi.org/10.1016/j.agrformet.2018.10.007

QUANTUM SENSOR Models SQ-100 and SQ-300 Series (including SS models). (2019). Retrieved from https://www.apogeeinstruments.com/content/SQ-100-300-manual.pdf

Rankine, C. J. (2016). *Monitoring Seasonal and Secondary Succession Processes in Deciduous Forests using Near-Surface Optical Remote Sensing and Wireless Sensor Networks*. 167. https://doi.org/10.7939/R32Z12V30

Rawat, P., Singh, K. D., Chaouchi, H., & Bonnin, J. M. (2014). Wireless sensor networks: A survey on recent developments and potential synergies. *Journal of Supercomputing*, *68*(1), 1–48. https://doi.org/10.1007/s11227-013-1021-9

Sanchez-Azofeifa, A., Antonio Guzmán, J., Campos, C. A., Castro, S., Garcia-Millan, V., Nightingale, J., & Rankine, C. (2017). Twenty-first century remote sensing technologies are revolutionizing the study of tropical forests. *Biotropica*, Vol. 49, pp. 604–619. https://doi.org/10.1111/btp.12454

Sanchez-Azofeifa, G. A., Rankine, C., do Espirito Santo, M. M., Fatland, R., & Garcia, M. (2011). Wireless Sensing Networks for Environmental Monitoring: Two Case Studies from Tropical Forests. *2011 IEEE Seventh International Conference on EScience*, (December 2011), 70–76. https://doi.org/10.1109/eScience.2011.18

Sánchez-Azofeifa, G. Arturo, Kalácska, M., Espírito-Santo, M. M. do, Fernandes, G. W., & Schnitzer, S. (2009). Tropical dry forest succession and the contribution of lianas to wood area index (WAI). *Forest Ecology and Management*, *258*(6), 941–948. https://doi.org/10.1016/j.foreco.2008.10.007

Sánchez-Azofeifa, G. Arturo, Quesada, M., Rodríguez, J. P., Nassar, J. M., Stoner, K. E., Castillo, A., … Cuevas-Reyes, P. (2005). Research priorities for neotropical dry forests. *Biotropica*, *37*(4), 477–485. https://doi.org/10.1111/j.1744-7429.2005.00066.x

Sánchez-Azofeifa, G., Kalacska, M., Quesada, M., Calvo-Alvarado, J. C., Nassar, J. M., & Rodríguez, J. P. (2005). Need for Integrated Research for a Sustainable Future in Tropical Dry Forests. *Conservation Biology*, *19*(2), 285–286. https://doi.org/10.1111/j.1523-1739.2005.s01

Sánchez-Azofeifa, Gerardo Arturo, Guzmán-Quesada, J. A., Vega-Araya, M., Campos-Vargas, C., Durán, S. M., D'Souza, N., … Sharp, I. (2017). Can terrestrial laser scanners (TLSs) and hemispherical photographs predict tropical dry forest succession with liana abundance? *Biogeosciences*, *14*(4), 977–988. https://doi.org/10.5194/bg-14-977-2017

Senna, M. C. A. (2005). Fraction of photosynthetically active radiation absorbed by Amazon tropical forest: A comparison of field measurements, modeling, and remote sensing. *Journal of Geophysical Research*, *110*(G1), G01008. https://doi.org/10.1029/2004JG000005

Shabanov, N. V., Wang, Y., Buermann, W., Dong, J., Hoffman, S., Smith, G. R., … Myneni, R. B. (2003). Effect of foliage spatial heterogeneity in the MODIS LAI and FPAR algorithm over broadleaf forests. *Remote Sensing of Environment*, *85*(4), 410–423. https://doi.org/10.1016/S0034-4257(03)00017-8

Steinberg, D., Goetz, S., & Hyer, E. (2006). Validation of MODIS F/sub PAR/products in boreal forests of Alaska. *Geoscience and Remote …*, *44*(7), 1–11. Retrieved from http://ieeexplore.ieee.org/xpls/abs_all.jsp?arnumber=1645282

Stenberg, P., Mõttus, M., & Rautiainen, M. (2016). Photon recollision probability in modelling the radiation regime of canopies — A review. *Remote Sensing of Environment*, *183*, 98–108. https://doi.org/10.1016/J.RSE.2016.05.013

Thomas, V., Finch, D. A., McCaughey, J. H., Noland, T., Rich, L., & Treitz, P. (2006). Spatial modelling of the fraction of photosynthetically active radiation absorbed by a boreal mixedwood forest using a lidar-hyperspectral approach. *Agricultural and Forest Meteorology*, *140*(1–4), 287–307. https://doi.org/10.1016/j.agrformet.2006.04.008

Van der Zande, D., Stuckens, J., Verstraeten, W. W., Muys, B., & Coppin, P. (2010). Assessment of light environment variability in broadleaved forest canopies using terrestrial laser scanning. *Remote Sensing*, *2*(6), 1564–1574. https://doi.org/10.3390/rs2061564

Verhoef, W. (1984). Light scattering by leaf layers with application to canopy reflectance modeling: The SAIL model. *Remote Sensing of Environment*, *16*(2), 125–141. https://doi.org/10.1016/0034-4257(84)90057-9

Vierling, L. A., & Wessman, C. A. (2000). Photosynthetically active radiation heterogeneity within a monodominant Congolese rain forest canopy. *Agricultural and Forest Meteorology*, *103*(3), 265–278. https://doi.org/10.1016/S0168-1923(00)00129-5

Walter, I. A. (Environmental and W. R. I. of the A. S. of C. E., Allen, R. . (Environmental and W. R. I. of the A. S. of C. E., Elliot, R. (Environmental and W. R. I. of the A. S. of C. E., Itenfisu, D. (Environmental and W. R. I. of the A. S. of C. E., Brown, P. (Environmental and W. R. I. of the A. S. of C. E., Jensen, M. E. (Environmental and W. R. I. of the A. S. of C. E., … Wright, J. L. (Environmental and W. R. I. of the A. S. of C. E. (2002). THE ASCE STANDARDIZED REFERENCE EVAPOTRANSPIRATION EQUATION Environmental and Water Resources Institute of the American Society of Civil Engineers Standardization

of Reference Evapotranspiration Task Committee. *American Society of Civil Engineers*, 1–51.

Wang, H. (2006). Extending the Linear Model with R: Generalized Linear, Mixed Effects and Nonparametric Regression Models Edited by Faraway J. J. *Biometrics*, *62*(4), 1278–1278. https://doi.org/10.1111/j.1541-0420.2006.00596_12.x

Widlowski, J.-L. (2010). On the bias of instantaneous FAPAR estimates in open-canopy forests. *Agricultural and Forest Meteorology*, *150*(12), 1501–1522. https://doi.org/10.1016/J.AGRFORMET.2010.07.011

Wilson, K. B., Baldocchi, D. D., & Hanson, P. J. (2001). Leaf age affects the seasonal pattern of photosynthetic capacityand net ecosystem exchange of carbon in a deciduous forest. *Plant, Cell and Environment*, *24*(6), 571–583. https://doi.org/10.1046/j.0016-8025.2001.00706.x

Younis, M., & Akkaya, K. (2008). Strategies and techniques for node placement in wireless sensor networks: A survey. *Ad Hoc Networks*, *6*(4), 621–655. https://doi.org/10.1016/J.ADHOC.2007.05.003

Zelazowski, P., Malhi, Y., Huntingford, C., Sitch, S., & Fisher, J. B. (2011). Changes in the potential distribution of humid tropical forests on a warmer planet. *Philosophical Transactions of the Royal Society A: Mathematical, Physical and Engineering Sciences*, *369*(1934), 137–160. https://doi.org/10.1098/rsta.2010.0238

Zhang, R., Zhou, Y., Luo, H., Wang, F., & Wang, S. (2017). Estimation and analysis of spatiotemporal dynamics of the net primary productivity integrating efficiency model with process model in Karst area. *Remote Sensing*, *9*(5). https://doi.org/10.3390/rs9050477

Zhang, X., Friedl, M. A., Schaaf, C. B., Strahler, A. H., Hodges, J. C. F., Gao, F., … Huete, A. (2003). Monitoring vegetation phenology using MODIS. *Remote Sensing of Environment*. https://doi.org/10.1016/S0034-4257(02)00135-9

Chapter 3: Employing wavelet-transforms and cross-wavelet analysis to validate the MODIS fPAR time-series over a tropical dry forest.

Abstract

The fraction of Photosynthetic Active Radiation (fPAR) is a component of determining the Photosynthetic Active Radiation (PAR) absorbed by vegetation for use in photosynthesis and is a crucial component of determining carbon flux products. Measuring this variable via satellite in the Northern Hemisphere has shown promising results, but still requires validation in the tropical climes, specifically in the Tropical Dry Forests which represent 42% of all tropical forests. By employing a Wireless Sensor Network, this study uses an *in-situ* Green fPAR product established in the Santa Rosa National Park Environmental Monitoring Super-site (SRNP-EMSS) for validating the MODIS Terra, Aqua, and MCD15A3H fPAR products between 2013-2017. This study implements both a Savitsky-Golay derivate-based smoothing method and continuous univariate wavelet transforms, to conduct cross-wavelet analysis to compare the phenometric variables of the *in-situ* and the MODIS fPAR products. The MODIS fPAR products are incapable of accurately predicting the onset of green-up or senescence, with detection of these events typically being delayed by 18-55 days; however, despite the temporal offset MODIS replicates the annual and interseasonal patterns detected by the *in-situ* product with significance ($p < 0.05$). These patterns broke down with the introduction of a hurricane, as the MODIS fPAR product was incapable of detecting a suppressed dry-season in 2016, instead over-predicting the extent of drought for that season. This study, therefore, illustrates the inflexibility and insensitivity of the MODIS observations, and therefore these products should not be relied upon to give feedback to rapid changes in the phenological cycle of tropical dry-forests or for the timing of phenological events.

Keywords: fPAR, tropical-dry forests, MODIS, wavelets, cross-wavelet analysis, phenometrics

1.0 – Introduction

Tropical Dry Forests (TDFs) occupy 49% of the Pacific Coast of Meso and South America and account for over 40% of all tropical ecosystems globally (Portillo-Quintero et al., 2010; Sánchez-Azofeifa et al., 2005). TDFs are deciduous broadleaf forests that undergo a distinct vegetation phenology cycle, driven by a minimum of 3-months drought making them precipitation-driven

systems, unlike that of temperate deciduous forests. Despite playing a fundamental role in the biogeochemical cycling between the Earth's biosphere, atmosphere, hydrosphere and geosphere these forests are drastically underrepresented in the scientific literature (Sánchez-Azofeifa et al., 2005). As a consequence, this has left a gap in the knowledge of how TDFs vegetation phenology, which is important in the moderation of local and regional climate, storing carbon, driving biomass productivity, and impacting the carbon flux exchange in the tropics, influences global dynamics or how it has behaved historically (Burguillos, et al., 2008; Cai, et al., 2009; Castro, et al., 2018; Pennington, 2010).

The semi-arid regions that tropical dry forests occupy have been marked by increasingly erratic and unpredictable climatic patterns, enhancing the stressors that already exist for this ecosystem that balances between water-scarcity and drought (Meir & Pennington, 2011). The erratic nature is predicted to get worse, as climate models project that the TDFs will experience an increase in temperatures between 1°C and 6°C; however, these models cannot predict the direction or magnitude of precipitation changes (Magrin et al., 2014). Given that TDFs are precipitation-driven, highly fragmented, secondary-growth forests, which are chronically degraded, suffering from insufficient conservation efforts, (Arroyo-Mora, et al., 2005; Calvo-Alvarado, et al., 2009; Sánchez-Azofeifa et al., 2005) understanding the changes in climate and the response of TDF forest phenology are increasingly important, because without understanding TDF resiliency under a changing climate, it is difficult to formulate land management practices (Stan & Sanchez-Azofeifa, 2019).

TDFS are exposed to an environment in which there are extended periods of high solar irradiance and little precipitation, leading to a greater mean annual loss of water through evapotranspiration than is received through precipitation. This has led to the biome being dominated by deciduous trees, as the seasonal foliage loss prevents loss of water through evapotranspiration until the first seasonal rains return, signalling these trees to initiate bud-break (Lieberman, 1982; Reich & Borchert, 1984). To track this interplay between climate and phenology, a suite of models and remote sensing products has been developed, but an area of discrepancy for these models is in the portioning of solar irradiance through the canopy (Fisher, et al., 2014; McDowell et al., 2015; Myneni et al., 1999). These models attempt to quantify the carbon storage and sequestration potential of ecosystems, using proxies like gross primary productivity, net ecosystem exchange, and above-ground biomass (Chazdon et al., 2016; J.

Demarty et al., 2007; Demarty & Bastien, 2011). Determining carbon and productivity values is often conducted by deriving them from vegetation indices, such as the Normalized Difference Vegetation Index (NDVI), Enhanced Vegetation Index (EVI), or the fraction of Photosynthetically Active Radiation (fPAR), as studies such as Zhang, et al., (2019) have connected these spectral indices with canopy dynamics (Lin et al., 2019; Peng et al., 2012; Phillips, Hansen, & Flather, 2008). The fact that these indices are widely available from remote sensing platforms, also gives them the ubiquity for employment (Jensen, 1986; Myneni et al., 1999).

The fraction of Photosynthetic Active Radiation is a variable that quantifies the amount of Photosynthetic Active Radiation (PAR; 400-700nm) that has been absorbed by photosynthesizing vegetation (Gower, et al., 1999). This has led fPAR to become a core component in estimating gross primary productivity, making it an essential element for carbon flux models, and can be determined either using satellite or *in-situ* sensors (Zhang et al., 2017; Zhang et al., 2019). Despite satellite fPAR having been validated across the globe, it is less accurate in places such as tropical forests which experience heavy cloud cover (Zhao, Heinsch, Nemani, & Running, 2005). Even with its global validation, MODIS fPAR products have not been validated with *in-situ* data over TDF's, a unique ecosystem that contributes heavily to global carbon fluxes. In part, this lack of validation is due to few long-term monitoring sites that are equipped with fPAR sensors existing. However, in the Santa Rosa National Park Environmental Monitoring Super-site (SRNP-EMSS) one site does exist, which is located in the TDF in Guanacaste, Costa Rica.

Testing and validating phenology time-series have often relied upon curve-fitting algorithms for determining the start and end of season dates. Curve-fitting methods typically determine a rate-of-change to determine the start of season and end of season metrics, and therefore ensure that rapid changes in the curve are identified and properly characterized. These methods were used by Zhang et al., (2003) to identify different land cover types based on the phenometrics derived from the curve-fitting of green leaf phenology, such as the start of season, dry season minimums, green phenology maximums and the amplitude of those maximums. The strengths of this method relies on its ability to determine absolute dates for certain phenometrics, making it possible to quantify the differences between two products or for different regions, but do not effectively analyze the synchronicity or behaviour of inter and intra-seasonal events.

When analyzing multiscale and non-stationary processes wavelet transforms (WTs) have proven to excel at describing these (Percival & Walden, 2006). The advantage of employing a wavelet transform is that it provides a method for time-frequency localization that is scale independent, and capable of adapting to non-stationary processes, unlike Fourier transforms or windowed Fourier transforms which may obscure information due to its non-stationarity (Gabor, 1946; Lau & Weng, 2002; Martínez & Gilabert, 2009). Wavelet transforms are described by a mother wavelet, which has a defined shape and frequency capable of transforming and translating continuously along a time-series, permitting the dissection of a time-series at different scales and resolutions. This flexibility in both the time and frequency domains, reveals patterns within the time-series according to the scale of the window that the wavelet is confined to; meaning, that narrow windows can be employed for capturing the presence of short-lived events (high-frequency variability), while broad-windows can capture low frequency events (Carvalho, 2001; Shumway & Stoffer, 2011; Torrence & Compo, 1998). Fortunately, the deconstruction of time-series into univariate wavelet transforms on different time-frequency scales does permit the cross-wavelet analysis of two or more univariate wavelets, to determine the coherence and multi-scale pattern recognition between these time-series (Grinsted, et al., 2004; Percival & Walden, 2006; Roesch & Schmidbauer, 2018; Torrence & Compo, 1998).

Given the gaps in knowledge surrounding the accuracy of satellite fPAR products in the TDF and the importance of this ecosystem to the global carbon system, it is imperative and integral to validate remote sensing fPAR with *in-situ* data at the SRNP-EMSS so that these uncertainties can be parameterized in future research and carbon models. Therefore, the purpose of this study is the following:

1. To determine the accuracy of the MODIS fPAR products in its estimation of phenological metrics such as the onset of green-up and senescence.
2. The capabilities of the MODIS fPAR product to detect intra-seasonal events and variation.
3. The capabilities of the MODIS fPAR product to detect inter-seasonal events and variation.
4. To determine the abilities of wavelet analysis for determining phenological cycles in TDFs.

2.0 Materials and Methods:

2.1 Study site

The SRNP-EMSS is a national park situated in the province of Guanacaste, Costa Rica (Figure 3-1). Hosted within the park is a transitional tropical dry forest (TDF), which, as described by Sánchez-Azofeifa et al., (2005) is a primarily deciduous forest that undergoes a distinct wet-dry seasonal cycle, where 900-2500mm of precipitation is unleashed during a 6 month period (June – December). During the first rains, initiating the green-up of the forest, two-stages of green-up can be exhibited, understorey green-up occurring prior to canopy green-up. The TDFs in the SRNP-EMSS are a mosaic of secondary TDFs at various stages of succession, due to the varied histories of anthropogenic uses and their integration into the park (Janzen, 1988; Janzen, 2000; Janzen & Hallwachs, 2016; Kalacska et al., 2004). Recently, an updated map was provided by Li, et al., (2017) which classifies the forest age stands within the SRNP-EMSS. Therefore, the wireless sensor network (WSN) site from which the *in-situ* Green fPAR data is provided is classified according to this map.

In the SRNP-EMSS there is a WSN encompassing an area of 75x65m (4875m^2) situated in an intermediate-stage forest. Intermediate-stage forests host the highest species diversity, largest variability in its canopy openness, and have significant differences in its species composition amongst themselves (Kalacska et al., 2004). To capture the canopy state of this forest, the WSN is equipped with 13 self-powered nodes that have temperature, relative humidity, soil moisture, and quantum PAR sensors that are located 1.3m above the forest floor; while, the height placement of these quantum sensors is standard practice (Nestola et al., 2017; Putzenlechner et al., 2019; Widlowski, 2010), due to the nature of TDFs, understorey vegetation may exceed the 1.3m height or vines and lianas may grow below the canopy, influencing the transmitted PAR measured at these locations. These Apogee SQ-110 quantum PAR sensors detect the amount of PAR transmitted through the canopy (Putzenlechner et al., 2019; Widlowski, 2010). The total incoming PAR (iPAR) is recorded at the local meteorological tower that is 200 m away from the WSN.

2.2 Data

To create an *in-situ* fPAR product for validating MODIS fPAR, this study estimates *2-flux fPAR* (Putzenlechner, et al., 2019; Widlowski, 2010) for the WSN by capturing data from both the

WSN and Tower in the SRNP-EMSS between the years 2013-2017. The WSN provides the PAR transmitted (tPAR) through the canopy which is not absorbed, reflected, or scattered by photosynthesizing vegetation (Widlowski, 2010) per node, while the tower collects iPAR which can be employed to calculate Green fPAR at each node for comparison against MODIS fPAR (Myneni, et al., 2015; Myneni et al., 1999). The *in-situ* product initially finds the 2-flux fPAR product using the equation (Putzenlechner et al., 2019; Widlowski, 2010), before converting it to Green fPAR:

$$2\ flux\ fPAR = \frac{iPAR_{tower} - tPAR_n}{iPAR_{tower}} \qquad 2.1$$

Where *n* represents each node. All fPAR values are filtered to based on small solar zenith angles ($27° < SZA < 60°$), low wind-speed ($WS < 3$m/s). The remaining fPAR values are adjusted according to the minimum fPAR values of the time-series. Based on the phenology of TDF's, this minimum *2-flux fPAR* value occurs during senescence when no photosynthesizing material remains and, consequently, any reported fPAR is an artifact of the scattering of photons or the interception of PAR by woody material (Reich & Borchert, 1984). Green fPAR is, therefore, calculated using the following formulae:

$$Green\ fPAR = t(2flux\ fPAR) - (2\ flux\ fPAR_{min}) \qquad 2.2$$

Where *t* represents each point in the time-series and $fPAR_{min}$ represents the absolute minimum value from the time-series. The *in-situ* Green fPAR product is then averaged across all the nodes (Green $fPAR_{Domain}$), creating an approximately 5000m^2 *in-situ* Green $fPAR_{Domain}$ product, that is spatially comparable for validating the MODIS fPAR (Steinberg, et al., 2006). The Green $fPAR_{Domain}$ was compared with both the Terra and Aqua satellites, matching *in-situ* observations with the pass-over times based on the NASA Satellite Overpass Predictor (Minnis, et al., 2008), but a linear regression analysis revealed that the two *in-situ* Green $fPAR_{Domain}$ products, yield similar results $R^2 = 0.968$, therefore, the study progresses using the *in-situ* Green $fPAR_{Domain}$ that is congruent with Terra overpass.

All MODIS-derived LAI and fPAR Collection 6 (Myneni et al., 2015) products were collected for the Network 1 WSN site between 2013-2017 using the ORNL DAAC subset tool (ORNL, 2018), and passed through the MODIS Quality Control filtering algorithm. The Terra (MOD15A2H) and Aqua (MYD15A2H) products are 8-day composites, whereas the

MCD15A3H product, is a hybridized 4-day composite taking data from both Terra and Aqua (Myneni & Park, 2015). These products are provided at 500m resolution from a sinusoidal grid and retrieve values based on the atmospherically-corrected L2G-Lite surface reflectance product, which also derives a Land Cover Classification (LCC) product. A Look-Up-Table in the main algorithm links the spectral reflectance values and LCC product to derive the MODIS fPAR (Knyazikhin et al., 1998; Myneni et al., 1999; Myneni & Park, 2015).

The resultant MODIS time-series was run through a Savitzky-Golay filter to create a temporally-smoothed and continuous time-series for comparison against the *in-situ* Green fPAR time-series. Savitzky-Golay filtering (Savitzky & Golay, 1964) adapts the MODIS fPAR time-series to reflect the upper-envelope of that time-series, reducing negative bias associated with clouds or poor atmospheric conditions (Cai, et al., 2017; Chen et al., 2004). Adaptation to the upper-envelope of the original MODIS fPAR time-series occurs through iteratively generating curves with weighted-averages that place lower weight on lower values of fPAR (Lange & Doktor, 2017; Savitzky & Golay, 1964). This method is implemented through the *R* package *'phenex'* (Lange and Doktor 2015). Finally, a moving-average interpolation is also applied to reduce the temporal frequency from an 8 or 4-day frequency, to a single day frequency, creating congruent time-series for analysis.

2.3 Derivative-based extraction of phenometrics, and calculation of other phenometrics.

To determine the precision of MODIS to precisely capture the phenological periods of a TDF at the SRNP-EMSS as represented by the *in-situ* Green fPAR product, phenometrics were extracted in two ways. A derivative-based approach to extract the dates for the onset of greenness and senescence based on the rate-of-change for the curvature of a wave, and a wavelet transformation. Zhang et al. (2003) breaks up the phenological cycle of a forest into four distinct phenophases: i) green-up which is the date upon which photosynthetic activity is first detected, ii) maturity described as the period at which leaves have reached maximum leaf area and maximum photosynthetic activity, iii) leaf senescence the date at which the photosynthetic activity of an ecosystems starts to decline rapidly, iv) canopy dormancy, the period at which no more photosynthetic activity is occurring within the environment. The onset of the green-up phase and the onset of senescence is determined when the rate of change between the maximum and minimum Green fPAR values crosses a threshold, calculated through the function

'*phenoPhase()'* from the package '*phenex'* (Lange and Doktor, 2015). Dormancy and maturity are determined by the $fPAR_{max}$ and $fPAR_{min}$ values during the time-series.

Other key phenometrics, such as the mean amount of photosynthesis (μfPAR), the amplitude of the annual phenological cycle (ΔfPAR) and $fPAR_{min}$ and $fPAR_{max}$ are also calculated for each growing season. These features were based on similar NDVI features derived from Martínez & Gilabert, (2009) study. The Mann-Kendall test is used to determine fPAR trend significance because the fPAR data is non-parametric (De Beurs & Henebry, 2005; Putzenlechner et al., 2019). The Mann-Kendall test is a widely used rank order based test, insensitive to any missing values it is easy to calculate and is robust against non-normality (De Beurs & Henebry, 2005; Martínez & Gilabert, 2009). The *Tau-b* coefficient is reported along with the significance and *p-values* to indicate the magnitude and strength of the trend.

2.4 Wavelet and cross-wavelet analysis of MODIS and in-situ Green $fPAR_{Domain}$ time series.

To understand the patterns and period-scales that they are occurring at, wavelet transforms are employed. Univariate wavelets and cross-wavelet analysis are versatile, as they deconstruct time-series into localized waves in time and or space, and have been widely used in the analysis of meteorology, for filtering operations on LiDAR data, and in land cover change (Khullar et al., 2011; Martínez & Gilabert, 2009; Sakamoto et al., 2005). Univariate and cross-wavelet analysis is also capable of determining discontinuities in the first-derivative and the rates of change of a time-series **(Vioyy et al., 1992; Park & Kim 2000).** Wavelets are calculated as follows:

$$Wf(a,b) = \int_{-\infty}^{+\infty} f(x) \frac{1}{\sqrt{a}} \varphi\left(\frac{x-b}{a}\right) dx \qquad 2.3$$

Where the wavelet is compacted or stretched by a scalar function (*a*) allowing it to represent multiple intervals of time, while also being shifted along the time axis (*b*) permitting 'daughter' wavelets (transforms of the 'mother' wavelet φ) to encapsulate an entire time series and detect patterns at smaller scales or higher frequencies. The 'mother' wavelet for the continuous wavelet employed is a Morlet wavelet and is calculated by using the package *'WaveletComp'* in R with the following formula (Roesch & Schmidbauer, 2018):

$$\varphi(t) = \pi^{-1/4} e^{i\omega t} e^{-t^2/2} \qquad 2.4$$

where the "angular frequency" ω is set to 6, allowing the "Morlet" wavelet to be analytical in nature and permitting its daughter wavelets to remain analytical as they are transformed.

By using the function '*wavelet.analysis'* from the '*WaveletComp'* package, each univariate wavelet transform is simulated 100 times for each of the MODIS and *in-situ* fPAR time-series. These simulations are compared against a white noise time series which highlights periods where the variance in fPAR significantly departs from a "white noise" time series. Periods which have variances consistently higher than that of white noise are identified in the power scale image by a "ridgeline" and allow for the isolation of periods which contribute significantly to the overall structure of time series. These significant period-scales are the recombined to recreate a basic representation of the original fPAR time-series (Torrence C. & Compo G., 1998). This recombination identifies critical time-series patterns and their interaction, allowing for the core components of fPAR to be identified and reconstructed around a normalized baseline.

The wavelet transforms from each fPAR time-seires are also compared using cross-wavelet power analysis, which is calculated with the following formula:

$$Wave.xy(b,a) = \frac{1}{a} * Wave.x(b,a) * Wave.y(b,a) \qquad 2.5$$

Where x_t and y_t are each a time-series and the modulus allows for the assessment of the similarity of the two series' wavelet power in the time-frequency domain. Analogously, this could be an analysis for the wavelets with significant covariance or joint periodicity between two time series ($p < 0.05$; Roesch and Schmidbauer, 2018). It should be noted that cross-wavelet power analysis does not display when time-series are 'in-phase' or the location where they have high degrees of correlation with one another. Coherence is used to resolve these gaps through the following formula:

$$Coherence = \frac{|aWave.xy|^2}{aPower.x * aPower.y} \qquad 2.6$$

In this case, there is no agreeance on the direction of smoothing in either time or scale to obtain the appropriate measure of coherence without loss of information (Torrence C. & Compo G., 1998). Therefore, to compare the coherence of the *in-situ* Green fPAR product with those of the MODIS fPAR products, it is necessary to employ a Bartlett window smoothing methodology, which eliminates low period (high frequency) signals but still allows for the analysis of the coherence between coarse resolution or low-frequency signals. Due to the absence of significant high-frequency signals after univariate wavelet analysis had been conducted, this study determined this to be the most appropriate smoothing method for the coherence analysis.

3.0 Results

3.1 Phenometric analysis

The *in-situ* Green fPAR time-series displays the greatest intra-seasonal amplitude with a ΔfPAR = 0.619 in 2016 (Figure 2), $fPAR_{min}$ that is much lower than any of the satellite products. This amplitude is 16% greater than the MCD15A3H fPAR product (Table 3-2), 24% greater than the Terra fPAR (Table 3-2) and 25% greater than the Aqua 8-day fPAR product (Table 3-1) for that same year. The MCD15A3H product presents the most marked intra-seasonal variations (Table 3-2), with ΔfPAR being 10% greater, on average, than Aqua (Table 3-1) or Terra (Table 3-2).

All of the fPAR products exhibit an increase in the μfPAR over all of the season, although there are changes in the dates and positions of $fPAR_{max}$ and $fPAR_{min}$. The inter-seasonal increase in μfPAR is significant when a Mann-Kendall test is employed ($p<0.05$; Table 2). The *Tau-b* values for each series are weakly positive, indicating a low strength change, which corresponds to the small change in μfPAR for all-time series. The *Tau-b* coefficient is similar in the Green, Terra and Aqua products (Table 2), while the combined product is the weakest (*Tau b* = 0.0582) and shows no association between paired observations.

The MODIS fPAR products display better congruency with *in-situ* Green fPAR for its $fPAR_{min}$ compared to the $fPAR_{max}$ dates. There is an average difference as low as 17 days (Terra), while Aqua displays a 47 day difference, and MCD15A3H a 57 day difference for $fPAR_{min}$ while $fPAR_{max}$ averages 75 days for Terra, 81 days for Aqua, and 91 days for MCD15A3H. The largest difference between MODIS and *in-situ* $fPAR_{max}$ occurs in 2013, where all three MODIS products have a difference ≥180 days. These differences between the MODIS and *in-situ* Green fPAR product are also reflected in the growing season length with the MCD15A3H growing

season length being 46 days longer than the *in-situ* product, compared to Aqua with 80 days or Terra with 111 days.

3.2 Univariate wavelet analysis

In the univariate analysis, no significant ($p < 0.05$) intra-seasonal patterns occur at scales smaller than a 64-day period for both *in-situ* Green fPAR (Figure 3-3a) and MCD15A3H fPAR (Figure 3-3b), and less than a 72-day period for both Aqua Figure 3-3c) and Terra fPAR (Figure 3-3d). The periods when significance in the covariance and symmetry is highest first appears in the combined product at 64-days, coinciding with $fPAR_{max}$. This ridgeline is discontinuous, fluctuating between 64-days and 96-days between 2015-2017, but is absent for 2014 (Figure 3-3b). The Terra product (Figure 3-3d) also exhibits an intra-seasonal ridgeline which consistently appears at a 96-day period scale beginning around its $fPAR_{max}$ date in 2015 (Table 3-2) and persists throughout 2016-2017. The next intra-seasonal ridgeline occurs at the 182-day period scale and is common between all four fPAR products, though it ends earlier for the *in-situ* product near its $fPAR_{max}$ in 2016. This disruption in the 182-day period corresponds with the landing of Hurricane Otto in the SRNP-EMSS on November 24, only 18 days after $fPAR_{max}$. Hurricane Otto delayed the onset of senescence in the study site, as evidenced by a 47% dampening of ΔfPAR in 2017 (Table 3-1) and a higher $fPAR_{min}$ which occurs a month later than average.

The final ridgeline of highest covariance and symmetry occurs at an inter-seasonal scale or 364-days. This ridge-line is present throughout all years, for all fPAR products except for the MCD15A3H 4-day fPAR product (Figure 3-3b). Here, during the time-frame immediately following $fPAR_{max}$ for MCD15A3H in 2015 (Table 3-2) the pattern is lost. The pattern is lost because the $fPAR_{max}$ in 2016 for the combined product occurs 3 months earlier than in previous years, which then proliferates into the timing of the $fPAR_{min}$ date in 2017, breaking the 364-day pattern. When analyzing the 364-day period ridgeline, it persists throughout the entire time series for the remaining products, each products ridgeline trends differently. The *in-situ* Green fPAR product (Figure 3-3a) declines, going from 364-days in 2013 to 298-days by 2017. The Aqua 8-day product (Figure 3-3c) acts conversely, expanding its 364-day period scale to a 438-day period scale between 2014 and 2017. Whereas the Terra 8-day product (Figure 3-3d) first

shortens its period-scale from 364 to 298 between 2013 and 2015 (Table 3-2), before lengthening from a 298 to 438-day period scale by the end of 2017.

When these significant wavelet periods are employed to reconstruct the fPAR time-series, the reconstructed time-series accurately reflect the *in-situ* cycle of green-up, maturity, brown-down and senescence. Wavelet reconstruction of the *in-situ* fPAR (Figure 3-6a) also captures the bi-annual peak events displayed during maturity, while also accurately displaying the loss of this bi-annual pattern and the reduced ΔfPAR in 2017 that occurs after the hurricane. Reconstructions of Terra (Figure 3-6b) and Aqua (Figure 3-6c) fPAR also capture the phenological cycle and double-peak during maturity. The amplitude of fPAR during maturity, coupled with a change in fPAR during senescence, differs between the reconstructed MODIS and ground data, with the *in-situ* data reaching a $fPAR_{min}$ 1.5x lower than the one from MODIS. The combined fPAR product has a discrepancy in that it displays a triple-peak events during maturity, between 2013 and 2015 (Figure 3-6d). The amplitude found in the combined product is also the greatest of the MODIS products. In general, all three MODIS fPAR reconstructions (Figures 3-6b-d) capture the timing of the phenological cycles and exhibit a bi-annual peak during the maturity phase, though the dates of these peaks differ from the *in-situ* data (Table 3-1/3-2).

3.3 Cross-wavelet power analysis between Green fPAR and MODIS fPAR products.

Using cross-wavelet analysis it is exhibited that each combination of Green and MODIS fPAR products have >95% confidence in the patterns detected at the 186-day, and 364-day scales (Figure 3-3). Bands of significant covariance between *in-situ* and MODIS fPAR also encompass period-scales between 256-512 days, indicating that every pair is detecting inter-seasonal scale patterns; however, the arrows within these inter-seasonal period-scales (Figure 3-4) indicates that although the patterns are in-phase, the *in-situ* fPAR product leads the MODIS fPAR products in each instance. This is confirmed by the phenometrics from the original time-series, where the *in-situ* fPARmin and fPARmax arrive, on average, 40-days and 82 days earlier, respectively than those of the MODIS fPAR products.

Transitioning to the intra-seasonal patterns (period scales $\leq$ 128-day) there is more variability between the *in-situ* and MODIS fPAR products. The Aqua and *in-situ* products (Figure 3-4a) are the most concordant but alternate between being in-phase, with Green fPAR leading at the 128-

day scale during 2015 and 2017, and Aqua leading at the 72-day scale in early 2015, late 2016, and mid-2017. These two products are out-of-phase during 2013, late 2015 and all of 2016 at the 96-day scale. For the MCD15A3H and *in-situ* products cross-wavelet power analysis (Figure 3-4b) the patterns are very similar to those exhibited with Aqua (Figure 3-4a); although, fewer small-scale features are shared between the two products with no similarities at period scales < 72-days. For Terra, it is seen that at the 128-day scale the *in-situ* product leads the Terra product for the entire time-series except during the end of 2013 and 2016 (Figure 3-4c). At scales smaller than 128-days, the *in-situ* and Terra products (Figure 3-4c) alternate between being $+\pi/2$ and $-\pi/2$ in-phase, meaning that the two products are destructively interfering with each other or completely out-of-phase. The positioning of these destructive interference signals is always during the growing-seasons too, meaning that while both Terra and *in-situ* products (Figure 3-4c) are detecting similar 2-3-month patterns, they are asynchronous with one another.

3.4 Cross-wavelet coherence between MODIS fPAR products and Green fPAR

The coherence analysis displays that Aqua and *in-situ* fPAR, despite detecting similar patterns at the 365-day scale are only in-phase during the mature phenophase's of 2013 and 2015, remaining incoherent in all other years and phenophase's (Figure 3-5a). A similar pattern emerges for the 186-day scale, where coherence occurs during the mature phenophase's of 2013, 2014, and 2015, with *in-situ* fPAR leading Aqua (Figure 3-5a). When comparing the *in-situ* product with the other MODIS products (MCD15A3H and Terra 8-day), many of the patterns exhibited between *in-situ* fPAR and Aqua fPAR are reflected. At periods of 182 and 364-days, differences in the continuity of the coherence between the two respective products change slightly, with Terra (Figure 3-5c) holding the longest period of coherence at the 182-day scale and MCD15A3H (Figure 3-5b) at the 364-day scale. All three MODIS fPAR products lose their coherence at the 182-day and 364-day period scales with the *in-situ* product during the green-up and maturity phenophases of 2016.

Investigating coherence at the intra-seasonal scales, between 128-day and 32-days, there are intermittent, randomly distributed periods in which Aqua and *in-situ* fPAR (Figure 3-5a) are coherent occurring during peak maturity in the years of 2014 and 2016, and during the green-up phenophase of 2016 and 2017. Additional periods of significance the 6-32-day windows, and are repeated during January 2013, 2014, 2015 and briefly during February of 2016 and 2017. These

periods correspond with decreasing fPAR, typically at rates of 1.3%-1.8% per day, rates which are shared between the Aqua and *in-situ* products (Figure 3-2). For the Terra and combined prodcuts, the period-scales between 128-days and 32-days exhibit periods of brief coherence (Figure 3-5b/c). At period-scales $\leq$ 32-days brief periods of coherence, typically lasting between 3-5 weeks, occur during the senescence periods of MCD15A3H (Figure 3-5b), Terra 8-day (Figure 3-5c) and *in-situ* fPAR with the strongest coherence occurring during January-February 2014 and November – December of 2014.

4.0 Discussion

Overall, we find that the Savitsky-Golay filter with a moving-average interpolation was useful in allowing the study to take advantage of those pixels that were flagged for cloud-contamination but interpolation to create a single-day product did not render additional advantages for pattern recognition at scales < 32-days. The study also determined that while the general phenological cycle is captured by MODIS, the small-scale, intra-seasonal features, such as those caused by hurricanes and drought events are missed in the satellite product. Additionally, MODIS products are not able to replicate the timing of the phenophases captured with this method of estimating *in-situ* fPAR, especially with regards to green-up and senescence. Moreover, the timing of phenological events between MODIS products are inconsistent amongst themselves, and Terra, the closest representation to the *in-situ* data is delayed by 1-3 months regarding *in-situ* $fPAR_{max}$ and $fPAR_{min}$ dates. Despite these issues, MODIS does capture the double peak fPAR feature found during maturity in an average year and reflects the correct long-term increase in the average fPAR per year at the SRNP-EMSS.

The Savitsky-Golay filter employed in conjunction with the moving-average interpolation was employed in this study to reduce the noise and errors of MODIS fPAR and model the daily satellite observations. This study employed a half-width smoothing window of 4 and a smoothing polynomial of 6, which has been shown to improve the detection and precision of long-term vegetation-index phenological trends (Cai et al., 2017; J. Chen et al., 2004; Lange & Doktor, 2017; Savitzky & Golay, 1964). While the wavelet-analysis supports the use of these filters for capturing inter-seasonal trends, such as the 182-day and 364-day cycles, this degree of smoothing on an 8-day product may have erased any small-scale patterns captured by MODIS. With few patterns captured at periods <32-days, and the delayed detection for green-up by MODIS products a lesser

degree of smoothing and a smaller half-width smoothing window may have enabled the detection of rapid small-scale events that were otherwise missed.

The differences exhibited between Terra and Aqua 8-day fPAR may be due to an offset in the overpass timing between the satellites, with Terra collecting data between 8:30-10:00 and Aqua acquiring data between 12:30-14:00. This timing difference changes the illumination geometry of the canopy; therefore, Terra acquires data when the solar zenith angle is 27-60°, and Aqua acquires data with a solar zenith angle <27°. This difference could change the resultant fPAR as this parameter notably saturates and has less variability at large solar zenith angles (Li & Fang, 2015; Widlowski, 2010). With smaller solar zenith angles, fPAR is subject to a 3-6% decrease in mean fPAR values and a 24% increase in its variance (Li & Fang, 2015). These effects are exhibited in the μfPAR, where Terra consistently reports a higher mean fPAR, with a smaller standard deviation than Aqua across all seasons. This difference in timing changes the illumination geometry resulting in an increase in the radiation reflected back to the Aqua satellite (Sellers, 1987; Walter-Shea et al., 1992), which in turn would also decrease the μfPAR reported by Aqua. These biases should be reduced in the combined product; however, even that product differs from the *in-situ* fPAR estimates.

The in-situ change in fPAR throughout the year differs from all MODIS products by up to 16%, indicating that there are errors or uncertainties that are not resolved between the ground and satellite data. These differences could partially be due to the fundamental differences in the methodologies of fPAR measurement. While MODIS fPAR is dependent on capturing the reflectivity off surfaces, or the two-way path of photons, and translating them into fPAR values (Knyazikhin et al., 1998; Myneni et al., 1999; Myneni & Park, 2015), the *in-situ* product is measuring the one-way path or direct radiation hitting the understory (Majasalmi, Stenberg, & Rautiainen, 2017; Nestola et al., 2017; Putzenlechner et al., 2019; Widlowski, 2010). This difference, might explain the subdued ΔfPAR exhibited by the MODIS products, as MODIS is measuring the difference between Near-Infrared Radiation (NIR) and red-radiation from the entire scene, which increases and saturates during maturity (Myneni et al., 2002; Myneni et al., 1999; Weiss, et al., 2000) therefore resulting in increased fPAR values for MODIS over the *in-situ* product. During senescence, surface reflectance may remain high as the soil reflectance for these areas increases as the soils dry-out (Myneni & Williams, 1994), and leaf-litter increases the

understory reflectance (Schlerf & Atzberger, 2006; Serbin, et al., 2013). This increase in the surface reflectivity during senescence may prevent MODIS fPAR values from decreasing and representing the true fPAR occurring during this period, also resulting in the ΔfPAR for MODIS in comparison with *in-situ* fPAR. Consequently, measuring *in-situ* fPAR from the local tower, rather than from the WSN may result in an *in-situ* fPAR product that is more reflective of what is observed by the MODIS satellite.

Other studies have found that ground data may be subject to understory phenological processes alongside that of the canopy dynamics. Not only would this impact the ΔfPAR, but also the timing of the phenophases. The ground data at the SRNP-EMSS enters green-up sooner than the satellite product, a phenomenon reflected in other biomes including the boreal, temperate deciduous, and temperate evergreen forests (Ryu et al. 2014; Pisek et al., 2015). The impact of the understory can be decoupled in the boreal forest where the canopy is sparser (Pisek et al., 2015); however, this is not possible in the dense TDF canopies where there are few canopy gaps and dense woody material. It is, therefore, crucial to develop a better understanding of the understory dynamics (Rankine et al., 2017) especially in early and intermediate-stage forests where grasses and shallow-rooted shrubs are subject to flush their leaves before trees and lianas in response to the first rain-events of the season (Kalacska et al., 2004, 2005).

Another source of error and uncertainty between the ground and satellite products is in the data collection process and sensor spectrography. MODIS uses a narrowband sensor which detects light in the red and near-infrared for its fPAR product (Myneni et al., 2015), while the WSN Apogee PAR sensor is a broadband sensor, which reports one value for the entire visible (400-700nm) spectrum to determine fPAR (Putzenlechner et al., 2019; *QUANTUM SENSOR Models SQ-100 and SQ-300 Series (including SS models)*, 2019). Furthermore, MODIS does not directly retrieve fPAR from the PAR signal and, instead, inputs a band-ratio product into a Look-up Table (LUT) which holds the parameters from interactions between PAR flux, LAI (retrieved from the same product) and the 3D canopy structure for the biome type it appears to observe, that is determined from the land cover classification product (Myneni et al., 1999). Furthermore, if the MODIS fPAR algorithm is incapable of deriving fPAR using the original formula, as a result of pixel contamination, it reverts to the backup algorithm which is based on the regression relationship between NDVI and fPAR (Myneni et al., 1999). The *in-situ* fPAR is instead calculated based on

the direct difference between incoming and transmitted PAR (Widlowski et al., 2010; Putzenlecher et al., 2019). These differences in both the data collected and in the algorithm used, ultimately mean that there is a comparison between a direct and indirect method of data collection, which has historically made cross-platform validation difficult (Huang et al., 2013).

Despite these differences, MODIS should remain sensitive to changes in the leaf area and chlorophyll content of the canopy (Shabanov et al., 2003; Yan et al., 2016). It has been demonstrated that the MODIS ΔfPAR found at the SRNP indicates that it is less sensitive to changes in PAR and more commonly reflects the behaviour of the NDVI, particularly during green-up. The congruency with NDVI could be due to the high proportion of clouds in the region during the wet season (Castro et al. 2018), which results in 62% of the pixels being cloud contaminated, resulting in the backup-algorithm regularly being used. The reliance on the back-up NDVI-fPAR relationship algorithm may explain the difference in green-up onset dates, lack of small scale coherence, and the reduced ΔfPAR in MODIS from green-up into late-maturity (Castro et al., 2018).

These errors and uncertainty do not, however, explain the disagreement between MODIS and *in-situ* fPAR during senescence. This discrepancy may be due to the LCC input in MODIS (Myneni et al., 2015). Each land cover type has a set of standard constants for the soil optical properties, vegetation optical properties, and 3D structural complexity which are changed for the fPAR algorithm. The pixels in this study are classified as savanna (62%), evergreen broadleaf forest (15%), grasses/cereal crops (13%), and deciduous broadleaf forest (10%), with inconsistent classification throughout the year, an added feature with the C6 update (Myneni & Park, 2015; Yan et al., 2016). Typically TDFs should be considered either as savanna or deciduous broadleaf forests (Myneni et al., 1999; Lieberman, 1982), meaning that there was misclassification at least 28% of the time. These types of misclassification have caused up to 50% differences in the related LAI product (Fang et al. 2013; Myneni et al., 2002; Gonsamo et al., 2011; Fang & Liang, 2005) and are considered especially problematic when herbaceous and woody ecosystems are misclassified with each other (Fang et al., 2013; Tian et al., 2000). Despite this, these types of misclassifications did not significantly impact the fPAR estimations in a similar dry ecosystem of Australia, though there was no ground validation product in that case (Schottker et al., 2010). Overall, the most numerous misclassification errors in the MODIS algorithm are found in

savannas, evergreen needle forests and broadleaf deciduous forests (Fang et al., 2013), indicating that this could be significantly impacting the fPAR estimations at the site and in this biome.

When looking at the intraseasonal discrepancies found in the cross-wavelet analysis, both with power and coherence, it should be noted that the LAI of the SRNP broadly changes with peaks in November-December and minimums in March-April (Kalácska et al., 2005). As change in LAI is the largest determining factor in PAR absorption (Majasalmi, 2015; Majasalmi et al., 2017; Myneni et al., 2002; Myneni, 1997), the broad-scale trends of the site are represented in the 182-day and 364-day period-scales of the cross-wavelet analysis. The TDF, however, is also highly responsive to changes in weather and the volumetric-soil water content (Cai et al., 2009; Castro et al., 2018) with changes in LAI from < 1 to > 4 occurring in less than <32 days at its maximum (Castro et al., 2018) during green-up. This is reflected in the bi-annual peak during maturity, where a 2-3 week drought results in a change in the physiology of the leaves as they yellow in response (Kalácska et al., 2005; Kalacska et al., 2005) to the decrease in soil moisture. While these changes are captured broadly, it is undetermined if the fPAR index is capable of capturing these changes at scales < 32-days or if the smoothing of the time-series has erased these changes from the record.

When looking at extreme events, the midseason precipitation lows and the drought in 2015 (Castro et al., 2018) are reflected in the *in-situ* fPAR with the double peak during maturity, the reductions in µfPAR in 2015 and 2016 and the shortened growing season in 2016. These reductions to µfPAR and the short growing season may be linked to the ecosystem being under severe water-stress after the drought in 2015, which exhibited a 64% decrease in precipitation compared to an average year (Castro et al., 2018). With every consecutive drought, the precipitation threshold necessary for bud-break to initiate increases (Daubenmire, 1972; Lieberman, 1982; Reich, 1984), and tree water storage drops, inducing changes in the leaf-physiology and canopy LAI of TDFs. These phenomena are possible to capture using Morlet-based continuous-wavelet transforms as seen in the reconstructed time-series, though they are only significant at the 182-day scale. The MODIS wavelets also encompass the double peak feature caused by the mid-season precipitation drop; yet, the reduced growing season in 2016 and reduction in the 2015 µfPAR caused by the drought is muted compared to the *in-situ* data, as evidenced by the loss of 182-day and 364-day coherence in 2015 and 2016. Similar trends have been observed in temperate broadleaf deciduous forests when using MODIS NDVI products (Hlásny et al., 2015).

The effects of dramatic precipitaiton events, such as with a hurricane, are not exhibited in the MODIS data. Immediately after $fPAR_{max}$ occurs for the *in-situ* product during the 2016 growing season, Hurricane Otto made landfall over the SRNP-EMSS (Brown, 2016). During this brief period, there was a large precipitation event of ~110mm with periodic smaller rain events lasting into mid-January of 2017 (Castro et al., 2018). These rainfall events reduced the ΔfPAR in the ground data by 281%, delayed $fPAR_{min}$ by 32 days, and extended the growing season by 191 days when compared to the average growing season lengths of 2013-2016. These features are not detected in the MODIS fPAR, noted by the lack of coherence with the ground product in the cross-wavelet analysis and the presence of the double peak in 2017, which is absent in the *in-situ* time-series reconstruction. The only indications that this event is detected by the MODIS fPAR products is the higher than average μfPAR for the 2017 growing season and the changes in the Aqua $fPAR_{max}$/$fPAR_{min}$ dates. Studies investigating the detection of hurricane disturbances using MODIS fPAR have not been conducted in the TDF; however, MODIS EVI has been used for tracking post-hurricane forest disturbance (Wang & D'sa, 2010). In that case, the results depended on the size of the hurricane and the level of disturbance in the forest, with smaller hurricanes such as Hurricane Otto, remaining undetected (Wang & D'sa, 2010). This analysis indicates that MODIS fPAR products may be unreliable for estimating fPAR in the subsequent season following a hurricane for TDFs.

The lack of congruence between the *in-situ* and MODIS fPAR products is particularly problematic as MODIS fPAR is frequently linked and depended on to estimate Gross Primary Productivity, to determine carbon fluxes and the sequestration potential in areas (Yu et al., 2018). Underestimation of fPAR, as found at this site, leads to the underestimation of the carbon sequestration potential (Cheng et al., 2014), and as these forests account for 42% of tropical forests globally (Portillo-Quintero et al., 2015), an underestimation of this carbon potential may lead to significant reductions in the global carbon budget. This underestimation is of special concern, for this ecosystem is frequently misclassified by the LCC product utilized by the MODIS algorithm, which paired with the high cloud cover during the growing season can lead to sustained underestimation for prolonged periods (Castro et al. 2018; Fang et al. 2013). Furthermore, other studies have also found that in deciduous ecosystems, particularly in the Southern Hemisphere, there is a weak relationship between the MODIS fPAR product and ground primary productivity estimates, with the savanna classification considered the worst globally (Cheng et al. 2014; Yu et al. 2018; Tao et

al. 2015). As the MODIS GPP product integrates the fPAR results, and both products are increasingly used in carbon and earth system models, it is important to parameterize the uncertainties, under-estimation, and restrict these products use to ecosystems where they are valid (Cheng et al. 2014; Mao et al. 2012; Demarty et al. 2007).

5.0 Conclusions

Overall, this study finds that the MODIS fPAR products are capable of correctly characterizing the long term, biannual, and yearly phenological cycles or trends, but that the method used to estimate the *in-situ* fPAR product may be incompatible for the validation of the MODIS fPAR product in a TDF environment. Differences in the methodologies of measuring fPAR, the inability to characterize the effects of understory vegetation on the *in-situ* product, and the need to characterize the effect of reflected PAR indicate a need for a study that characterizes these differences at the TDF in the SRNP-EMSS. Despite this, this study was capable of highlighting that the MODIS fPAR product had difficulty in determining the length and onset timing of different phenophases, particularly green-up and senescence. While inter-seasonal phenological patterns are similar between MODIS and *in-situ* fPAR, the intra-seasonal events are not well characterized by either product, despite the high temporal resolution of the *in-situ* product. Moreover, MODIS fPAR did capture, though underestimated, drought-related events, it did not capture the extension of the growing season and changes to the forest phenology caused by the extreme rain events, such as hurricanes. Some or all these errors in the MODIS data may be due to the lack of TDF biome characterization in the MODIS algorithm, which instead inconsistently classifies this biome, instead of classifying it as either deciduous broadleaf or woody savanna. These errors could be extenuated by the inconsistent classification, or because TDFs exhibit different canopy behaviours and adaptive strategies than both the deciduous forests and woody savannas.

While some of the differences in growing season lengths and the onset of phenophase timing may be linked to the sensitivity of the *in-situ* fPAR products to understory vegetation green-up, it should still be considered an unreliable product for its inability to capture $fPAR_{max}$ dates consistently. Reliance on the MODIS-derived fPAR products for TDF phenological cycles is likely to lead to the consistent underestimation of total fPAR during the growing season. This underestimation of fPAR could translate into an underestimation of carbon flux exchanges in

regional or global models, which often rely on MODIS fPAR products. This is especially prevalent, as TDFs comprise 42% of all tropical vegetation, resulting in a significant alteration of the global carbon cycle in these models and future predictions. Furthermore, underestimating the effects of drought and the inability to detect the effects of hurricanes or major precipitation events on TDF phenology in the satellite data could lead to the mismanagement of government response to extreme precipitation as the magnitude of these events is inadequately contextualized. These findings lead the study to the conclusion that the MODIS C6 fPAR products, as they currently exist, are inappropriate for the monitoring of TDF phenology and are inappropriate for characterizing the canopies response to drought-related or extreme weather events.

Despite this studies conclusion on the MODIS fPAR products ability to track TDF phenology, or the magnitude of TDF canopy response to extreme weather events, it does reveal the strength of using both derivative-based phenological metrics in conjunction with continuous-wavelet transformations and cross-wavelet analysis for the validation of satellite-derived VI products. While the univariate and cross-wavelet analyses capture both intra and inter-seasonal scale patterns, determine the strength of those patterns, and compare multiple products for the same patterns, using them in conjunction with a Savitzky-Golay filter may make them incapable of providing precise dates for rapid-changes. The derivative-based method does, however, compliment the continuous-wavelet method with its ability to establish general dates for the occurrence of bud-break or senescence. Using these two methods of analysis in concert can, therefore, provide more robust quantitative temporal metrics and temporal pattern recognition techniques for validating satellite-derived VI's with ground-based measurements.

Acknowledgements

This study was conducted with the aid of a grant from the Inter-American Institute for Global Change Research (IAI), which is supported by the US National Science Foundation. We are also grateful for the financial, technical and infrastructural support provided by International Business Machines (IBM). We would also like to thank Roger Blanco and Maria Marta Chavarría from the Santa Rosa National Park. Finally, we would like to thank the field assistants from the University of Alberta and the Instituto Tecnologico de Costa Rica for their help in the collection

of data and the maintenance of equipment at the Santa Rosa National Park Environmental Monitoring Super-site.

I would also like to acknowledge Dr. Martin Sharp who, after viewing a presentation of mine, presented the idea of continuous-wavelet transforms to extract more temporal patterns from my current data. This gave inspiration to the idea of using cross-wavelet transforms to compare wavelet-transforms between *in-situ* and satellite-derived fPAR products.

Tables Legend

Table 3-1 **Key values for key features, for the Green fPAR and Aqua 8-day fPAR products.** Numerical and date values for the key features: µfPAR, ΔfPAR, $fPAR_{max}$, $fPAR_{min}$, and Growing Season Length for the selected MODIS & *in-situ* fPAR products. $fPAR_{max}$ and $fPAR_{min}$ are given both their Julian calendar date and Julian day.

Table 3-2 **Key features for Terra 8-day and MCD15A3H 4-day.** Numerical values for the key features: µfPAR, ΔfPAR, $fPAR_{max}$, $fPAR_{min}$, and Growing Season Length (as described in Table 1). $fPAR_{max}$ and $fPAR_{min}$ are given both their Julian calendar date and Julian day.

Table 3-3 **Several statistics derived from the non-parametric Mann-Kendall test to identify trends in the original time-series.** Tau-b coefficient, two-sided p-value ($p < 0.05$ indicates a significant trend), and S-statistic where $S = 0$ indicates the null-hypothesis is true meaning that there is no deviation from the mean.

Figures Legend

Figure 3-1 The location of the Santa Rosa National Park - Environmental Monitoring Super-site (SRNP-EMSS). Network 1 refers to the WSN that is employed in the creation of the in-situ Green FPAR product.

Figure 3-2 **Time-series of each MODIS fPAR data product, and the *in-situ* Green fPAR data product from the SRNP-EMSS.** Each time-series displayed is the modeled output from the 'phenex' package, resulting in daily fPAR values. Each MODIS fPAR product has therefore been interpolated from their 4 or 8-day product to a daily product, whereas the *in-situ* Green fPAR product is directly resulted from daily averages taken from the WSN.

Figure 3-3 **A univariate analysis of the Green and MODIS fPAR time-series employing the Morlet Wavelet.** The left axis indicates the Morlet wavelet period (in days), whereas the bottom-axis indicates time. Coloured contours are normalized variances which are dependent on the scale of the time-series itself. The white contour lines enclose the regions of greater than 95% confidence for a red-noise process. Shaded areas on either end of the graphs indicate a "cone of influence", where edge effects become important. a) Green fPAR, b) MCD15A3H fPAR, c) Aqua 8-day fPAR, d) Terra 8-day fPAR.

Figure 3-4 **Cross-wavelet power analysis between Green fPAR and MODIS fPAR**. Areas found within the white-boundary are areas where the Morlet-wavelet deconstructions of the two time-series align with significance. Arrows are indicative of which time-series leads the other, if arrows point right the 2-flux $fPAR_{Domain}$ product leads the MODIS fPAR product, up and down indicate the direction towards the nearest "ridge" or period of highest significance between the two time-series. a) Green fPAR and Aqua 8-Day fPAR, b) Green fPAR and MCD15A3H 4-day fPAR, c) Green fPAR and Terra 8-Day fPAR

Figure 3-5 **Cross-wavelet coherence between Green fPAR and MODIS fPAR**. Areas found within the white-boundary are areas where the two time-series align with significance and for what length of period those time-series align. Arrows are indicative of which time-series leads the other, if arrows point right the Green $fPAR_{Domain}$ product leads the MODIS fPAR product, up and down indicate the direction towards the nearest "ridge" or period of highest significance between the two time-series. a) Green $fPAR_{Domain}$ and Aqua 8-Day fPAR, b) Green $fPAR_{Domain}$ and MCD15A3H 4-day fPAR, c) Green $fPAR_{Domain}$ and Terra 8-Day fPAR.

Figure 3-6 **Reconstructions of each fPAR time series using time-frequency periods of significance.** The reconstruction of the time-series employs the periods of highest significance between the Morlet wavelet and the MODIS and *in-situ* Green fPAR. a) *In-situ* Green fPAR, b) Terra 8-day, c) Aqua MODIS 8-day, d) MCD15A3H 4-day. Black lines indicate the original time-series after smoothing, whereas the red line indicates the reconstruction of the time-series based on utilizing the significant periods.

(Table 3-1)

Product	Green fPAR					Aqua 8-day				
Year	μfPAR	ΔfPAR	$fPAR_{max}$	$fPAR_{min}$	Length	μfPAR	ΔfPAR	$fPAR_{max}$	$fPAR_{min}$	Length
2013	0.494	0.452	June 17 (169)	Apr 4 (95)	192	0.555	0.345	Dec 26 (360)	May 18 (139)	114
2014	0.522	0.541	Nov 12 (317)	Mar 28 (88)	168	0.642	0.263	Jan 12 (12)	Apr 24 (115)	357
2015	0.395	0.578	Nov 18 (323)	Apr 3 (94)	236	0.638	0.388	Dec 15 (349)	Apr 28 (119)	239
2016	0.398	0.619	Nov 06 (311)	Mar 30 (90)	87	0.583	0.373	Nov 29 (332)	Mar 28 (88)	204
2017	0.587	0.260	Sept 18 (262)	May 2 (123)	361	0.656	0.395	Jan 5 (5)	Sept 14 (258)	348

(Table 3-2)

Product			Terra 8-day					MCD15A3H 4-day		
Year	μfPAR	ΔfPAR	$fPAR_{max}$	$fPAR_{min}$	Length	μfPAR	ΔfPAR	$fPAR_{max}$	$fPAR_{min}$	Length
2013	0.612	0.283	Dec 19 (354)	May 14 (135)	190	0.572	0.507	Dec 14 (349)	May 5 (146)	180
2014	0.638	0.252	Jan 15 (15)	Apr 4 (95)	353	0.644	0.347	Jan 3 (3)	Apr 16 (107)	199
2015	0.636	0.416	Dec 5 (340)	Apr 22 (113)	166	0.62	0.453	Dec 9 (344)	May 13 (134)	238
2016	0.62	0.379	Nov 19 (324)	Mar 29 (89)	213	0.572	0.456	July 20 (202)	Apr 18 (109)	213
2017	0.677	0.317	Dec 26 (361)	Apr 14 (105)	187	0.633	0.458	Dec 22 (357)	Oct 7 (281)	302

(Table 3-3)

	Green fPAR	Aqua 8-day fPAR	Terra 8-day fPAR	MCD15A3H 4-day fPAR
Tau-b	*0.132*	*0.132*	*0.146*	*0.0582*
p-value	$<2.2x\ 10^{-16}$	$<2.2x\ 10^{-16}$	$<2.2x\ 10^{-16}$	$1.95\ x\ 10^{-4}$
S - statistic	$2.2\ x\ 10^{5}$	$2.2\ x\ 10^{5}$	$2.44\ x\ 10^{5}$	$9.69\ x\ 10^{4}$

(Figure 3-1)

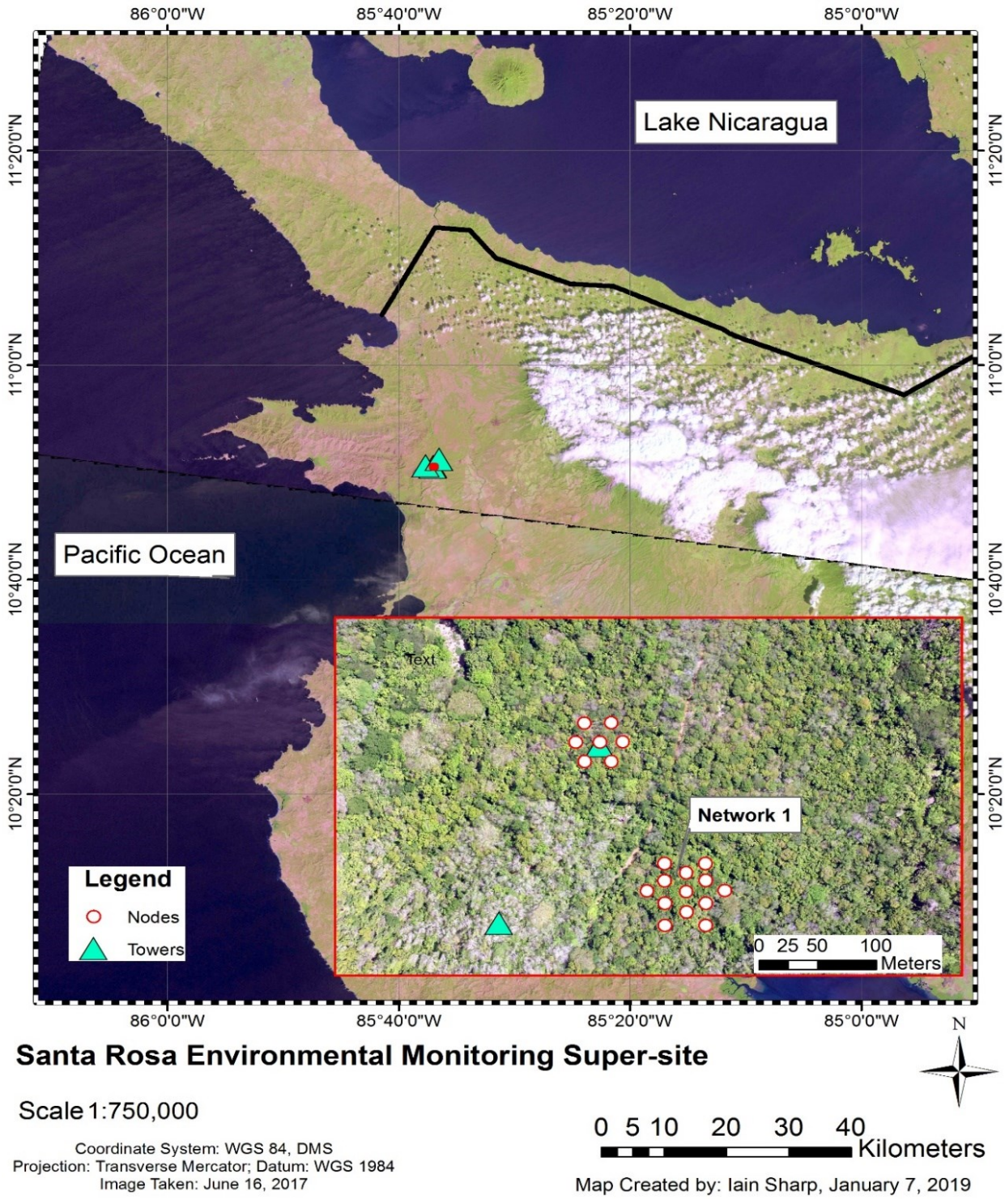
86°0'0"W
85°40'0"W
85°20'0"W
85°0'0"W
11°20'0"N
11°0'0"N
10°40'0"N
10°20'0"N
Lake Nicaragua
Pacific Ocean
Text
Network 1
Legend
Nodes
Towers
0 25 50 100
Meters
N
Santa Rosa Environmental Monitoring Super-site
Scale 1:750,000
Coordinate System: WGS 84, DMS
Projection: Transverse Mercator; Datum: WGS 1984
Image Taken: June 16, 2017
0 5 10 20 30 40
Kilometers
Map Created by: Iain Sharp, January 7, 2019

(Figure 3-2)

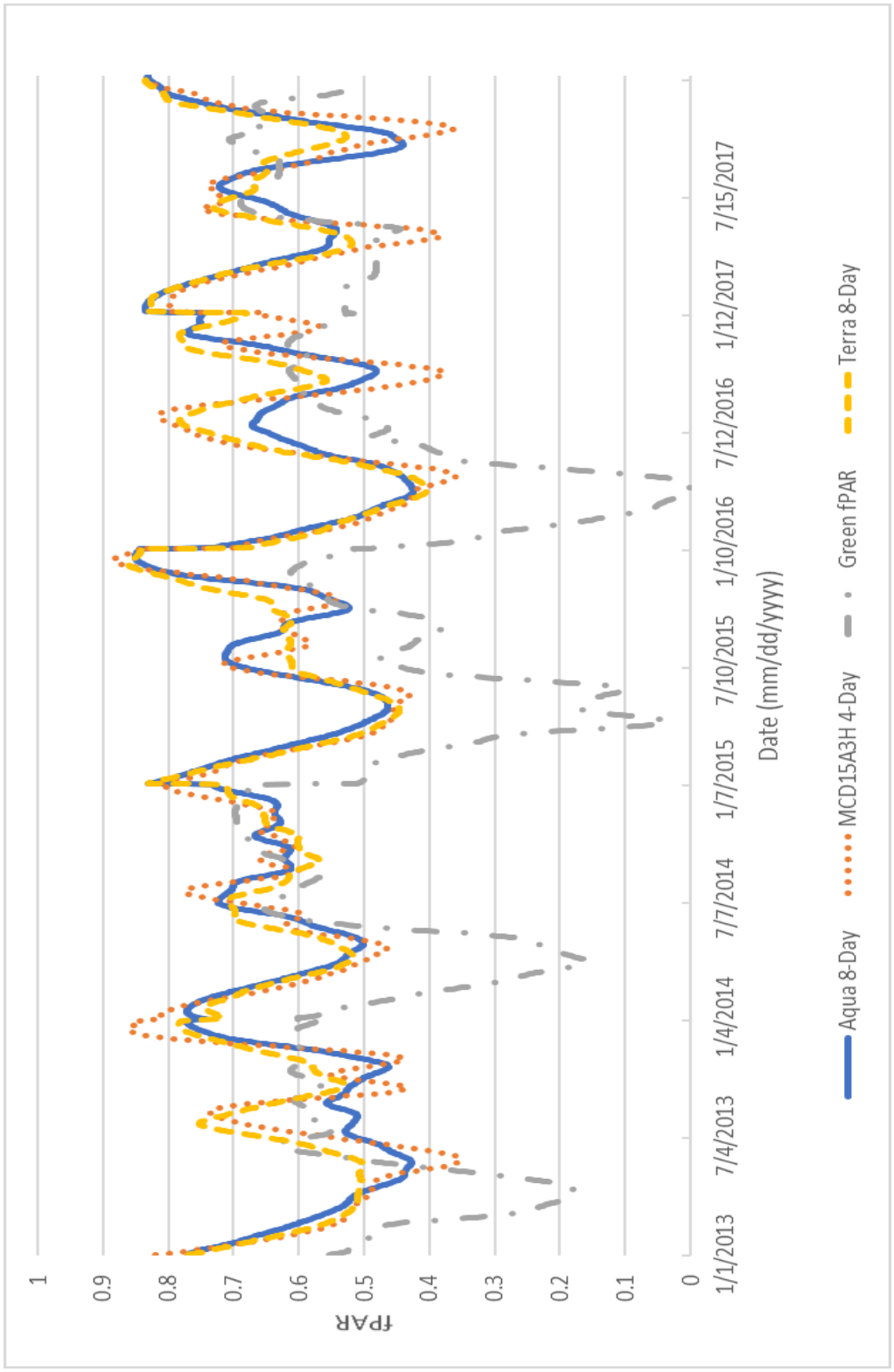
fPAR
1
0.9
0.8
0.7
0.6
0.5
0.4
0.3
0.2
0.1
0
1/1/2013
7/4/2013
1/4/2014
7/7/2014
1/7/2015
7/10/2015
1/10/2016
7/12/2016
1/12/2017
7/15/2017
Date (mm/dd/yyyy)
Aqua 8-Day
MCD15A3H 4-Day
Green fPAR
Terra 8-Day

(Figure 3-3)

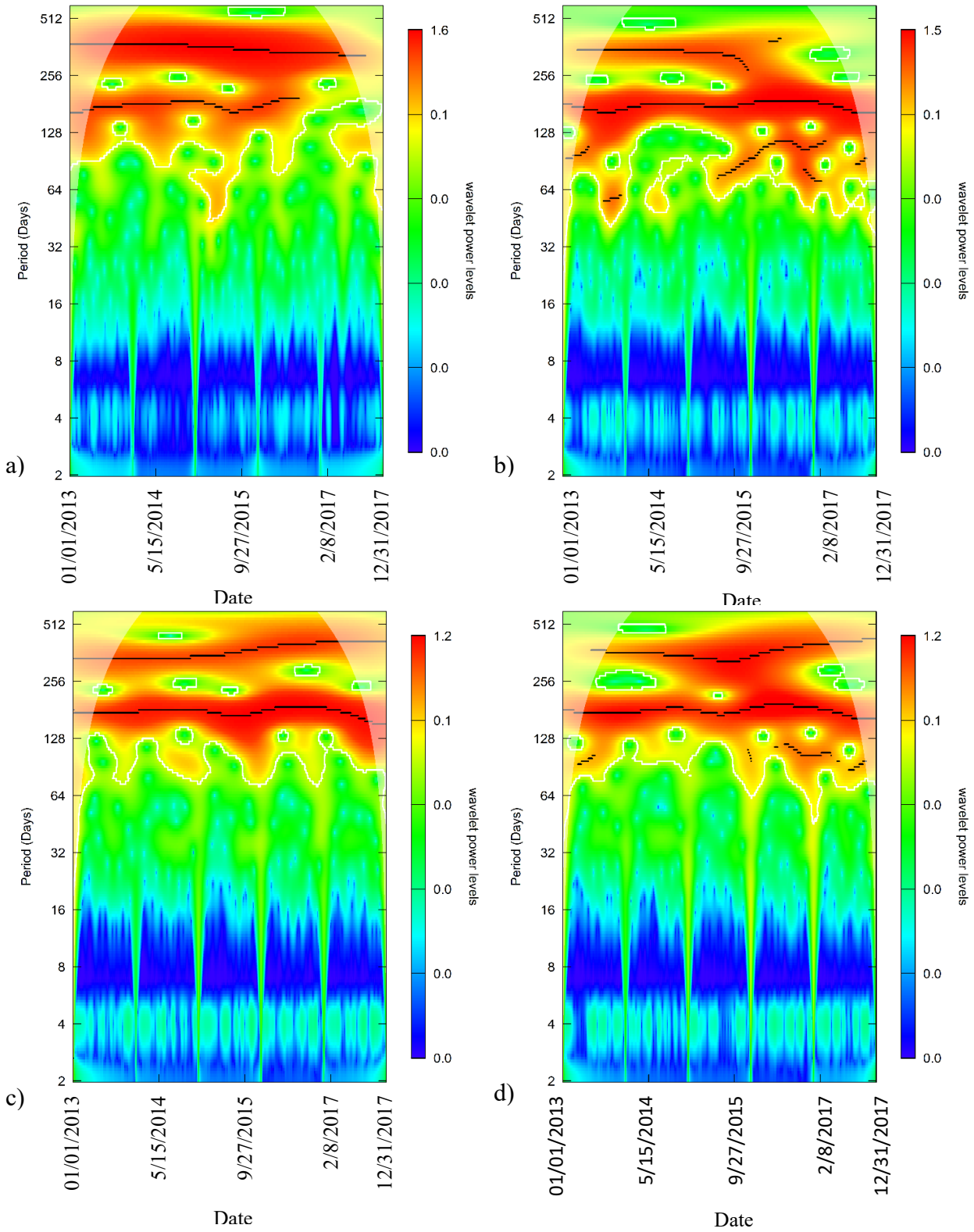
a)
b)
c)
d)
Period (Days)
512
256
128
64
32
16
8
4
2
01/01/2013
5/15/2014
9/27/2015
2/8/2017
12/31/2017
Date
wavelet power levels
1.6
1.5
1.2
0.1
0.0

(Figure 3-4)

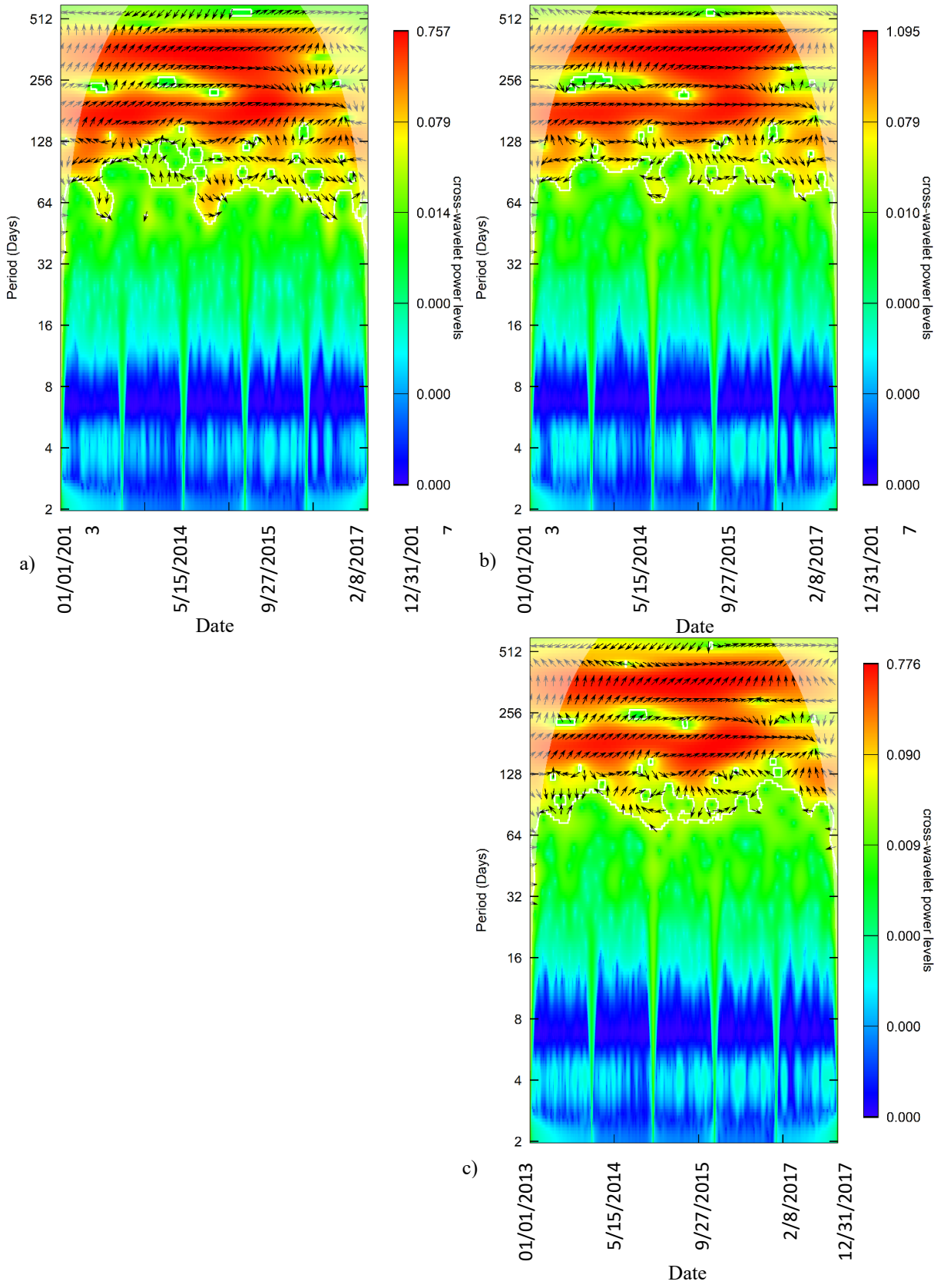
a)
b)
c)
Period (Days)
512
256
128
64
32
16
8
4
2
Date
01/01/201 3
5/15/2014
9/27/2015
2/8/2017
12/31/201 7
01/01/2013
12/31/2017
cross-wavelet power levels
0.757
0.079
0.014
0.000
0.000
1.095
0.010
0.776
0.090
0.009

(Figure 3-5)

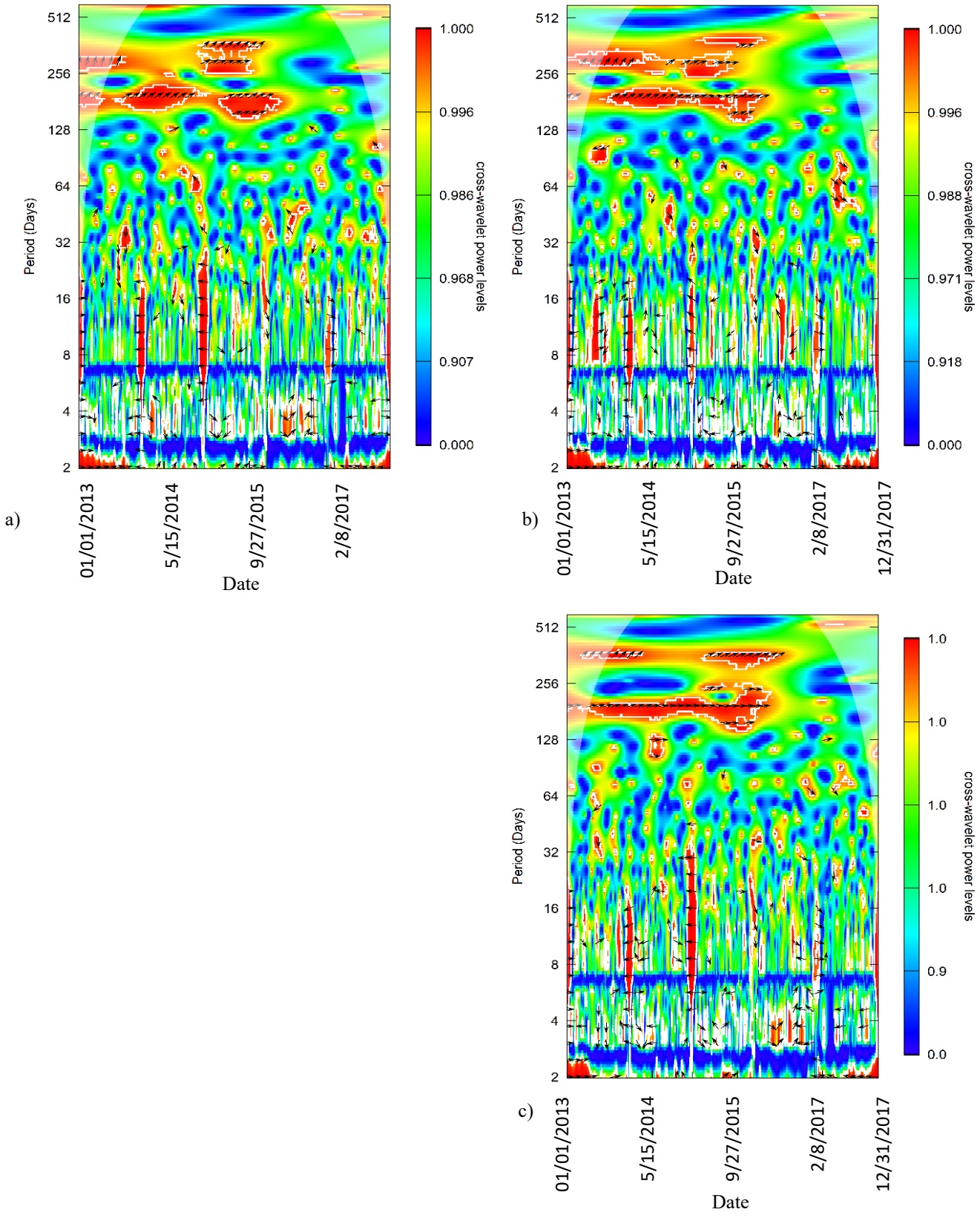
a)
b)
c)
Period (Days)
512
256
128
64
32
16
8
4
2
01/01/2013
5/15/2014
9/27/2015
2/8/2017
12/31/2017
Date
cross-wavelet power levels
1.000
0.996
0.986
0.968
0.907
0.000
0.988
0.971
0.918
1.0
0.9
0.0

(Figure 3-6)

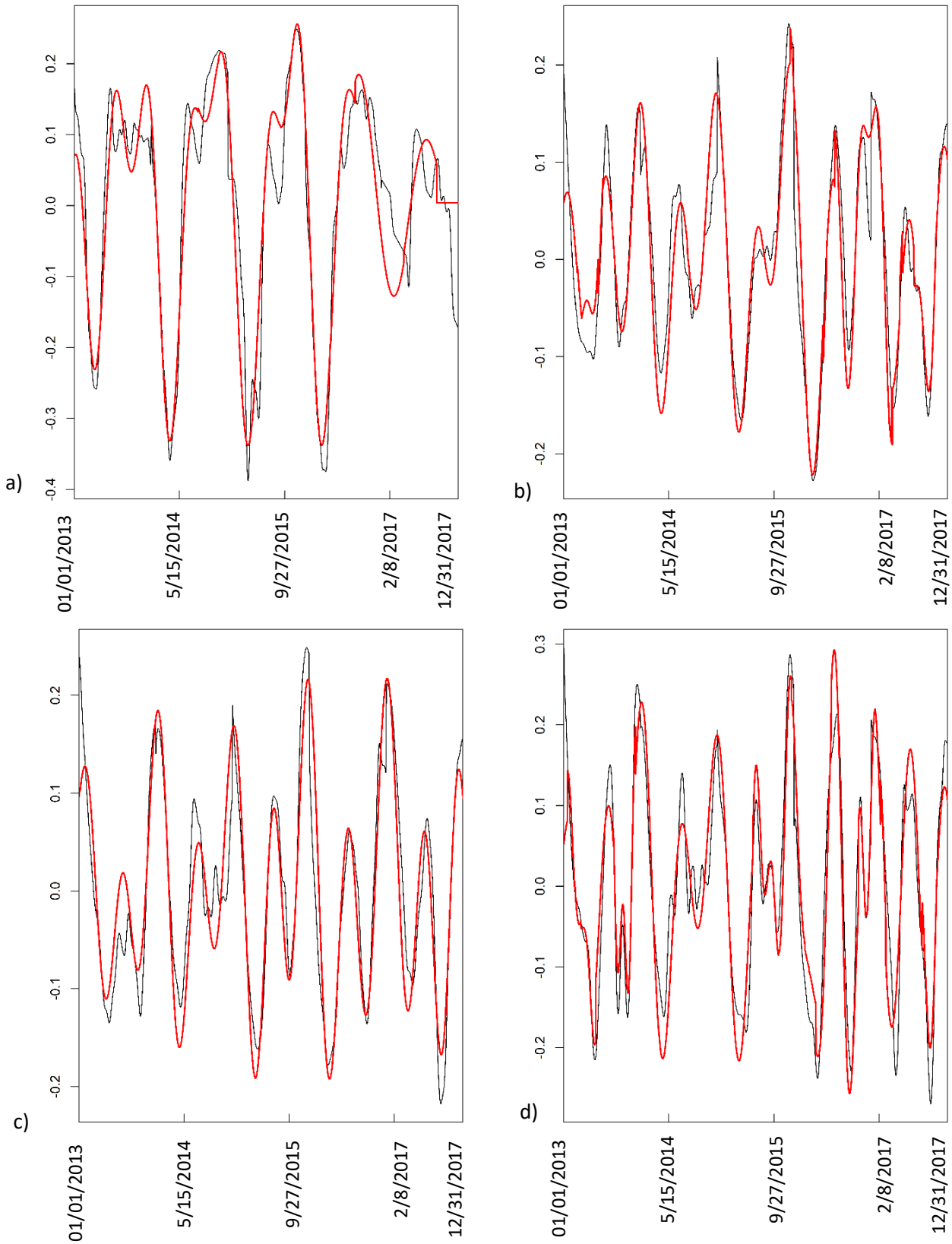

Literature Cited:

Arroyo-Mora, J. P., Sánchez-Azofeifa, G. A., Rivard, B., Calvo, J. C., & Janzen, D. H. (2005). Dynamics in landscape structure and composition for the Chorotega region, Costa Rica from 1960 to 2000. *Agriculture, Ecosystems and Environment*, *106*(1), 27–39. https://doi.org/10.1016/j.agee.2004.07.002

Brown, D. P. (2016). *HURRICANE OTTO NASA TERRA MODIS VISIBLE SATELLITE IMAGE OF HURRICANE OTT0 AT 1605 UTC 24 NOVEMBER 2016 JUST BEFORE LANDFALL AS A CATEGORY 3 HURRICANE IN SOUTHERN NICARAGUA. IMAGE COURTESY OF NASA'S EARTH OBSERVATORY*.

Burguillos, L., Parra, L., & Wagner, E. (2008). Human, ecologican, and biophysical dimensions of tropical dry forests. In *Manual of methods. Human, Ecologican, and Biophysical Dimensions of Tropical Dry Forests*.

Cai, Z., Jönsson, P., Jin, H., & Eklundh, L. (2017). Performance of smoothing methods for reconstructing NDVI time-series and estimating vegetation phenology from MODIS data. *Remote Sensing*, *9*(12). https://doi.org/10.3390/rs9121271

Cai, Z. Q., Schnitzer, S. A., & Bongers, F. (2009a). Seasonal differences in leaf-level physiology give lianas a competitive advantage over trees in a tropical seasonal forest. *Oecologia*, *161*(1), 25–33. https://doi.org/10.1007/s00442-009-1355-4

Cai, Z. Q., Schnitzer, S. A., & Bongers, F. (2009b). Seasonal differences in leaf-level physiology give lianas a competitive advantage over trees in a tropical seasonal forest. *Oecologia*, *161*(1), 25–33. https://doi.org/10.1007/s00442-009-1355-4

Calvo-Alvarado, J. C., McLennan, B., Sanchez-Azofeifa, G. A., & Garvin, T. (2009). Deforestation and forest restoration in Guanacaste, Costa Rica: Putting conservation policies in context. *For*, *258*, 931–940. https://doi.org/10.1016/j.foreco.2008.10.035

Carvalho, L. M. T., Clevers, J. G. P. W., Fonseca, L. M. G., & Murtagh, F. (2001). Digital change detection with the aid of multiresolution wavelet analysis. *International Journal of Remote Sensing*. https://doi.org/10.1080/01431160110069836

Castro, S. M., Sanchez-Azofeifa, G. A., & Sato, H. (2018). Effect of drought on productivity in a Costa Rican tropical dry forest Effect of drought on productivity in a Costa Rican tropical dry forest. *Environ. Res. Lett*, *13*. Retrieved from https://doi.org/10.1088/1748-9326/aaacbc

Chazdon, R. L., Broadbent, E. N., Rozendaal, D. M. A., Bongers, F., Zambrano, A. M. A., Aide, T. M., … Poorter, L. (2016). Carbon sequestration potential of second-growth forest regeneration in the Latin American tropics. *Science Advances*, *2*(5). https://doi.org/10.1126/sciadv.1501639

Chen, J., Jönsson, P., Tamura, M., Gu, Z., Matsushita, B., & Eklundh, L. (2004). A simple method for reconstructing a high-quality NDVI time-series data set based on the Savitzky-Golay filter. *Remote Sensing of Environment*. https://doi.org/10.1016/j.rse.2004.03.014

Daubenmire, R. (1972). Phenology and Other Characteristics of Tropical Semi-Deciduous Forest in North-Western Costa Rica. *The Journal of Ecology*, *60*(1), 147.

https://doi.org/10.2307/2258048

De Beurs, K. M., & Henebry, G. M. (2005). A statistical framework for the analysis of long image time series. *International Journal of Remote Sensing*. https://doi.org/10.1080/01431160512331326657

Demarty, J., Chevallier, F., Friend, A. D., Viovy, N., Piao, S., & Ciais, P. (2007). Assimilation of global MODIS leaf area index retrievals within a terrestrial biosphere model. *Geophysical Research Letters*, *34*(15), 1–6. https://doi.org/10.1029/2007GL030014

Demarty, M., & Bastien, J. (2011). GHG emissions from hydroelectric reservoirs in tropical and equatorial regions: Review of 20 years of CH4 emission measurements. *Energy Policy*, *39*(7), 4197–4206. https://doi.org/10.1016/j.enpol.2011.04.033

Fisher, J. B., Huntzinger, D. N., Schwalm, C. R., & Sitch, S. (2014). Modeling the terrestrial biosphere. *Annual Review of Environment and Resources*, *39*(1), 91–123. https://doi.org/10.1146/annurev-environ-012913-093456

Gabor, D. (1946). Theory of communication. Part 1: The analysis of information. *Journal of the Institution of Electrical Engineers - Part III: Radio and Communication Engineering*. https://doi.org/10.1049/ji-3-2.1946.0074

Gower, S. T., Kucharik, C. J., & Norman, J. M. (1999). Direct and indirect estimation of leaf area index, f(APAR), and net primary production of terrestrial ecosystems. *Remote Sensing of Environment*, *70*(1), 29–51. https://doi.org/10.1016/S0034-4257(99)00056-5

Grinsted, A., Moore, J. C., & Jevrejeva, S. (2004). Application of the cross wavelet transform and wavelet coherence to geophysical time series Nonlinear Processes in Geophysics Application of the cross wavelet transform and wavelet coherence to geophysical time series. In *European Geosciences Union (EGU)* (Vol. 11). Retrieved from http://www.pol.ac.uk/home/research/waveletcoherence/

Hlásny, T., Barka, I., Sitková, Z., Bucha, T., Konôpka, M., & Lukáč, M. (2015). MODIS-based vegetation index has sufficient sensitivity to indicate stand-level intra-seasonal climatic stress in oak and beech forests. *Annals of Forest Science*. https://doi.org/10.1007/s13595-014-0404-2

Huang, W., Huang, J., Wang, X., Wang, F., & Shi, J. (2013). Comparability of red/near-infrared reflectance and NDVI based on the spectral response function between MODIS and 30 other satellite sensors using rice canopy spectra. *Sensors (Basel, Switzerland)*, *13*(12), 16023–16050. https://doi.org/10.3390/s131216023

Janzen, D. H. (1988). Tropical dry forests. *Biodiversity*, 130–137.

Janzen, Daniel H. (2000). Costa Rica's Area de Conservación Guanacaste: A long march to survival through non-damaging biodevelopment. *Biodiversity*, *1*(2), 7–20. https://doi.org/10.1080/14888386.2000.9712501

Janzen, Daniel H, & Hallwachs, W. (2016). Biodiversity Conservation History and Future in Costa Rica: The Case of Área de Conservación Guanacaste (ACG). *Costa Rican Ecosystems*, 290.

Jensen, J. R. (1986). *Original Title: Introductory Digital Image Processing (Prentice Hall Series in Geographic Information Science) Introductory Digital Image Processing*.

Kalácska, M., Calvo-Alvarado, J. C., & Sánchez-Azofeifa, G. a. (2005). Calibration and assessment of seasonal changes in leaf area index of a tropical dry forest in different stages of succession. *Tree Physiology*, *25*(6), 733–744. https://doi.org/10.1093/treephys/25.6.733

Kalacska, M. E. R., Sanchez-Azofeifa, G. a, & … J. C. C.-. (2005). Effects of Season and Successional Stage on Leaf Area Index and Spectral Vegetation Indices in Three …. *Biotropica*, *37*(4), 486–496. Retrieved from http://www.ingentaconnect.com/content/bsc/btp/2005/00000037/00000004/art00002

Kalacska, M., Sanchez-Azofeifa, G. A., Calvo-Alvarado, J. C., Quesada, M., Rivard, B., & Janzen, D. H. (2004). Species composition, similarity and diversity in three successional stages of a seasonally dry tropical forest. *Forest Ecology and Management*, *200*(1–3), 227–247. https://doi.org/10.1016/j.foreco.2004.07.001

Khullar, S., Michael, A., Correa, N., Adali, T., Baum, S. A., & Calhoun, V. D. (2011). Wavelet-based fMRI analysis: 3-D denoising, signal separation, and validation metrics. *NeuroImage*, *54*(4), 2867–2884. https://doi.org/10.1016/j.neuroimage.2010.10.063

Knyazikhin, Y., Martonchik, J. V., Myneni, R. B., Diner, D. J., & Running, S. W. (1998). Synergistic algorithm for estimating vegetation canopy leaf area index and fraction of absorbed photosynthetically active radiation from MODIS and MISR data. *Journal of Geophysical Research*, *103*(D24), 32257. https://doi.org/10.1029/98JD02462

Lange, M., & Doktor, D. (2017). *phenex: Auxiliary Functions for Phenological Data Analysis. R package version 1.4-5.* Retrieved from https://cran.r-project.org/web/packages/phenex/phenex.pdf

Lau, K.-M., & Weng, H. (2002). Climate Signal Detection Using Wavelet Transform: How to Make a Time Series Sing. *Bulletin of the American Meteorological Society*, *76*(12), 2391–2402. https://doi.org/10.1175/1520-0477(1995)076<2391:csduwt>2.0.co;2

Li, Wei, Cao, S., Campos-Vargas, C., & Sanchez-Azofeifa, A. (2017). Identifying tropical dry forests extent and succession via the use of machine learning techniques. *International Journal of Applied Earth Observation and Geoinformation*, *63*, 196–205. https://doi.org/10.1016/J.JAG.2017.08.003

Li, Wenjuan, & Fang, H. (2015). Estimation of direct, diffuse, and total FPARs from Landsat surface reflectance data and ground-based estimates over six FLUXNET sites. *Journal of Geophysical Research: Biogeosciences*, *120*(1), 96–112. https://doi.org/10.1002/2014JG002754

Lieberman, D. (1982). Seasonality and Phenology in a Dry Tropical Forest in Ghana. *The Journal of Ecology*, *70*(3), 791. https://doi.org/10.2307/2260105

Lin, S., Li, J., Liu, Q., Li, L., Zhao, J., & Yu, W. (2019). Evaluating the Effectiveness of Using Vegetation Indices Based on Red-Edge Reflectance from Sentinel-2 to Estimate Gross Primary Productivity. *Remote Sensing*, *11*(11), 1303.

Magrin, G. O., Marengo, J. A., Boulanger, J. P., Buckeridge, M. S., Castellanos, E., Poveda, G.,

… Vicuña, S. (2014). Central and South America Coordinating Lead Authors : Lead Authors : Contributing Authors : Review Editors : *Climate Change 2014: Impacts, Adaptation, and Vulnerability. Part B: Regional Aspects. Contribution of Working Group II to the Fifth Assessment Report of the Intergovernmental Panel on Climate Change [Barros, V.R., C.B. Field, D.J. Dokken, M.D. Mastrandre*, *Central an*, 1499–1566.

Majasalmi, T. (2015). *Estimation of leaf area index and the fraction of absorbed photosynthetically active radiation in a boreal*. https://doi.org/10.14214/df.187

Majasalmi, T., Stenberg, P., & Rautiainen, M. (2017). Comparison of ground and satellite-based methods for estimating stand-level fPAR in a boreal forest. *Agricultural and Forest Meteorology*, *232*, 422–432. https://doi.org/10.1016/j.agrformet.2016.09.007

Martínez, B., & Gilabert, M. A. (2009). Vegetation dynamics from NDVI time series analysis using the wavelet transform. *Remote Sensing of Environment*, *113*(9), 1823–1842. https://doi.org/10.1016/j.rse.2009.04.016

McDowell, N. G., Coops, N. C., Beck, P. S. A., Chambers, J. Q., Gangodagamage, C., Hicke, J. A., … Allen, C. D. (2015). Global satellite monitoring of climate-induced vegetation disturbances. *Trends in Plant Science*. https://doi.org/10.1016/j.tplants.2014.10.008

Meir, P., & Pennington, R. T. (2011). Climatic change and seasonally dry tropical forests. In *Seasonally Dry Tropical Forests* (pp. 279–299). Springer.

Minnis, P., Doelling, D. R., Nguyen, L., Miller, W. F., & Chakrapani, V. (2008). Assessment of the visible channel calibrations of the VIRS on TRMM and MODIS on Aqua and Terra. *Journal of Atmospheric and Oceanic Technology*, *25*(3), 385–400. https://doi.org/10.1175/2007JTECHA1021.1

Myneni, R. B., Hoffman, S., Knyazikhin, Y., Privette, J. L., Glassy, J., Tian, Y., … Running, S. W. (2002). Global products of vegetation leaf area and fraction absorbed PAR from year one of MODIS data. *Remote Sensing of Environment*, *83*(1–2), 214–231. https://doi.org/10.1016/S0034-4257(02)00074-3

Myneni, R. B., & Williams, D. L. (1994). On the relationship between FAPAR and NDVI. *Remote Sensing of Environment*, *49*(3), 200–211. https://doi.org/10.1016/0034-4257(94)90016-7

Myneni, R., Knyazikhin, Y., & Park, T. (2015). MOD15A2H MODIS Leaf Area Index/FPAR 8-Day L4 Global 500m SIN Grid V006. NASA EOSDIS Land Processes DAAC. *LP DAAC*, *Terra*(6), 1. https://doi.org/https://doi.org/10.5067/modis/mod15a2h.006

Myneni, R.B., Knyazikhin, Y., Privette, J. L., Running, S. W., Nemani, R., Zhang, Y., … Votava, P. (1999). MODIS Leaf Area Index (LAI) And Fraction Of Photosynthetically Active Radiation Absorbed By Vegetation (FPAR) Product. *Modis Atbd*, *Version 4.*(4.0), 130. https://doi.org/http://eospso.gsfc.nasa.gov/atbd/modistables.html

Myneni, R.B., & Park, T. (2015). *MCD15A3H MODIS/Terra+Aqua Leaf Area Index/FPAR 4-Day L4 Global 500m SIN Grid V006. NASA EOSDIS Land Processes DAAC*. https://doi.org/https://doi.org/10.5067/MODIS/MCD15A3H.006

Myneni, Ranga B. (1997). Estimation of global leaf area index and absorbed par using radiative

transfer models. *IEEE Transactions on Geoscience and Remote Sensing*, *35*(6), 1380–1393. https://doi.org/10.1109/36.649788

Nestola, E., Sánchez-Zapero, J., Latorre, C., Mazzenga, F., Matteucci, G., Calfapietra, C., & Camacho, F. (2017). Validation of PROBA-V GEOV1 and MODIS C5 & C6 fAPAR products in a deciduous beech forest site in Italy. *Remote Sensing*, *9*(2), 126. https://doi.org/10.3390/rs90201026

ORNL. (2018). *ORNL DAAC. 2017. MODIS Collection 6 Land Products Global Subsetting and Visualization Tool. ORNL DAAC, Oak Ridge, Tennessee, USA. Accessed April 04, 2018. Subset obtained for MCD15A3H product at 10.8415N,85.6157W, time period: 2017-07-20 to 2018-03-22, an*. https://doi.org/https://doi.org/10.3334/ORNLDAAC/1379

Peng, D., Zhang, B., Liu, L., Fang, H., Chen, D., Hu, Y., & Liu, L. (2012). Characteristics and drivers of global NDVI-based FPAR from 1982 to 2006. *Global Biogeochemical Cycles*, *26*(3).

Pennington, T. (2010). Human, Ecological and Biophysical Dimensions of Tropical Dry Forests. Manual of Methods (Book review). In *Interciencia* (Vol. 35).

Percival, D. B., & Walden, A. T. (2006). *Wavelet methods for time series analysis* (Vol. 4). Cambridge university press.

Phillips, L. B., Hansen, A. J., & Flather, C. H. (2008). Evaluating the species energy relationship with the newest measures of ecosystem energy: NDVI versus MODIS primary production. *Remote Sensing of Environment*, *112*(9), 3538–3549. https://doi.org/10.1016/j.rse.2008.04.012

Portillo-Quintero, C. A., & Sánchez-Azofeifa, G. A. (2010). Extent and conservation of tropical dry forests in the Americas. *Biological Conservation*, *143*(1), 144–155. https://doi.org/10.1016/j.biocon.2009.09.020

Putzenlechner, B., Marzahn, P., Kiese, R., Ludwig, R., & Sanchez-Azofeifa, A. (2019). Assessing the variability and uncertainty of two-flux FAPAR measurements in a conifer-dominated forest. *Agricultural and Forest Meteorology*, *264*(October 2018), 149–163. https://doi.org/10.1016/j.agrformet.2018.10.007

QUANTUM SENSOR Models SQ-100 and SQ-300 Series (including SS models). (2019). Retrieved from https://www.apogeeinstruments.com/content/SQ-100-300-manual.pdf

Rankine, C., Sánchez-Azofeifa, G. A., Guzmán, J. A., Espirito-Santo, M. M., & Sharp, I. (2017). Comparing MODIS and near-surface vegetation indexes for monitoring tropical dry forest phenology along a successional gradient using optical phenology towers Comparing MODIS and near-surface vegetation indexes for monitoring tropical dry forest phenology . *Environ. Res. Lett*, *12*. https://doi.org/10.1088/1748-9326/aa838c

Reich, P. B., & Borchert, R. (1984). Water Stress and Tree Phenology in a Tropical Dry Forest in the Lowlands of Costa Rica. *The Journal of Ecology*, *72*(1), 61. https://doi.org/10.2307/2260006

Roesch, A., & Schmidbauer, H. (2018). *WaveletComp: Computational Wavelet Analysis*. Retrieved from https://cran.r-project.org/package=WaveletComp

Sakamoto, T., Yokozawa, M., Toritani, H., Shibayama, M., Ishitsuka, N., & Ohno, H. (2005). A crop phenology detection method using time-series MODIS data. *Remote Sensing of Environment*, *96*(3–4), 366–374. https://doi.org/10.1016/j.rse.2005.03.008

Sánchez-Azofeifa, G. A., Quesada, M., Rodríguez, J. P., Nassar, J. M., Stoner, K. E., Castillo, A., … Cuevas-Reyes, P. (2005). Research priorities for neotropical dry forests. *Biotropica*, *37*(4), 477–485. https://doi.org/10.1111/j.1744-7429.2005.00066.x

Savitzky, A., & Golay, M. J. E. (1964). Smoothing and Differentiation of Data by Simplified Least Squares Procedures. *Analytical Chemistry*. https://doi.org/10.1021/ac60214a047

Schlerf, M., & Atzberger, C. (2006). Inversion of a forest reflectance model to estimate structural canopy variables from hyperspectral remote sensing data. *Remote Sensing of Environment*. https://doi.org/10.1016/j.rse.2005.10.006

Sellers, P. J. (1987). Canopy reflectance, photosynthesis, and transpiration, II. The role of biophysics in the linearity of their interdependence. *Remote Sensing of Environment*, *21*(2), 143–183. https://doi.org/10.1016/0034-4257(87)90051-4

Serbin, S. P., Ahl, D. E., & Gower, S. T. (2013). Spatial and temporal validation of the MODIS LAI and FPAR products across a boreal forest wildfire chronosequence. *Remote Sensing of Environment*, *133*, 71–84. https://doi.org/10.1016/j.rse.2013.01.022

Shabanov, N. V., Wang, Y., Buermann, W., Dong, J., Hoffman, S., Smith, G. R., … Myneni, R. B. (2003). Effect of foliage spatial heterogeneity in the MODIS LAI and FPAR algorithm over broadleaf forests. *Remote Sensing of Environment*, *85*(4), 410–423. https://doi.org/10.1016/S0034-4257(03)00017-8

Shumway, R. H., & Stoffer, D. S. (2011). *Time Series Analysis and Its Applications*. https://doi.org/10.1007/978-1-4419-7865-3

Stan, K., & Sanchez-Azofeifa, A. (2019). Deforestation and secondary growth in Costa Rica along the path of development. *Regional Environmental Change*, *19*(2), 587–597. https://doi.org/10.1007/s10113-018-1432-5

Steinberg, D., Goetz, S., & Hyer, E. (2006). Validation of MODIS F/sub PAR/products in boreal forests of Alaska. *Geoscience and Remote …*, *44*(7), 1–11. Retrieved from http://ieeexplore.ieee.org/xpls/abs_all.jsp?arnumber=1645282

Torrence C., & Compo G. (1998). A practical guide to wavelet analysis. *Bulletin of the American Meteorological Society*, *79 (1)*, 61--78. Retrieved from https://journals.ametsoc.org/doi/pdf/10.1175/1520-0477%281998%29079%3C0061%3AAPGTWA%3E2.0.CO%3B2

Walter-Shea, E. A., Blad, B. L., Hays, C. J., Mesarch, M. A., Deering, D. W., & Middleton, E. M. (1992). Biophysical properties affecting vegetative canopy reflectance and absorbed photsynthetically active radiation at the FIFE site. *Journal of Geophysical Research*, *97*(D17), 925–943. https://doi.org/10.1029/92jd00656

Wang, F., & D'Sa, E. J. (2010). Potential of MODIS EVI in identifying hurricane disturbance to coastal vegetation in the Northern Gulf of Mexico. *Remote Sensing*, *2*(1), 1–18. https://doi.org/10.3390/rs2010001

Weiss, M., Baret, F., Myneni, R. B., Pragnère, A., & Knyazikhin, Y. (2000). Investigation of a model inversion technique to estimate canopy biophysical variables from spectral and directional reflectance data. *Agronomie*, *20*(1), 3–22. https://doi.org/10.1051/agro:2000105

Widlowski, J.-L. (2010). On the bias of instantaneous FAPAR estimates in open-canopy forests. *Agricultural and Forest Meteorology*, *150*(12), 1501–1522. https://doi.org/10.1016/J.AGRFORMET.2010.07.011

Yan, K., Park, T., Yan, G., Liu, Z., Yang, B., Chen, C., … Myneni, R. B. (2016). Evaluation of MODIS LAI/FPAR product collection 6. Part 1: Consistency and Improvements. *Remote Sensing*, *8*(6), 1–16. https://doi.org/10.3390/rs8060460

Zhang, R., Zhou, Y., Luo, H., Wang, F., & Wang, S. (2017). Estimation and analysis of spatiotemporal dynamics of the net primary productivity integrating efficiency model with process model in Karst area. *Remote Sensing*, *9*(5). https://doi.org/10.3390/rs9050477

Zhang, X., Friedl, M. A., Schaaf, C. B., Strahler, A. H., Hodges, J. C. F., Gao, F., … Huete, A. (2003). Monitoring vegetation phenology using MODIS. *Remote Sensing of Environment*. https://doi.org/10.1016/S0034-4257(02)00135-9

Zhang, Y., Song, C., Band, L. E., & Sun, G. (2019). No proportional increase of terrestrial gross carbon sequestration from the greening Earth. *Journal of Geophysical Research: Biogeosciences*, *124*(8), 2540–2553.

Zhao, M., Heinsch, F. A., Nemani, R. R., & Running, S. W. (2005). Improvements of the MODIS terrestrial gross and net primary production global data set. *Remote Sensing of Environment*, *95*(2), 164–176. https://doi.org/10.1016/j.rse.2004.12.011

Chapter 4 – Significance, Contributions & Conclusions

The field of remote sensing science is radically transforming humanities understanding of how the atmosphere and biogeosphere interact with one another, unveiling the utility of these interactions to discover more about our globe. As landscape-level changes continue to accelerate in their frequency and magnitude, it has been imperative for humanity to employ satellites to capture imagery of the globe to quantify and monitor how this expansive change is influencing the globe. These satellites images act not only as tools to extract the current state of the globe, but as repositories to archive the planets' past, establishing a baseline or reference for how Earths' biosphere, atmosphere, and hydrosphere used to behave. Due to the capabilities of these satellites to extract multi-spectral information about the Earth's surface, it has been possible to employ this data for historical and long-term forest monitoring, extracting information about important vegetative physiological processes such as photosynthesis (Ryu, et al., 2019). These satellites are tools useful for us in determining the behaviour of biomes photosynthetic capabilities and the response of these biomes to weather events and climatic change. As the scientific community marches forward, increasing the number of vegetation monitoring programs available there comes a need for the establishment of methods to test for the reliability, adaptability, and validity of these satellite-derived biophysical products to understand the limitations and capabilities of these products. As a response to this new demand, near surface remote sensing techniques such as wireless sensor networks, capable of replicating comparable biophysical products from those derived by satellites are necessary.

Wireless sensor networks have started to gain popularity as passive-monitoring instruments for meteorological and biophysical variables, primarily in the northern hemisphere due to the prohibitive capital costs restricting their application to regions where institutions with more funding can afford them (Burgess, et al., 2010; Nestola et al., 2017; Putzenlechner, et al., 2019; Rawat, et al., 2014; Younis & Akkaya, 2008). Despite this, the high temporal and spatial resolution that these wireless sensor networks can provide allows for the collection of vast amounts of highly detailed data about ecosystem health and productivity. In a time where the climate is rapidly changing, these datasets collected provide the temporal resolution necessary to establish baselines for the behaviour of biomes to regular climatic cycles, extreme weather events, and disruptions or rapid changes in the climate (Burgess et al., 2010; Sanchez-Azofeifa et

al., 2017). As the technology and data science techniques advance, these wireless sensor networks may become integral parts in the monitoring of environments helping inform governments of impending droughts, water & air quality issues, or extreme temperature events providing the means to be proactive in responding to these events (Sanchez-Azofeifa et al., 2017). Subsequently, if these networks are to become tools to be relied upon, research on the setup, utilization, and influences that environmental factors have on these networks in a variety of environments is necessary to exploit this tool to its maximum benefit.

This need led to the installation and development of a WSN in the tropical dry forest of Costa Rica's, Santa Rosa National Park. Tropical Dry Forests (TDFs) are broadly classified as broadleaf deciduous forests (Sánchez-Azofeifa et al., 2005) but are unique in that these forests phenology is tied to precipitation and atmospheric events transforming them from arid, leafless forests to lush, highly productive environments capable of hosting many endemic species in the span of ten to twenty days (Lieberman, 1982; Reich & Borchert, 1984). The sensitivity and responsiveness of TDFs to changes in the atmospheric and soil water content makes it an ideal ecosystem-level bio-indicator for climate change impacts in the tropics. Much remains unclear in the scientific literature about the influence that climate change will have on the productivity and health of tropical forests, especially in comparison with northern forests which have been exhibiting earlier spring bud-burst timing in response to an increase in temperature (Menzel et al., 2006). Currently, no clear relationship between tree species community assemblages, ecosystem succession, and phenology has been established in the tropics, making it essential to establish baselines for the phenological behaviour of TDFs found in different successional stages. Establishing a baseline for how TDFs behave during regular climatic patterns will help assess, identify, and link anomalous phenological behaviour to climatic patterns, changes or weather events. With Huang, et al., (2013) already having predicted that tropical precipitation patterns are likely to become more temporally abrupt, spatially concentrated, and irregular, following the suns latitudinal position, concerns arise that this inter-annual variability of the seasonal timing and intensity of precipitation events will have significant effects on the regional and global biogeochemical cycles. These concerns extend to the unknown consequences for those local communities that co-exist in these regions as well, many of which rely upon the predictability of seasonal phenological cycles for their livelihood. Understanding how climatic

change will affect these environments is therefore crucial to preserving, conserving, and utilizing them to minimize the impact that climate change will have.

Therefore, given that forest ecosystem phenology is a major driver for landscape, regional, and global annual exchanges of atmospheric carbon, it is important to acknowledge that climate-induced shifts in phenology currently significantly limit our ability to predict the biospheres responses to the multitude of future climate regimes. Therefore, it is important to establish a methodology to capture the current phenologic behaviour of these forests, which can be employed in understanding how forests will respond to future changes in phenology (Collins, 2007; Dessai, et al., 2009). To monitor forest phenology, it is necessary to implement a tool that is capable of both providing information about the total amount of photosynthesizing vegetation and the health of vegetation. One biophysical variable that is capable of encapsulating these two qualities in a single value is the fraction of Photosynthetic Active Radiation (fPAR). The fPAR quantifies the amount of photosynthetic radiation being utilized by vegetation, which directly corresponds to the amount of photosynthesizing vegetation present and the capacity for that vegetation to photosynthesize which is consequently related to the health of vegetation. This study then focuses on the implementation of a wireless sensor network in a tropical dry forest to study fPAR, to further the understanding of TDF response to seasonal and climatic patterns.

Research Contributions and Implications for Future Work

The studies that are presented in this thesis are unique in that it both reviews the environmental and methodological influences on the creation of an *in-situ 2-flux fPAR* product in a TDF and then implements that product to test and validate the MODIS-derived fPAR product for its ability to detect phenological patterns that occur in a TDF. As a biophysical variable, fPAR has been tested extensively in the forests of the northern hemisphere (Nestola et al., 2017; Putzenlechner et al., 2019; Widlowski, 2010) but any testing in tropical forests has been scarce (Senna, 2005) or absent for TDFs. The results therefore are presented to address the limitations and pitfalls of using wireless sensor networks for the long-term monitoring of phenological cycles in TDFs and to promote the validity of using a WSN-derived fPAR products for the validation of satellite-derived fPAR products. Identifying the phenological patterns of TDFs in this study is meant to promote the scientific communities current understanding of the function and behaviour of tropical dry forests, to better implement conservation and management

practices for the preservation of these ecosystems. The time-series presented in this study, and the subsequent data are also meant to establish a baseline or reference for the long-term behaviour of tropical dry forest phenology, to be used in future works for the evaluation of tropical dry forest health, productivity, and phenologic variability in the semi-arid landscapes of Central and South America.

Chapter Two: *Characterization of PAR sensors and an in-situ fraction of Photosynthetic Active Radiation product in a tropical dry-forest.*

Wireless sensor networks can be quickly and easily installed in a variety of configurations with an adjustable number of nodes, permitting a networks expansion and enabling it to cover space equivalent to that of a satellite pixel. Regardless, it is determined that a minimum of ten or more nodes is necessary for a WSN to create a network-averaged fPAR product that is statistically invariant enough to be relied on as a reference for satellite-validation or comparative purposes. Of the environmental factors tested in the study, it was determined that solar zenith angle is the most influential variable for the estimation of *in-situ* fPAR, followed by the sky condition and then wind speed. While wind speeds greater than 5m/s were determined to cause a detectable increase in the variability of *in-situ 2-flux fPAR,* the frequency of wind speeds reaching this speed is low during maturity and green-up, and therefore should be more strongly considered during senescence when wind speeds greater than 5 m/s are more common. This study also supports the conclusions made by Li & Fang, (2015) that estimates of fPAR made under larger solar zenith angles ($SZA > 27°$) promotes the overestimation of *in-situ* fPAR due to an increase in the length of the path for a photon to reach a PAR sensor, subsequently, increasing the likelihood of interception for that photon. To capture the true canopy state during maturity, under clear-sky conditions, while keeping variation to under 10% as set by the GCOS, 10+ sensors are necessary with the condition that measurements are taken when $WS < 3$ m/s. The study also determined that sky condition had a significant effect on the estimation of 2-flux fPAR, especially during the transitional phenophases, where clear-sky conditions typically led to unimodal distributions with less variance compared to those measurements taken under diffuse sky conditions that typically exhibited bimodal distributions with larger degrees of variability. The results from the study indicate that it is necessary to split the analysis of *in-situ 2-flux fPAR* into is respective phenophases to accurately describe how fPAR reacts to seasonal variation, but

also indicates the need for physical evidence to determine how leaf area and leaf colour influence the estimation of *in-situ 2-flux fPAR* in a TDF. It is also indicated in this study that sensor recalibration should be considered for PAR sensors, especially for those that have been deployed for long periods as to ensure the integrity of a studies data when utilizing WSNs.

Chapter Three: *Employing wavelet-transforms and cross-wavelet analysis to validate the MODIS fPAR time-series over a tropical dry forest*.

The study utilized two different methodologies to compare the phenological patterns captured by the *in-situ* Green fPAR product created from the WSN and fPAR products derived from the MODIS platforms mounted to the satellites Terra and Aqua. The first, a derivative-based method, made it possible to extract a date for the onset of green-up and senescence which identified that the MODIS fPAR products were, as a total, performing better for the estimation of the onset of green-up than the onset of senescence. MODIS fPAR products were consistently at least two to six weeks delayed in the estimation of these dates when compared with the *in-situ* Green fPAR product. The second method implemented the continuous-wavelet transform, which led to the univariate analysis of each fPAR products time-series determining that time-period scales of 364 days, 186 days, and 98 days seemed to co-vary with the shape of the Morlet wavelet. The longer time-period scales of 364 days and 186 days were more consistent and had significant covariance with the Morlet wavelet for all the years analyzed for all the products, whereas the time-period scales between 64-128 days were much less consistent. Once cross-wavelet analysis was performed between the *in-situ* Green fPAR product and the respective MODIS fPAR products, the study determines that the MODIS-derived fPAR products are capable of detecting the yearly 364-day phenological cycle and the bi-annual double peaking feature present during the maturity phenophase at the 184-day scale, but are inaccurate in capturing the timing of such events. The *in-situ* Green fPAR product consistently led or detected these cycles prior to the MODIS fPAR products resulting in incoherence between the *in-situ* Green fPAR product and the MODIS fPAR products, especially during the 2016 and 2017 phenological cycles. The only period in which the *in-situ* fPAR product and MODIS fPAR products achieve coherence at time-period scales > 128 days is during the senescence phenophase, when both fPAR products are decreasing significantly towards their yearly minima. Of note, is that the MODIS fPAR product seemed incapable of capturing a change in the

phenological cycle of the TDF, in regard to its response to a late-season hurricane event which prolonged the maturity phenophase for 2016, significantly shortening its senescence phase. The inability for the MODIS fPAR product to capture this disruption in the phenological cycle, along with its depressed intra-seasonal amplitude seems to indicate that the MODIS fPAR products may not be sensitive enough to precisely capture changes in fPAR. Therefore, the MODIS fPAR products ability to accurately assess fine-scale changes in phenology cannot be relied upon, limiting its functionality to assessing the existence, but not the timing, of broad-scale phenologic patterns for TDFs.

Overall Significance

The findings and results presented in this thesis should be used to broaden the scientific communities' knowledge regarding the development of *in-situ fPAR* products in tropical dry forests, its uses and limitations in the validation of satellite-derived fPAR products, and to bring to light the concepts of phenological monitoring as a relevant conservation parameter. It also pursues the idea that satellite remote sensing techniques need to be complimented with near surface remote sensing techniques to ensure that satellite-derived biophysical products continue to improve in their temporal accuracy and the scalability of information for biophysical dynamics. As climate-induced phenological change becomes a more pressing issue, understanding how secondary tropical dry forests respond to these changes is imperative to our ability to assess forest health, and prioritize forest conservation and regeneration efforts. Exploring new tools and techniques to implement into these assessments will provide rapid and reliable evaluations about the condition of these Neotropical dry forests and its ecosystem dynamics. It is the hope of this thesis that the concepts and methodologies discussed will contribute to the conversation about establishing standardized protocols and methods for the validation of satellite-derived biophysical products, therefore contributing to the fields of Earth observation and forestry conservation sciences.

Literature Cited:

Burgess, S. S. O., Kranz, M. L., Turner, N. E., Cardell-Oliver, R., & Dawson, T. E. (2010). Harnessing wireless sensor technologies to advance forest ecology and agricultural research. *Agricultural and Forest Meteorology*, *150*(1), 30–37. https://doi.org/10.1016/j.agrformet.2009.08.002

Collins, M. A. T. (2007). Ensembles and probabilities: A new era in the prediction of climate change. *Philosophical Transactions of the Royal Society A: Mathematical, Physical and Engineering Sciences*. https://doi.org/10.1098/rsta.2007.2068

Dessai, S., Hulme, M., Lempert, R., & Pielke, R. (2009). Do We Need Better Predictions to Adapt to a Changing Climate? *Eos, Transactions American Geophysical Union*. https://doi.org/10.1029/2009eo130003

Huang, P., Xie, S. P., Hu, K., Huang, G., & Huang, R. (2013). Patterns of the seasonal response of tropical rainfall to global warming. *Nature Geoscience*. https://doi.org/10.1038/ngeo1792

Li, W., & Fang, H. (2015). Estimation of direct, diffuse, and total FPARs from Landsat surface reflectance data and ground-based estimates over six FLUXNET sites. *Journal of Geophysical Research: Biogeosciences*, *120*(1), 96–112. https://doi.org/10.1002/2014JG002754

Lieberman, D. (1982). Seasonality and Phenology in a Dry Tropical Forest in Ghana. *The Journal of Ecology*, *70*(3), 791. https://doi.org/10.2307/2260105

Menzel, A., Sparks, T. H., Estrella, N., Koch, E., Aaasa, A., Ahas, R., … Zust, A. (2006). European phenological response to climate change matches the warming pattern. *Global Change Biology*. https://doi.org/10.1111/j.1365-2486.2006.01193.x

Nestola, E., Sánchez-Zapero, J., Latorre, C., Mazzenga, F., Matteucci, G., Calfapietra, C., & Camacho, F. (2017). Validation of PROBA-V GEOV1 and MODIS C5 & C6 fAPAR products in a deciduous beech forest site in Italy. *Remote Sensing*, *9*(2). https://doi.org/10.3390/rs90201026

Putzenlechner, B., Marzahn, P., Kiese, R., Ludwig, R., & Sanchez-Azofeifa, A. (2019). Assessing the variability and uncertainty of two-flux FAPAR measurements in a conifer-dominated forest. *Agricultural and Forest Meteorology*, *264*(October 2018), 149–163. https://doi.org/10.1016/j.agrformet.2018.10.007

Rawat, P., Singh, K. D., Chaouchi, H., & Bonnin, J. M. (2014). Wireless sensor networks: A survey on recent developments and potential synergies. *Journal of Supercomputing*, *68*(1), 1–48. https://doi.org/10.1007/s11227-013-1021-9

Reich, P. B., & Borchert, R. (1984). Water Stress and Tree Phenology in a Tropical Dry Forest in the Lowlands of Costa Rica. *The Journal of Ecology*, *72*(1), 61. https://doi.org/10.2307/2260006

Ryu, Y., Berry, J. A., & Baldocchi, D. D. (2019). What is global photosynthesis? History, uncertainties and opportunities. *Remote Sensing of Environment*, *223*(January), 95–114. https://doi.org/https://doi.org/10.1016/j.rse.2019.01.016

Sanchez-Azofeifa, A., Antonio Guzmán, J., Campos, C. A., Castro, S., Garcia-Millan, V., Nightingale, J., & Rankine, C. (2017). Twenty-first century remote sensing technologies are revolutionizing the study of tropical forests. *Biotropica*, Vol. 49, pp. 604–619. https://doi.org/10.1111/btp.12454

Sánchez-Azofeifa, G. A., Quesada, M., Rodríguez, J. P., Nassar, J. M., Stoner, K. E., Castillo, A., … Cuevas-Reyes, P. (2005). Research priorities for neotropical dry forests. *Biotropica*, *37*(4), 477–485. https://doi.org/10.1111/j.1744-7429.2005.00066.x

Senna, M. C. A. (2005). Fraction of photosynthetically active radiation absorbed by Amazon tropical forest: A comparison of field measurements, modeling, and remote sensing. *Journal of Geophysical Research*, *110*(G1), G01008. https://doi.org/10.1029/2004JG000005

Widlowski, J.-L. (2010). On the bias of instantaneous FAPAR estimates in open-canopy forests. *Agricultural and Forest Meteorology*, *150*(12), 1501–1522. https://doi.org/10.1016/J.AGRFORMET.2010.07.011

Younis, M., & Akkaya, K. (2008). Strategies and techniques for node placement in wireless sensor networks: A survey. *Ad Hoc Networks*, *6*(4), 621–655. https://doi.org/10.1016/J.ADHOC.2007.05.003

Literature Cited for the Complete Thesis

Ahl, D. E., Gower, S. T., Burrows, S. N., Shabanov, N. V., Myneni, R. B., & Knyazikhin, Y. (2006). Monitoring spring canopy phenology of a deciduous broadleaf forest using MODIS. *Remote Sensing of Environment*, *104*(1), 88–95. https://doi.org/10.1016/J.RSE.2006.05.003

Akitsu, T., Nasahara, K. N., Hirose, Y., Ijima, O., & Kume, A. (2017). Quantum sensors for accurate and stable long-term photosynthetically active radiation observations. *Agricultural and Forest Meteorology*, *237–238*, 171–183. https://doi.org/10.1016/J.AGRFORMET.2017.01.011

Alton, P. B. (2018). Decadal trends in photosynthetic capacity and leaf area index inferred from satellite remote sensing for global vegetation types. *Agricultural and Forest Meteorology*, *250–251*, 361–375. https://doi.org/10.1016/j.agrformet.2017.11.020

Apogee Quantum Sensor Calibration Certificate. (2019).

Arivazhagan, S., & Ganesan, L. (2003). Texture classification using wavelet transform. *Pattern Recognition Letters*. https://doi.org/10.1016/S0167-8655(02)00390-2

Arroyo-Mora, J. P., Sánchez-Azofeifa, G. A., Rivard, B., Calvo, J. C., & Janzen, D. H. (2005). Dynamics in landscape structure and composition for the Chorotega region, Costa Rica from 1960 to 2000. *Agriculture, Ecosystems and Environment*, *106*(1), 27–39. https://doi.org/10.1016/j.agee.2004.07.002

Asner, G. P., & Wessman, C. A. (1997). Scaling PAR absorption from the leaf to landscape level in spatially heterogeneous ecosystems. *Ecological Modelling*, *103*(1), 81–97. https://doi.org/10.1016/S0304-3800(97)00080-X

Atkins, J. W., Fahey, R. T., Hardiman, B. H., & Gough, C. M. (2018). Forest Canopy Structural Complexity and Light Absorption Relationships at the Subcontinental Scale. *Journal of Geophysical Research: Biogeosciences*, *123*(4), 1387–1405. https://doi.org/10.1002/2017JG004256

Bondeau, A., Kicklighter, D. W., & Kaduk, J. (1999). Comparing global models of terrestrial net primary productivity (NPP): Importance of vegetation structure on seasonal NPP estimates. *Global Change Biology*, *5*(SUPPL. 1), 35–45. https://doi.org/10.1046/j.1365-2486.1999.00005.x

Bradley, B. A., Jacob, R. W., Hermance, J. F., & Mustard, J. F. (2007). A curve fitting procedure to derive inter-annual phenologies from time series of noisy satellite NDVI data. *Remote Sensing of Environment*. https://doi.org/10.1016/j.rse.2006.08.002

Brown, D. P. (2016). *HURRICANE OTTO NASA TERRA MODIS VISIBLE SATELLITE IMAGE OF HURRICANE OTT0 AT 1605 UTC 24 NOVEMBER 2016 JUST BEFORE LANDFALL AS A CATEGORY 3 HURRICANE IN SOUTHERN NICARAGUA. IMAGE COURTESY OF NASA'S EARTH OBSERVATORY*.

Burgess, S. S. O., Kranz, M. L., Turner, N. E., Cardell-Oliver, R., & Dawson, T. E. (2010). Harnessing wireless sensor technologies to advance forest ecology and agricultural research. *Agricultural and Forest Meteorology*, *150*(1), 30–37.

https://doi.org/10.1016/j.agrformet.2009.08.002

Burguillos, L., Parra, L., & Wagner, E. (2008). Human, ecologican, and biophysical dimensions of tropical dry forests. In *Manual of methods. Human, Ecologican, and Biophysical Dimensions of Tropical Dry Forests*.

Cai, Z., Jönsson, P., Jin, H., & Eklundh, L. (2017). Performance of smoothing methods for reconstructing NDVI time-series and estimating vegetation phenology from MODIS data. *Remote Sensing*, *9*(12). https://doi.org/10.3390/rs9121271

Cai, Z. Q., Schnitzer, S. A., & Bongers, F. (2009). Seasonal differences in leaf-level physiology give lianas a competitive advantage over trees in a tropical seasonal forest. *Oecologia*, *161*(1), 25–33. https://doi.org/10.1007/s00442-009-1355-4

Calvo-Alvarado, J. C., McLennan, B., Sanchez-Azofeifa, G. A., & Garvin, T. (2009). Deforestation and forest restoration in Guanacaste, Costa Rica: Putting conservation policies in context. *For*, *258*, 931–940. https://doi.org/10.1016/j.foreco.2008.10.035

Calvo-Alvarado, J., McLennan, B., Sánchez-Azofeifa, A., & Garvin, T. (2009). Deforestation and forest restoration in Guanacaste, Costa Rica: Putting conservation policies in context. *Forest Ecology and Management*, *258*(6), 931–940. https://doi.org/10.1016/j.foreco.2008.10.035

Campos, F. A. (2018). *A Synthesis of Long-Term Environmental Change in Santa Rosa, Costa Rica*. https://doi.org/10.1007/978-3-319-98285-4_16

Canadell, J. G., & Raupach, M. R. (2008, June 13). Managing forests for climate change mitigation. *Science*, Vol. 320, pp. 1456–1457. https://doi.org/10.1126/science.1155458

Cao, S., & Sanchez-Azofeifa, A. (2017). Modeling seasonal surface temperature variations in secondary tropical dry forests. *International Journal of Applied Earth Observation and Geoinformation*, *62*(October), 122–134. https://doi.org/10.1016/j.jag.2017.06.008

Cao, S., Yu, Q., Sanchez-Azofeifa, A., Feng, J., Rivard, B., & Gu, Z. (2015). Mapping tropical dry forest succession using multiple criteria spectral mixture analysis. *ISPRS Journal of Photogrammetry and Remote Sensing*, *109*, 17–29. https://doi.org/10.1016/j.isprsjprs.2015.08.009

Carrara, A., Kolari, P., Op De Beeck, M., Arriga, N., Berveiller, D., Dengel, S., … Biraud, S. C. (2018). Radiation measurements at ICOS ecosystem stations. *Int. Agrophys*, *32*, 589–605. https://doi.org/10.1515/intag-2017-0049

Carter, G. A., Mitchell, R. J., Chappelka, A. H., & Brewer, C. H. (1992). Response of Leaf Spectral Reflectance in Loblolly Pine to Increased Atmospheric Ozone and Precipitation Acidity. In *Journal of Experimental Botany* (Vol. 43). Retrieved from https://academic.oup.com/jxb/article-abstract/43/4/577/610818

Castillo-Núñez, M., Sánchez-Azofeifa, G. A., Croitoru, A., Rivard, B., Calvo-Alvarado, J., & Dubayah, R. O. (2011). Delineation of secondary succession mechanisms for tropical dry forests using LiDAR. *Remote Sensing of Environment*, *115*(9), 2217–2231. https://doi.org/10.1016/j.rse.2011.04.020

Castro, S. M., Sanchez-Azofeifa, G. A., & Sato, H. (2018). Effect of drought on productivity in a Costa Rican tropical dry forest Effect of drought on productivity in a Costa Rican tropical dry forest. *Environ. Res. Lett*, *13*. Retrieved from https://doi.org/10.1088/1748-9326/aaacbc

Chadwick, R., Good, P., Martin, G., & Rowell, D. P. (2016). Large rainfall changes consistently projected over substantial areas of tropical land. *Nature Climate Change*, *6*(2), 177–181. https://doi.org/10.1038/nclimate2805

Chanthorn, W., Ratanapongsai, Y., Brockelman, W. Y., Allen, M. A., Favier, C., & Dubois, M. A. (2016). Viewing tropical forest succession as a three-dimensional dynamical system. *Theoretical Ecology*, *9*(2), 163–172. https://doi.org/10.1007/s12080-015-0278-4

Chave, J., Réjou-Méchain, M., Búrquez, A., Chidumayo, E., Colgan, M. S., Delitti, W. B. C., … Vieilledent, G. (2014). Improved allometric models to estimate the aboveground biomass of tropical trees. *Global Change Biology*, *20*(10), 3177–3190. https://doi.org/10.1111/gcb.12629

Chazdon, R. L., & Fetcher, N. (1984). Photosynthetic Light Environments in a Lowland Tropical Rain Forest in Costa Rica. In *The Journal of Ecology* (Vol. 72). https://doi.org/10.2307/2260066

Chen, J., Jönsson, P., Tamura, M., Gu, Z., Matsushita, B., & Eklundh, L. (2004). A simple method for reconstructing a high-quality NDVI time-series data set based on the Savitzky-Golay filter. *Remote Sensing of Environment*. https://doi.org/10.1016/j.rse.2004.03.014

Chen, J. M. (1996). Canopy architecture and remote sensing of the fraction of photosynthetically active radiation absorbed by boreal conifer forests. *IEEE Transactions on Geoscience and Remote Sensing*, *34*(6), 1353–1368. https://doi.org/10.1109/36.544559

Claverie, M., Vermote, E. F., Weiss, M., Baret, F., Hagolle, O., & Demarez, V. (2013). Validation of coarse spatial resolution LAI and FAPAR time series over cropland in southwest France. *Remote Sensing of Environment*, *139*, 216–230. https://doi.org/10.1016/j.rse.2013.07.027

Cliff, N. (1993). Dominance statistics: Ordinal analyses to answer ordinal questions. *Psychological Bulletin*, *114*(3), 494.

Collins, M. A. T. (2007). Ensembles and probabilities: A new era in the prediction of climate change. *Philosophical Transactions of the Royal Society A: Mathematical, Physical and Engineering Sciences*. https://doi.org/10.1098/rsta.2007.2068

D'Odorico, P., Gonsamo, A., Pinty, B., Gobron, N., Coops, N., Mendez, E., & Schaepman, M. E. (2014). Intercomparison of fraction of absorbed photosynthetically active radiation products derived from satellite data over Europe. *Remote Sensing of Environment*, *142*, 141–154. https://doi.org/10.1016/j.rse.2013.12.005

Daubenmire, R. (1972). Phenology and Other Characteristics of Tropical Semi-Deciduous Forest in North-Western Costa Rica. *The Journal of Ecology*, *60*(1), 147. https://doi.org/10.2307/2258048

De Beurs, K. M., & Henebry, G. M. (2005). A statistical framework for the analysis of long image time series. *International Journal of Remote Sensing*.

https://doi.org/10.1080/01431160512331326657

Dessai, S., Hulme, M., Lempert, R., & Pielke, R. (2009). Do We Need Better Predictions to Adapt to a Changing Climate? *Eos, Transactions American Geophysical Union*. https://doi.org/10.1029/2009eo130003

DeWalt, S. J., Schnitzer, S. A., Chave, J., Bongers, F., Burnham, R. J., Cai, Z., … Thomas, D. (2010). Annual rainfall and seasonality predict pan-tropical patterns of liana density and basal area. *Biotropica*, *42*(3), 309–317. https://doi.org/10.1111/j.1744-7429.2009.00589.x

Drake, J. E., Davis, S. C., Raetz, L. M., & Delucia, E. H. (2011). Mechanisms of age-related changes in forest production: The influence of physiological and successional changes. *Global Change Biology*, *17*(4), 1522–1535. https://doi.org/10.1111/j.1365-2486.2010.02342.x

Duursma, R. A., Falster, D. S., Valladares, F., Sterck, F. J., Pearcy, R. W., Lusk, C. H., … Ellsworth, D. S. (2012). Light interception efficiency explained by two simple variables: A test using a diversity of small- to medium-sized woody plants. *New Phytologist*, *193*(2), 397–408. https://doi.org/10.1111/j.1469-8137.2011.03943.x

FAO. (2015a). Global Forest Resources Assessment 2015. In *FAO Forestry*. https://doi.org/10.1002/2014GB005021

FAO. (2015b). *How are the world's forests changing?* Retrieved from www.fao.org/publications

Fensholt, R., Sandholt, I., & Rasmussen, M. S. (2004). Evaluation of MODIS LAI, fAPAR and the relation between fAPAR and NDVI in a semi-arid environment using in situ measurements. *Remote Sensing of Environment*, *91*(3–4), 490–507. https://doi.org/10.1016/J.RSE.2004.04.009

Foley, J. A., Asner, G. P., Costa, M. H., Coe, M. T., DeFries, R. S., Gibbs, H. K., … Snyder, P. K. (2007). Amazonian revealed: Forest degradation and loss of ecosystem goods and services in the Amazon Basin. *Frontiers in Ecology and the Environment*, *5*(1), 25–32. Retrieved from http://www.jstor.org/stable/20440556

Fonseca, L. M. G., Costa, M. H. M., & Castellari, S. P. (2003). *Automatic registration of radar imagery*. https://doi.org/10.1109/igarss.2002.1026579

Furon, A. C., Wagner-Riddle, C., Smith, C. R., & Warland, J. S. (2008). Wavelet analysis of wintertime and spring thaw CO2 and N2O fluxes from agricultural fields. *Agricultural and Forest Meteorology*. https://doi.org/10.1016/j.agrformet.2008.03.006

Gabor, D. (1946). Theory of communication. Part 1: The analysis of information. *Journal of the Institution of Electrical Engineers - Part III: Radio and Communication Engineering*. https://doi.org/10.1049/ji-3-2.1946.0074

Gabrielsen, E. K. (1948). Effects of Different Chlorophyll Concentrations on Photosynthesis in Foliage Leaves. *Physiologia Plantarum*, *1*(1), 5–37. https://doi.org/10.1111/j.1399-3054.1948.tb07108.x

Galford, G. L., Mustard, J. F., Melillo, J., Gendrin, A., Cerri, C. C., & Cerri, C. E. P. (2008). Wavelet analysis of MODIS time series to detect expansion and intensification of row-crop

agriculture in Brazil. *Remote Sensing of Environment*, *112*(2), 576–587. https://doi.org/10.1016/j.rse.2007.05.017

Garrigues, S., Shabanov, N. V., Swanson, K., Morisette, J. T., Baret, F., & Myneni, R. B. (2008). Intercomparison and sensitivity analysis of Leaf Area Index retrievals from LAI-2000, AccuPAR, and digital hemispherical photography over croplands. *Agricultural and Forest Meteorology*, *148*(8–9), 1193–1209. https://doi.org/10.1016/J.AGRFORMET.2008.02.014

GCOS. (2011). *WORLD METEOROLOGICAL ORGANIZATION INTERGOVERNMENTAL OCEANOGRAPHIC COMMISSION SYSTEMATIC OBSERVATION REQUIREMENTS FOR SATELLITE-BASED DATA PRODUCTS FOR CLIMATE 2011 Update Supplemental details to the satellite-based component of the "Implementation Pl*. Retrieved from https://library.wmo.int/doc_num.php?explnum_id=3710

Ghazoul, J., Burivalova, Z., Garcia-Ulloa, J., & King, L. A. (2015, October 1). Conceptualizing Forest Degradation. *Trends in Ecology and Evolution*, Vol. 30, pp. 622–632. https://doi.org/10.1016/j.tree.2015.08.001

Gobron, N., Pinty, B., Aussedat, O., Chen, J. M., Cohen, W. B., Fensholt, R., … Widlowski, J. L. (2006). Evaluation of fraction of absorbed photosynthetically active radiation products for different canopy radiation transfer regimes: Methodology and results using Joint Research Center products derived from SeaWiFS against ground-based estimations. *Journal of Geophysical Research Atmospheres*, *111*(13), 1–15. https://doi.org/10.1029/2005JD006511

Goel, N. S., & Qin, W. (1994). Influences of canopy architecture on relationships between various vegetation indices and LAI and Fpar: A computer simulation. *Remote Sensing Reviews*, *10*(4), 309–347. https://doi.org/10.1080/02757259409532252

Goward, S. N., & Huemmrich, K. F. (1992). Vegetation canopy PAR absorptance and the normalized difference vegetation index: An assessment using the SAIL model. *Remote Sensing of Environment*, *39*(2), 119–140. https://doi.org/10.1016/0034-4257(92)90131-3

Gower, S. T., Kucharik, C. J., & Norman, J. M. (1999). Direct and indirect estimation of leaf area index, f(APAR), and net primary production of terrestrial ecosystems. *Remote Sensing of Environment*, *70*(1), 29–51. https://doi.org/10.1016/S0034-4257(99)00056-5

Gower, S. T., McMurtrie, R. E., & Murty, D. (1996). Aboveground net primary production decline with stand age: Potential causes. *Trends in Ecology and Evolution*, Vol. 11, pp. 378–382. https://doi.org/10.1016/0169-5347(96)10042-2

Gu, L., Baldocchi, D., Verma, S. B., Black, T. A., Vesala, T., Falge, E. M., & Dowty, P. R. (2002). Advantages of diffuse radiation for terrestrial ecosystem productivity. *Journal of Geophysical Research: Atmospheres*, *107*(D6), ACL 2-1-ACL 2-23. https://doi.org/10.1029/2001JD001242

Hlásny, T., Barka, I., Sitková, Z., Bucha, T., Konôpka, M., & Lukáč, M. (2015). MODIS-based vegetation index has sufficient sensitivity to indicate stand-level intra-seasonal climatic stress in oak and beech forests. *Annals of Forest Science*. https://doi.org/10.1007/s13595-014-0404-2

Horgan, G. (1998). Wavelets for SAR image smoothing. *Photogrammetric Engineering and Remote Sensing*, *64*(12), 1171–1177.

Hosonuma, N., Herold, M., De Sy, V., De Fries, R. S., Brockhaus, M., Verchot, L., … Romijn, E. (2012, December 1). An assessment of deforestation and forest degradation drivers in developing countries. *Environmental Research Letters*, Vol. 7, p. 044009. https://doi.org/10.1088/1748-9326/7/4/044009

Huang, P., Xie, S. P., Hu, K., Huang, G., & Huang, R. (2013). Patterns of the seasonal response of tropical rainfall to global warming. *Nature Geoscience*. https://doi.org/10.1038/ngeo1792

Huang, W., Huang, J., Wang, X., Wang, F., & Shi, J. (2013). Comparability of red/near-infrared reflectance and NDVI based on the spectral response function between MODIS and 30 other satellite sensors using rice canopy spectra. *Sensors (Basel, Switzerland)*, *13*(12), 16023–16050. https://doi.org/10.3390/s131216023

Hwang, T., Gholizadeh, H., Sims, D. A., Novick, K. A., Brzostek, E. R., Phillips, R. P., … Rahman, A. F. (2017). Capturing species-level drought responses in a temperate deciduous forest using ratios of photochemical reflectance indices between sunlit and shaded canopies. *Remote Sensing of Environment*, *199*, 350–359. https://doi.org/10.1016/J.RSE.2017.07.033

Janzen, D. H. (1988). Tropical dry forests. *Biodiversity*, 130–137.

Janzen, Daniel H. (2000). Costa Rica's Area de Conservación Guanacaste: A long march to survival through non-damaging biodevelopment. *Biodiversity*, *1*(2), 7–20. https://doi.org/10.1080/14888386.2000.9712501

Janzen, Daniel H, & Hallwachs, W. (2016). Biodiversity Conservation History and Future in Costa Rica: The Case of Área de Conservación Guanacaste (ACG). *Costa Rican Ecosystems*, 290.

JCGM. (2008). *Evaluation of measurement data-Guide to the expression of uncertainty in measurement Évaluation des données de mesure-Guide pour l'expression de l'incertitude de mesure*. Retrieved from www.bipm.org

Jensen, J. R. (1986). *Original Title: Introductory Digital Image Processing (Prentice Hall Series in Geographic Information Science) Introductory Digital Image Processing*.

Kalácska, M., Calvo-Alvarado, J. C., & Sánchez-Azofeifa, G. a. (2005). Calibration and assessment of seasonal changes in leaf area index of a tropical dry forest in different stages of succession. *Tree Physiology*, *25*(6), 733–744. https://doi.org/10.1093/treephys/25.6.733

Kalacska, M., Sanchez-Azofeifa, G. A., Calvo-Alvarado, J. C., Quesada, M., Rivard, B., & Janzen, D. H. (2004). Species composition, similarity and diversity in three successional stages of a seasonally dry tropical forest. *Forest Ecology and Management*, *200*(1–3), 227–247. https://doi.org/10.1016/j.foreco.2004.07.001

Kalácska, M., Sánchez-Azofeifa, G. A., Rivard, B., Calvo-Alvarado, J. C., Journet, A. R. P., Arroyo-Mora, J. P., & Ortiz-Ortiz, D. (2004). Leaf area index measurements in a tropical moist forest: A case study from Costa Rica. *Remote Sensing of Environment*, *91*(2), 134–152. https://doi.org/10.1016/j.rse.2004.02.011

Kalacska, M E R, Sanchez-Azofeifa, G. a, & … J. C. C.-. (2005). Effects of Season and Successional Stage on Leaf Area Index and Spectral Vegetation Indices in Three …. *Biotropica*, *37*(4), 486–496. Retrieved from http://www.ingentaconnect.com/content/bsc/btp/2005/00000037/00000004/art00002

Kalacska, Margaret E R, Sánchez-azofeifa, G. A., & Calvo-alvarado, J. C. (2017). *Effects of Season and Successional Stage on Leaf Area Index and Spectral Vegetation Indices in Three Mesoamerican Tropical Dry Forests Benoit Rivard and Mauricio Quesada Published by : Association for Tropical Biology and Conservation Stable URL : http://*. *37*(4), 486–496.

Khullar, S., Michael, A., Correa, N., Adali, T., Baum, S. A., & Calhoun, V. D. (2011). Wavelet-based fMRI analysis: 3-D denoising, signal separation, and validation metrics. *NeuroImage*, *54*(4), 2867–2884. https://doi.org/10.1016/j.neuroimage.2010.10.063

Knyazikhin, Y., Martonchik, J. V., Myneni, R. B., Diner, D. J., & Running, S. W. (1998). Synergistic algorithm for estimating vegetation canopy leaf area index and fraction of absorbed photosynthetically active radiation from MODIS and MISR data. *Journal of Geophysical Research*, *103*(D24), 32257. https://doi.org/10.1029/98JD02462

Lau, K.-M., & Weng, H. (2002). Climate Signal Detection Using Wavelet Transform: How to Make a Time Series Sing. *Bulletin of the American Meteorological Society*, *76*(12), 2391–2402. https://doi.org/10.1175/1520-0477(1995)076<2391:csduwt>2.0.co;2

Leuchner, M., Hertel, C., & Menzel, A. (2011). Spatial variability of photosynthetically active radiation in European beech and Norway spruce. *Agricultural and Forest Meteorology*, *151*(9), 1226–1232. https://doi.org/10.1016/J.AGRFORMET.2011.04.014

Li, Jiang. (2004). Wavelet-based feature extraction for improved endmember abundance estimation in linear unmixing of hyperspectral signals. *IEEE Transactions on Geoscience and Remote Sensing*. https://doi.org/10.1109/TGRS.2003.822750

Li, Jin, & Heap, A. D. (2014). Spatial interpolation methods applied in the environmental sciences: A review. *Environmental Modelling & Software*, *53*, 173–189. https://doi.org/10.1016/J.ENVSOFT.2013.12.008

Li, Wei, Cao, S., Campos-Vargas, C., & Sanchez-Azofeifa, A. (2017a). Identifying tropical dry forests extent and succession via the use of machine learning techniques. *International Journal of Applied Earth Observation and Geoinformation*, *63*(April), 196–205. https://doi.org/10.1016/j.jag.2017.08.003

Li, Wei, Cao, S., Campos-Vargas, C., & Sanchez-Azofeifa, A. (2017b). Identifying tropical dry forests extent and succession via the use of machine learning techniques. *International Journal of Applied Earth Observation and Geoinformation*, *63*, 196–205. https://doi.org/10.1016/J.JAG.2017.08.003

Li, Wenjuan, & Fang, H. (2015). Estimation of direct, diffuse, and total FPARs from Landsat surface reflectance data and ground-based estimates over six FLUXNET sites. *Journal of Geophysical Research: Biogeosciences*, *120*(1), 96–112. https://doi.org/10.1002/2014JG002754

Li, Wenjuan, Weiss, M., Waldner, F., Defourny, P., Demarez, V., Morin, D., … Baret, F. (2015). A generic algorithm to estimate LAI, FAPAR and FCOVER variables from SPOT4_HRVIR and landsat sensors: Evaluation of the consistency and comparison with ground measurements. *Remote Sensing*, *7*(11), 15494–15516. https://doi.org/10.3390/rs71115494

Lieberman, D. (1982). Seasonality and Phenology in a Dry Tropical Forest in Ghana. *The Journal of Ecology*, *70*(3), 791. https://doi.org/10.2307/2260105

Lin, J., & Qu, L. (2000). Feature extraction based on morlet wavelet and its application for mechanical fault diagnosis. *Journal of Sound and Vibration*. https://doi.org/10.1006/jsvi.2000.2864

Liu, R., Sun, J., Wang, J., Li, X., Yang, F., Chen, P., & District, C. (2010). *STUDY OF REMOTE SENSING BASED PARAMETER UNCERTAINTY IN PRODUCTION EFFICIENCY MODELS State Key Laboratory of Resources and Environmental Information Systems , Institute of Geographical Sciences and Natural Resources Research , Chinese Academy of Sciences ,*. 3303–3306.

Madani, N., Kimball, J. S., & Running, S. W. (2017). Improving Global Gross Primary Productivity Estimates by Computing Optimum Light Use Efficiencies Using Flux Tower Data. *Journal of Geophysical Research: Biogeosciences*, *122*(11), 2939–2951. https://doi.org/10.1002/2017JG004142

Majasalmi, T. (2015). *Estimation of leaf area index and the fraction of absorbed photosynthetically active radiation in a boreal*. https://doi.org/10.14214/df.187

Majasalmi, T., Stenberg, P., & Rautiainen, M. (2017). Comparison of ground and satellite-based methods for estimating stand-level fPAR in a boreal forest. *Agricultural and Forest Meteorology*, *232*, 422–432. https://doi.org/10.1016/j.agrformet.2016.09.007

Martínez, B., & Gilabert, M. A. (2009). Vegetation dynamics from NDVI time series analysis using the wavelet transform. *Remote Sensing of Environment*, *113*(9), 1823–1842. https://doi.org/10.1016/j.rse.2009.04.016

McDowell, N. G., Coops, N. C., Beck, P. S. A., Chambers, J. Q., Gangodagamage, C., Hicke, J. A., … Allen, C. D. (2015). Global satellite monitoring of climate-induced vegetation disturbances. *Trends in Plant Science*. https://doi.org/10.1016/j.tplants.2014.10.008

Menzel, A., Sparks, T. H., Estrella, N., Koch, E., Aaasa, A., Ahas, R., … Zust, A. (2006). European phenological response to climate change matches the warming pattern. *Global Change Biology*. https://doi.org/10.1111/j.1365-2486.2006.01193.x

Moran, P. A. P. (1950). Notes on Continuous Stochastic Phenomena. *Biometrika*, *37*(1/2), 17. https://doi.org/10.2307/2332142

Morlet, J., Arens, G., Fourgeau, E., & Glard, D. (1982). Wave propagation and sampling theory—Part I: Complex signal and scattering in multilayered media. *GEOPHYSICS*, *47*(2), 203–221. https://doi.org/10.1190/1.1441328

Myneni, R. B., Hoffman, S., Knyazikhin, Y., Privette, J. L., Glassy, J., Tian, Y., … Running, S. W. (2002). Global products of vegetation leaf area and fraction absorbed PAR from year

one of MODIS data. *Remote Sensing of Environment*, *83*(1–2), 214–231. https://doi.org/10.1016/S0034-4257(02)00074-3

Myneni, R. B., & Williams, D. L. (1994). On the relationship between FAPAR and NDVI. *Remote Sensing of Environment*, *49*(3), 200–211. https://doi.org/10.1016/0034-4257(94)90016-7

Myneni, R., Knyazikhin, Y., & Park, T. (2015). MOD15A2H MODIS Leaf Area Index/FPAR 8-Day L4 Global 500m SIN Grid V006. NASA EOSDIS Land Processes DAAC. *LP DAAC*, *Terra*(6), 1. https://doi.org/https://doi.org/10.5067/modis/mod15a2h.006

Myneni, R.B., Knyazikhin, Y., Privette, J. L., Running, S. W., Nemani, R., Zhang, Y., … Votava, P. (1999). MODIS Leaf Area Index (LAI) And Fraction Of Photosynthetically Active Radiation Absorbed By Vegetation (FPAR) Product. *Modis Atbd*, *Version 4.*(4.0), 130. https://doi.org/http://eospso.gsfc.nasa.gov/atbd/modistables.html

Myneni, R.B., & Park, T. (2015). *MCD15A3H MODIS/Terra+Aqua Leaf Area Index/FPAR 4-Day L4 Global 500m SIN Grid V006. NASA EOSDIS Land Processes DAAC*. https://doi.org/https://doi.org/10.5067/MODIS/MCD15A3H.006

Myneni, Ranga B. (1997). Estimation of global leaf area index and absorbed par using radiative transfer models. *IEEE Transactions on Geoscience and Remote Sensing*, *35*(6), 1380–1393. https://doi.org/10.1109/36.649788

Nestola, E., Sánchez-Zapero, J., Latorre, C., Mazzenga, F., Matteucci, G., Calfapietra, C., & Camacho, F. (2017a). Validation of PROBA-V GEOV1 and MODIS C5 & C6 fAPAR products in a deciduous beech forest site in Italy. *Remote Sensing*, *9*(2), 126. https://doi.org/10.3390/rs90201026

Nestola, E., Sánchez-Zapero, J., Latorre, C., Mazzenga, F., Matteucci, G., Calfapietra, C., & Camacho, F. (2017b). Validation of PROBA-V GEOV1 and MODIS C5 & C6 fAPAR products in a deciduous beech forest site in Italy. *Remote Sensing*, *9*(2). https://doi.org/10.3390/rs90201026

Nightingale, J., Schaepman-Strub, G., & Nickeson, J. (2011). Assessing satellite-derived land product quality for Earth system science applications: overview of the CEOS LPV sub-group. *Proceedings of the 34th International Symposium on Remote Sensing of Environment*, (1).

ORNL. (2018). *ORNL DAAC. 2017. MODIS Collection 6 Land Products Global Subsetting and Visualization Tool. ORNL DAAC, Oak Ridge, Tennessee, USA. Accessed April 04, 2018. Subset obtained for MCD15A3H product at 10.8415N,85.6157W, time period: 2017-07-20 to 2018-03-22, an*. https://doi.org/https://doi.org/10.3334/ORNLDAAC/1379

Pan, Y., Birdsey, R. A., Phillips, O. L., & Jackson, R. B. (2013). The Structure, Distribution, and Biomass of the World's Forests. *Annual Review of Ecology, Evolution, and Systematics*, *44*(1), 593–622. https://doi.org/10.1146/annurev-ecolsys-110512-135914

Pastorello, G. Z., Sanchez-Azofeifa, G. A., & Nascimento, M. A. (2011). Enviro-Net : A Network of Ground-based Sensors for Tropical Dry Forests in the Americas. *Sensors*, *11.6*, 6454–6479.

Pennington, T. (2010). Human, Ecological and Biophysical Dimensions of Tropical Dry Forests. Manual of Methods (Book review). In *Interciencia* (Vol. 35).

Percival, D. B., & Walden, A. T. (2006). *Wavelet methods for time series analysis* (Vol. 4). Cambridge university press.

Pickett-Heaps, C. A., Canadell, J. G., Briggs, P. R., Gobron, N., Haverd, V., Paget, M. J., … Raupach, M. R. (2014). Evaluation of six satellite-derived Fraction of Absorbed Photosynthetic Active Radiation (FAPAR) products across the Australian continent. *Remote Sensing of Environment*, *140*, 241–256. https://doi.org/10.1016/j.rse.2013.08.037

Pineda-García, F., Paz, H., & Meinzer, F. C. (2012). *Drought resistance in early and late secondary successional species from a tropical dry forest: the interplay between xylem resistance to embolism, sapwood water storage and leaf sheddingp ce_2582 405..418*. https://doi.org/10.1111/j.1365-3040.2012.02582.x

Pinty, B., Jung, M., Kaminski, T., Lavergne, T., Mund, M., Plummer, S., … Widlowski, J. L. (2011). Evaluation of the JRC-TIP 0.01° products over a mid-latitude deciduous forest site. *Remote Sensing of Environment*, *115*(12), 3567–3581. https://doi.org/10.1016/j.rse.2011.08.018

Pisek, J., Rautiainen, M., Nikopensius, M., & Raabe, K. (2015). Estimation of seasonal dynamics of understory NDVI in northern forests using MODIS BRDF data: Semi-empirical versus physically-based approach. *Remote Sensing of Environment*. https://doi.org/10.1016/j.rse.2015.03.003

Portillo-Quintero, C. A., & Sánchez-Azofeifa, G. A. (2010). Extent and conservation of tropical dry forests in the Americas. *Biological Conservation*, *143*(1), 144–155. https://doi.org/10.1016/j.biocon.2009.09.020

Poulter, B., Heyder, U., & Cramer, W. (2009). Modeling the sensitivity of the seasonal cycle of GPP to dynamic LAI and soil depths in tropical rainforests. *Ecosystems*, *12*(4), 517–533. https://doi.org/10.1007/s10021-009-9238-4

Power, M. J., Whitney, B. S., Mayle, F. E., Neves, D. M., de Boer, E. J., & Maclean, K. S. (2016). Fire, climate and vegetation linkages in the bolivian chiquitano seasonally dry tropical forest. *Philosophical Transactions of the Royal Society B: Biological Sciences*, *371*(1696). https://doi.org/10.1098/rstb.2015.0165

Putzenlechner, B., Marzahn, P., Kiese, R., Ludwig, R., & Sanchez-Azofeifa, A. (2019). Assessing the variability and uncertainty of two-flux FAPAR measurements in a conifer-dominated forest. *Agricultural and Forest Meteorology*, *264*(October 2018), 149–163. https://doi.org/10.1016/j.agrformet.2018.10.007

QUANTUM SENSOR Models SQ-100 and SQ-300 Series (including SS models). (2019). Retrieved from https://www.apogeeinstruments.com/content/SQ-100-300-manual.pdf

Quesada, M., Sanchez-Azofeifa, G. A., Alvarez-Añorve, M., Stoner, K. E., Avila-Cabadilla, L., Calvo-Alvarado, J., … Sanchez-Montoya, G. (2009). Succession and management of tropical dry forests in the Americas: Review and new perspectives. *Forest Ecology and Management*, *258*(6), 1014–1024. https://doi.org/10.1016/j.foreco.2009.06.023

Ramsfield, T. D., Bentz, B. J., Faccoli, M., Jactel, H., & Brockerhoff, E. G. (2016). Forest health in a changing world: Effects of globalization and climate change on forest insect and pathogen impacts. *Forestry*, *89*(3), 245–252. https://doi.org/10.1093/forestry/cpw018

Rankine, C. J. (2016). *Monitoring Seasonal and Secondary Succession Processes in Deciduous Forests using Near-Surface Optical Remote Sensing and Wireless Sensor Networks*. 167. https://doi.org/10.7939/R32Z12V30

Rankine, C., Sánchez-Azofeifa, G. A., Guzmán, J. A., Espirito-Santo, M. M., & Sharp, I. (2017). Comparing MODIS and near-surface vegetation indexes for monitoring tropical dry forest phenology along a successional gradient using optical phenology towers Comparing MODIS and near-surface vegetation indexes for monitoring tropical dry forest phenology . *Environ. Res. Lett*, *12*. https://doi.org/10.1088/1748-9326/aa838c

Rawat, P., Singh, K. D., Chaouchi, H., & Bonnin, J. M. (2014). Wireless sensor networks: A survey on recent developments and potential synergies. *Journal of Supercomputing*, *68*(1), 1–48. https://doi.org/10.1007/s11227-013-1021-9

Reich, P. B., & Borchert, R. (1984). Water Stress and Tree Phenology in a Tropical Dry Forest in the Lowlands of Costa Rica. *The Journal of Ecology*, *72*(1), 61. https://doi.org/10.2307/2260006

Roesch, A., & Schmidbauer, H. (2018). *WaveletComp: Computational Wavelet Analysis*. Retrieved from https://cran.r-project.org/package=WaveletComp

Rullan-Silva, C. D., Olthoff, A. E., Delgado de la Mata, J. A., & Pajares-Alonso, J. A. (2013). Remote monitoring of forest insect defoliation. A review. *Forest Systems*, *22*(3), 377–391. https://doi.org/10.5424/fs/2013223-04417

Ryu, Y., Berry, J. A., & Baldocchi, D. D. (2019). What is global photosynthesis? History, uncertainties and opportunities. *Remote Sensing of Environment*, *223*(January), 95–114. https://doi.org/https://doi.org/10.1016/j.rse.2019.01.016

Ryu, Y., Lee, G., Jeon, S., Song, Y., & Kimm, H. (2014). Monitoring multi-layer canopy spring phenology of temperate deciduous and evergreen forests using low-cost spectral sensors. *Remote Sensing of Environment*. https://doi.org/10.1016/j.rse.2014.04.015

Sakamoto, T., Yokozawa, M., Toritani, H., Shibayama, M., Ishitsuka, N., & Ohno, H. (2005). A crop phenology detection method using time-series MODIS data. *Remote Sensing of Environment*, *96*(3–4), 366–374. https://doi.org/10.1016/j.rse.2005.03.008

Sanchez-Azofeifa, A., Antonio Guzmán, J., Campos, C. A., Castro, S., Garcia-Millan, V., Nightingale, J., & Rankine, C. (2017). Twenty-first century remote sensing technologies are revolutionizing the study of tropical forests. *Biotropica*, Vol. 49, pp. 604–619. https://doi.org/10.1111/btp.12454

Sanchez-Azofeifa, G. A., Rankine, C., do Espirito Santo, M. M., Fatland, R., & Garcia, M. (2011). Wireless Sensing Networks for Environmental Monitoring: Two Case Studies from Tropical Forests. *2011 IEEE Seventh International Conference on EScience*, (December 2011), 70–76. https://doi.org/10.1109/eScience.2011.18

Sánchez-Azofeifa, G. Arturo, Quesada, M., Rodríguez, J. P., Nassar, J. M., Stoner, K. E.,

Castillo, A., … Cuevas-Reyes, P. (2005). Research priorities for neotropical dry forests. *Biotropica*, *37*(4), 477–485. https://doi.org/10.1111/j.1744-7429.2005.00066.x

Sánchez-Azofeifa, G. Arturo, Rankine, C., Do Espirito Santo, M. M., Fatland, R., & Garcia, M. (2011). Wireless sensing networks for environmental monitoring: Two case studies from tropical forests. *Proceedings - 2011 7th IEEE International Conference on EScience, EScience 2011*, (December 2011), 70–76. https://doi.org/10.1109/eScience.2011.18

Sánchez-Azofeifa, G., Kalacska, M., Quesada, M., Calvo-Alvarado, J. C., Nassar, J. M., & Rodríguez, J. P. (2005). Need for Integrated Research for a Sustainable Future in Tropical Dry Forests. *Conservation Biology*, *19*(2), 285–286. https://doi.org/10.1111/j.1523-1739.2005.s01

Sánchez-Azofeifa, G A, Kalácska, M., Espírito-Santo, M. M. do, Fernandes, G. W., & Schnitzer, S. A. (2009). Tropical dry forest succession and the contribution of lianas to wood area index (WAI). *Forest Ecology and Management*, *258*(6), 941–948. https://doi.org/10.1016/j.foreco.2008.10.007

Sánchez-Azofeifa, Gerardo Arturo, Guzmán-Quesada, J. A., Vega-Araya, M., Campos-Vargas, C., Durán, S. M., D'Souza, N., … Sharp, I. (2017). Can terrestrial laser scanners (TLSs) and hemispherical photographs predict tropical dry forest succession with liana abundance? *Biogeosciences*, *14*(4), 977–988. https://doi.org/10.5194/bg-14-977-2017

Savitzky, A., & Golay, M. J. E. (1964). Smoothing and Differentiation of Data by Simplified Least Squares Procedures. *Analytical Chemistry*. https://doi.org/10.1021/ac60214a047

Sellers, P. J. (1985). Canopy reflectance, photosynthesis and transpiration. *International Journal of Remote Sensing*, *6*(8), 1335–1372. https://doi.org/10.1080/01431168508948283

Sellers, P J. (1987). Canopy reflectance, photosynthesis, and transpiration, II. The role of biophysics in the linearity of their interdependence. *Remote Sensing of Environment*, *21*(2), 143–183. https://doi.org/10.1016/0034-4257(87)90051-4

Sellers, Piers J., Nickeson, J. E., Goetz, S. J., Hall, F. G., & Huemmrich, K. F. (2012). Satellite remote sensing of surface energy balance: Success, failures, and unresolved issues in FIFE. *Journal of Geophysical Research*, *97*(D17), 19061. https://doi.org/10.1029/92jd02189

Seneviratne, S. I., Donat, M. G., Mueller, B., & Alexander, L. V. (2014). No pause in the increase of hot temperature extremes. *Nature Climate Change*, *4*(3), 161–163. https://doi.org/10.1038/nclimate2145

Senna, M. C. A. (2005). Fraction of photosynthetically active radiation absorbed by Amazon tropical forest: A comparison of field measurements, modeling, and remote sensing. *Journal of Geophysical Research*, *110*(G1), G01008. https://doi.org/10.1029/2004JG000005

Serbin, S. P., Ahl, D. E., & Gower, S. T. (2013). Spatial and temporal validation of the MODIS LAI and FPAR products across a boreal forest wildfire chronosequence. *Remote Sensing of Environment*, *133*, 71–84. https://doi.org/10.1016/j.rse.2013.01.022

Shabanov, N. V., Wang, Y., Buermann, W., Dong, J., Hoffman, S., Smith, G. R., … Myneni, R. B. (2003). Effect of foliage spatial heterogeneity in the MODIS LAI and FPAR algorithm over broadleaf forests. *Remote Sensing of Environment*, *85*(4), 410–423.

https://doi.org/10.1016/S0034-4257(03)00017-8

Shumway, R. H., & Stoffer, D. S. (2011). *Time Series Analysis and Its Applications*. https://doi.org/10.1007/978-1-4419-7865-3

Souza, R., Feng, X., Antonino, A., Montenegro, S., Souza, E., & Porporato, A. (2016). Vegetation response to rainfall seasonality and interannual variability in tropical dry forests. *Hydrological Processes*, *30*(20), 3583–3595. https://doi.org/10.1002/hyp.10953

Steinberg, D. C., & Goetz, S. (2008). Assessment and extension of the MODIS FPAR products in temperate forests of the eastern United States. *International Journal of Remote Sensing*, *30*(1), 169–187. https://doi.org/10.1080/01431160802244276

Steinberg, D., Goetz, S., & Hyer, E. (2006). Validation of MODIS F/sub PAR/products in boreal forests of Alaska. *Geoscience and Remote …*, *44*(7), 1–11. Retrieved from http://ieeexplore.ieee.org/xpls/abs_all.jsp?arnumber=1645282

Stenberg, P., Mõttus, M., & Rautiainen, M. (2016). Photon recollision probability in modelling the radiation regime of canopies — A review. *Remote Sensing of Environment*, *183*, 98–108. https://doi.org/10.1016/J.RSE.2016.05.013

Temperli, C., Bugmann, H., & Elkin, C. (2012). Adaptive management for competing forest goods and services under climate change. *Ecological Applications*, *22*(8), 2065–2077. https://doi.org/10.1890/12-0210.1

Thomas, V., Finch, D. A., McCaughey, J. H., Noland, T., Rich, L., & Treitz, P. (2006). Spatial modelling of the fraction of photosynthetically active radiation absorbed by a boreal mixedwood forest using a lidar-hyperspectral approach. *Agricultural and Forest Meteorology*, *140*(1–4), 287–307. https://doi.org/10.1016/j.agrformet.2006.04.008

Tian, Y., Myneni, R. ., Morisette, J. ., Privette, J. ., Votava, P., Lotsch, A., … Glassy, J. (2002). Global products of vegetation leaf area and fraction absorbed PAR from year one of MODIS data. *Remote Sensing of Environment*. https://doi.org/10.1016/s0034-4257(02)00074-3

Torrence C., & Compo G. (1998). A practical guide to wavelet analysis. *Bulletin of the American Meteorological Society*, *79 (1)*, 61--78. Retrieved from https://journals.ametsoc.org/doi/pdf/10.1175/1520-0477%281998%29079%3C0061%3AAPGTWA%3E2.0.CO%3B2

Trenberth, K. E., Fasullo, J. T., & Shepherd, T. G. (2015, July 24). Attribution of climate extreme events. *Nature Climate Change*, Vol. 5, pp. 725–730. https://doi.org/10.1038/nclimate2657

Van der Zande, D., Stuckens, J., Verstraeten, W. W., Muys, B., & Coppin, P. (2010). Assessment of light environment variability in broadleaved forest canopies using terrestrial laser scanning. *Remote Sensing*, *2*(6), 1564–1574. https://doi.org/10.3390/rs2061564

Verbesselt, J., Hyndman, R., Newnham, G., & Culvenor, D. (2010). Detecting trend and seasonal changes in satellite image time series. *Remote Sensing of Environment*, *114*(1), 106–115. https://doi.org/10.1016/j.rse.2009.08.014

Verhoef, W. (1984). Light scattering by leaf layers with application to canopy reflectance modeling: The SAIL model. *Remote Sensing of Environment*, *16*(2), 125–141. https://doi.org/10.1016/0034-4257(84)90057-9

Vermote, E. F., El Saleous, N. Z., & Justice, C. O. (2002). Atmospheric correction of MODIS data in the visible to middle infrared: First results. *Remote Sensing of Environment*, *83*(1–2), 97–111. https://doi.org/10.1016/S0034-4257(02)00089-5

Vierling, L. A., & Wessman, C. A. (2000). Photosynthetically active radiation heterogeneity within a monodominant Congolese rain forest canopy. *Agricultural and Forest Meteorology*, *103*(3), 265–278. https://doi.org/10.1016/S0168-1923(00)00129-5

Walter-, E. A., Blad, B. L., Hays, C. J., Mesarch, M. A., Deering, D. W., & Middleton, E. M. (1992). Biophysical Properties Affecting Vegetative Canopy Reflectance and Absorbed Photosynthetically Active Radiation at the FIFE Site. In *JOURNAL OF GEOPHYSICAL RESEARCH* (Vol. 97). Retrieved from https://agupubs.onlinelibrary.wiley.com/doi/pdf/10.1029/92JD00656

Wan, Z. (2014). New refinements and validation of the collection-6 MODIS land-surface temperature/emissivity product. *Remote Sensing of Environment*, *140*, 36–45. https://doi.org/10.1016/j.rse.2013.08.027

Wang, F., & D'Sa, E. J. (2010). Potential of MODIS EVI in identifying hurricane disturbance to coastal vegetation in the Northern Gulf of Mexico. *Remote Sensing*, *2*(1), 1–18. https://doi.org/10.3390/rs2010001

Wang, H. (2006). Extending the Linear Model with R: Generalized Linear, Mixed Effects and Nonparametric Regression Models Edited by Faraway J. J. *Biometrics*, *62*(4), 1278–1278. https://doi.org/10.1111/j.1541-0420.2006.00596_12.x

White, M. A., & Nemani, R. R. (2006). Real-time monitoring and short-term forecasting of land surface phenology. *Remote Sensing of Environment*, *104*(1), 43–49. https://doi.org/10.1016/j.rse.2006.04.014

Widlowski, J.-L. (2010). On the bias of instantaneous FAPAR estimates in open-canopy forests. *Agricultural and Forest Meteorology*, *150*(12), 1501–1522. https://doi.org/10.1016/J.AGRFORMET.2010.07.011

Wilson, K. B., Baldocchi, D. D., & Hanson, P. J. (2001). Leaf age affects the seasonal pattern of photosynthetic capacityand net ecosystem exchange of carbon in a deciduous forest. *Plant, Cell and Environment*, *24*(6), 571–583. https://doi.org/10.1046/j.0016-8025.2001.00706.x

Wright, C., Nyberg, D., Rickards, L., & Freund, J. (2018, July 1). Organizing in the Anthropocene. *Organization*, Vol. 25, pp. 455–471. https://doi.org/10.1177/1350508418779649

Wright, S. J., & Muller-Landau, H. C. (2006). The future of tropical forest species. *Biotropica*, *38*(3), 287–301. https://doi.org/10.1111/j.1744-7429.2006.00154.x

Yan, K., Park, T., Yan, G., Liu, Z., Yang, B., Chen, C., … Myneni, R. B. (2016). Evaluation of MODIS LAI/FPAR product collection 6. Part 1: Consistency and Improvements. *Remote Sensing*, *8*(6), 1–16. https://doi.org/10.3390/rs8060460

Younis, M., & Akkaya, K. (2008). Strategies and techniques for node placement in wireless sensor networks: A survey. *Ad Hoc Networks*, *6*(4), 621–655. https://doi.org/10.1016/J.ADHOC.2007.05.003

Zelazowski, P., Malhi, Y., Huntingford, C., Sitch, S., & Fisher, J. B. (2011). Changes in the potential distribution of humid tropical forests on a warmer planet. *Philosophical Transactions of the Royal Society A: Mathematical, Physical and Engineering Sciences*, *369*(1934), 137–160. https://doi.org/10.1098/rsta.2010.0238

Zhang, R., Zhou, Y., Luo, H., Wang, F., & Wang, S. (2017). Estimation and analysis of spatiotemporal dynamics of the net primary productivity integrating efficiency model with process model in Karst area. *Remote Sensing*, *9*(5). https://doi.org/10.3390/rs9050477

Zhang, X., Friedl, M. A., Schaaf, C. B., Strahler, A. H., Hodges, J. C. F., Gao, F., … Huete, A. (2003). Monitoring vegetation phenology using MODIS. *Remote Sensing of Environment*. https://doi.org/10.1016/S0034-4257(02)00135-9

Zhou, J., Civco, D. L., & Silander, J. A. (1998). A wavelet transform method to merge Landsat TM and SPOT panchromatic data. *International Journal of Remote Sensing*. https://doi.org/10.1080/014311698215973

Zhu, Q., Zhao, J., Zhu, Z., Zhang, H., Zhang, Z., Guo, X., … Sun, L. (2017). *Remotely Sensed Estimation of Net Primary Productivity (NPP) and Its Spatial and Temporal Variations in the Greater Khingan Mountain Region, China*. https://doi.org/10.3390/su9071213